UNIVERSITY OF CALIFORNIA, SAN DIEGO

Implementation and Advancement of Novel Technologies for Understanding Skeletal Myogenesis and Treating Peripheral Artery Disease

A dissertation submitted in partial satisfaction of the
requirements for the degree
Doctor of Philosophy

in

Bioengineering with a Specialization in Multi-Scale Biology

by

Nikhil Rao

Committee in charge:

Professor Karen Christman, Chair
Professor Shaochen Chen
Professor Adam Engler
Professor Farah Sheikh
Professor Shyni Varghese

2014

The dissertation of Nikhil Rao is approved, and it is acceptable in quality and form for publication on microfilm and electronically:

_____

_____

_____

_____

_____
Chair

University of California, San Diego

2014

DEDICATION

To my loving mother and father.

EPIGRAPH

Don't let a mad world tell you that success is anything other than a successful present moment.

—Eckhart Tolle

TABLE OF CONTENTS

LIST OF FIGURES

ACKNOWLEDGEMENTS

Throughout my time in San Diego and particularly at UC San Diego, there have been numerous people that have contributed to my excelling and success as a bioengineer. Due to my somewhat unrelated technical background in nucleic acid technology, cancer, and biomolecular engineering, it was no easy task to understand cardiac/skeletal muscle physiology and the associated skill sets. First and foremost, I want to thank my mentor, Dr. Karen Christman. I felt that she took a risk taking me in as a student with no prior cardiac tissue engineering knowledge. I appreciate her confidence she had in me to create scientific value in a lab that had already incredible growth and potential for the future. She has allowed me to grow in multiple dimensions - to expand in breadth of what types of projects I can carry out and in depth in terms of helping me realize a story behind my research. She was extraordinarily respectful of my needs and expectations in graduate school and the mutually understanding relationship created a great working environment for me. She has provided a schedule with amazing flexibility, some of the best resources in the world, and a collaborative working environment. She also allowed and encouraged me to pursue leadership in the community and present my work at numerous conferences nationwide. I have learned a great deal just by interacting and working under her, and because of her I believe I have been blessed with a successful Ph.D. degree.

The peers within the lab were more than helpful and eager to help me with the transition into graduate school and the work in this lab. For that I would like to thank Drs. Jennifer Singelyn, Aboli Rane, Sonya Sonnenberg, and Jessica Dequach. However, more specifically I would like to thank Dr. Adam Young. He took me into the lab as a mentor - teaching me technical and soft skills related to bioengineering. I learned and admired his leadership, work ethic, and professionalism. It's because of him that I was bold enough to become a leader within the UCSD bioengineering department. He not only was a great mentor, but ended up as one of my better friends and roommate for two years at UCSD.

There were a number of coworkers that have helped me along the way and without them I would not have had nearly as success or the resources to generate

such promising data. Ludovic Vincent, Dr. Yu Suk Choi, Dr. Gregory Grover, Dr. Roberto Gaetani, Samantha Evans, Rebecca Braden and Gillie Agmon are a few of the many that made my work much easier and that much more powerful.

In the transition into *in vivo* work I would like to thank the rest of the members of the lab that have helped me throughout to learn in parallel and provide assistance as needed: Todd Johnson, Sophia Suarez, and Jean Wang.

During my grad life I felt there was a constant need for a healthy-work life balance. My water bottle, coffee, running, yoga, craft beer and cocktails, concerts, and my ipod are a few of the many requirements to maintain my sanity. There are a number of people that also helped me through this process, through hard times and good times: Dr. Aarash Bordbar, Todd Johnson, Mimi Wang, David Nelles, Lisa Dieu, Brian Meckes, Dr. Gaurav Kaushik, Matthew Bergman, Kristen Meyer, Jeffrey Shin, Michael Rozen, Ranvir Mangat, Carson Fuller, Asaf Savion, Devjeet Mishra, Siddharth Bhandari, Amy Tran, Rajiv Mallipudi, Dr. Gregory Grover, Shahed Alam, Mary Mallaney, and many, many more. My social interactions throughout these last few years have made me confident and a leader and I must thank these people.

Most importantly, I would not have been here in the first place without my wonderful and supportive parents, Anita and Ramesh. They provided me with the best education imaginable from grade school through high school and on to college. They have supported my dreams and desires throughout and have never once doubted my abilities even when times were difficult. They always believed that I could do and be the best at what my passions and goals in life have been. To them, I dedicate this thesis.

Chapter 2 in part is a reprint of the material in: Rao N, Evans S, Stewart D, Spencer K, Sheikh F, Hui, E E, Christman K L. Fibroblasts influence muscle progenitor differentiation and alignment in contact independent and dependent manners in organized co-culture devices. *Biomedical Microdevices*, 2013; 15:161-9. The dissertation author was the primary author.

Chapter 3 in part is a reprint of the material Rao N, Grover G N, Vincent L G, Evans S, Choi Y S, Spencer K, Hui E E, Engler A J, Christman K L. A co-culture device with a tunable stiffness to understand combinatorial cell-cell and cell-matrix interactions. *Integrative Biology.* 2013; 5: 1344-54. Inside cover article. The dissertation author was the primary author.

Chapter 4 in part currently being prepared for submission for publication of the material: Rao N, Agmon G, Tierney M, Vincent L G, Engler A J, Sacco A, Christman KL. A two-pronged approach to increasing myoblast retention and viability and hind limb ischemia perfusion with skeletal fibroblasts and a decellularized skeletal muscle matrix hydrogel. The dissertation author was the primary author.

VITA

2009	B.S. in Chemical Biomolecular Engineering, Johns Hopkins University, Baltimore
2014	Ph.D. in Bioengineering with a Specialization in Multi-Scale Biology, University of California, San Diego

PUBLICATIONS

1. **Rao N**, Agmon G, Tierney M, Braden R, Sacco A, Christman K L. Improving myoblast cell viability by co-delivery of an injectable skeletal-muscle specific microenvironment for treatment of peripheral artery disease. (*In Preparation*)
2. Sonnenberg S, Rane A, Liu C J, **Rao N**, Bajaj V, Zhang S, Braden, R, Schup-Magoffin P.J., Kwan O L, DeMaria A, Cochran J R, Christman K L. Delivery of an engineered HGF fragment in an extracellular matrix-derived hydrogel prevents negative LV remodeling post-myocardial infarction. (*Submitted*)
3. **Rao N**, Grover G N, Vincent L G, Evans S, Choi Y S, Spencer K, Hui E E, Engler A J, Christman K L. A co-culture device with a tunable stiffness to understand combinatorial cell-cell and cell-matrix interactions. Integrative Biology. 2013; 5: 1344-54. Inside cover article.
4. Grover G N, **Rao N**, Christman K L. Myocardial Matrix Polyethylene Glycol Hybrid Hydrogels for Tissue Engineering. Nanotechnology. 2013; 25:014011. 25th anniversary issue.
5. **Rao N**, Evans S, Stewart D, Spencer K, Sheikh F, Hui, E E, Christman K L. Fibroblasts influence muscle progenitor differentiation and alignment in contact independent and dependent manners in organized co-culture devices. Biomedical Microdevices, 2013; 15:161-9.

ABSTRACT OF THE DISSERTATION

Implementation and Advancement of Novel Technologies for Understanding Skeletal Myogenesis and Treating Peripheral Artery Disease

by

Nikhil Rao

Doctor of Philosophy in Bioengineering with a Specialization in Multi-Scale Biology

University of California, San Diego, 2014

Professor Karen Christman, Chair

Tissue engineered therapies have demonstrated promise for multiple injuries and diseases that in particular affect muscle. Over the last decade, many groups have shown that these therapies could provide an alternate avenue for biological therapies that obviate the need for systemic drugs, invasive procedures, and repeated treatments. In particular, cell therapy has shown much promise in repairing damaged muscle tissue. This has mainly been exemplified in damaged cardiac tissue but more recently has been used to treat skeletal muscle ailments such as peripheral artery disease (PAD). PAD effects over 27 million people in

Europe and North America alone. This chronic disease is typically caused by an atherosclerosis of the leg, decreasing blood flow, and leading to eventual muscle atrophy. This can cause extreme pain at rest and could lead to amputation. Skeletal myoblast cell therapy has been shown to be a promising therapy by increasing blood vessel formation by paracrine signaling and repairing damaged muscle by engraftment into host tissue. However, few of these cells upon injection stay viable and localized to the site of delivery. The inability to administer, remain viable, and engraft efficiently has led scientists to explore alternative ways to deliver these cells. In this thesis, we examine the behavior of myoblasts in response to fibroblasts via a state-of-the-art co-culture device *in vitro*. Next, we make the system more physiologically relevant by adding a substrate that can be tuned to a specific stiffness. Then we utilize previous co-culture findings and implement them into a decellularized skeletal muscle matrix hydrogel (SkECM) that can be easily injected *in vivo*. We show that combining both myoblasts and fibroblasts in the SkECM improves myoblast differentiation and metabolic activity when cultured in 3D. We also show that the SkECM and fibroblasts promote myoblast engraftment in muscle tissue compared to injections in saline. Lastly, we demonstrate an increase in blood perfusion in ischemic limbs when myoblasts are injected with SkECM. This work provides a way to study myoblast differentiation and viability in vitro and a delivery system that improves on the current method used in clinical trials for PAD treatment.

Chapter 1

Introduction to skeletal muscle tissue engineering

1.1 Introduction

Developing or improving a tissue-engineered therapy to translate into humans can be researched at various stages of development. This scale ranges from understanding the basic biology and its implications at a molecular level to a macroscopic analysis of functional improvement and quality of life. Cell and molecular biologists are involved in the former while clinicians and doctors in the latter. Tissue engineers bridge the gap between the two by translating findings at a micro level to apply to a physiologically relevant macroscale. This thesis acknowledges the steps in the "process development" of a viable tissue engineering therapeutic. This involves observational cell biology, understanding cell-cell and cell-matrix interactions, engineering and improving a novel *in vitro* technology, and translating such findings to advancing the treatments utilized in clinical trials. In this thesis we use this methodology to improve on the current treatments for peripheral artery disease (PAD) [1].

1.2 Skeletal muscle physiology

Skeletal muscle is a highly organized organ that controls most of the voluntary movements in our body. The ability to voluntarily move skeletal muscle makes this organ distinct from other muscle types, such as smooth or cardiac. It comprises approximately 40% of all muscle mass [2]. It is a striated muscle made up of striped and aligned muscle fibers. These muscle fibers are composed of myocytes, muscle cells that are cylindrical and multi-nucleated. This muscle movement (muscle contraction) is carried out by the contractile entities of myocytes, i.e. the interplay of actin and myosin proteins in sarcomeres [2]. Movement of myosin is governed by calcium concentration and ATP binding and subsequent conversion to ADP. Not only is intracellular protein movement important but functional force generation by these cells is also governed by the extracellular matrix (ECM). This ECM provides the scaffolding and structure necessary to allow for passive force, but also helps in stabilizing muscle, facilitating muscle growth, and housing important cells responsible for overall muscle function. It has also been shown to be important in the biochemical framework surrounding the muscle cells.

Collagen makes up the majority of this ECM and can account for up to 10% of muscle's dry weight [3]. Multiple sub-types of collagen (collagen I, II, V, VI, etc.) make up the total collagen content in the muscle. In the basement membrane, in particular, a large number of collagen interacts with proteoglycans, most noteably Decorin [4]. Proteoglycans along with glycosaminoglycans are responsible for binding various growth factors that regulate collagen synthesis. In healthy muscle, MMP-2, MMP-9, and other secreted collagenases are present and increase in concentration when injury occurs to help in general muscle repair [5, 4]. They are responsible for normal muscle ECM turnover, degradation and subsequent muscle growth.

The ECM greatly influences overall stiffness of the tissue. Skeletal muscle has an "intermediate" stiffness relative to the other organs in the body. At the extremes lie fat tissue (extremely soft < 1 kPa) and bone (extremely stiff > 100 kPa). Individual muscle fibers are on the order of 10 kPa [6]. Fibers supported by extracellular matrix have an increased modulus of approximately 40kPa [4].

This demonstrates that the ECM is a very important biochemical and structural component of the muscle. Furthermore, skeletal fibroblasts in the basal lamina and surrounding the myocytes in muscle are responsible for producing this extracellular matrix [4]. These cells have been shown to also secrete important paracrine factors for maintaining healthy muscle tissue [7, 8]. They are not the only important cell type involved in muscle function but will be a major focus in the following chapters.

1.3 Skeletal myoblasts

Muscle has a limited reparative capacity. Intrinsic muscle repair is due to an acute signaling cascade that occurs upon injury that leads to quiescent satellite cells to be activated [9]. These quiescent cells lie nascent to mature muscle fibers in the basal membrane (ECM) and are considered "precursor" muscle cells [10]. Upon activation, they proliferate and migrate to the site of injury and become what is known as the "myoblast." At the damaged region, they fuse with endogeneous muscle and with one another to form multi-nucleated myotubes [11]. This differentiation is key in creating myotubes, the functional building blocks of muscle fibers. Myoblast cells go through a very complex albeit well-studied change in gene and protein expression as a function of differentiation. Transcription factors such as Pax 7, MyoD, and Myf 5 are prevalent at the early stages of satellite cell activation [12]. Myogenin, a later transcription factor turns on as these myoblasts begin to differentiate while Pax 7 and Myf 5 are no longer expressed. [12]. Proteins such as desmin, myosin heavy chain, and z-proteins responsible for mature muscle formation tend to increase as a function of this differentiation process.

1.4 Peripheral artery disease

We are interested in developing technologies for skeletal muscle repair specifically for peripheral artery disease (PAD). PAD currently affects 8 million people in the United States alone today [13]. Due to the growing number of people affected by the disease every year, there is an increasing need for a successful treatment.

There are a number of factors that put an individual at risk for the disease including diabetes, smoking, obesity, hypertension, coronary arterial disease, cerebrovascular disease, and a host of other variables [14, 15, 16]. In early stages of PAD onset, blood vessels are partially occluded by either calcification or atherosclerotic plaques. This leads to decreased blood flow in the legs. Over time, this lack of blood flow causes a scarcity of nutrients to the tissues in the leg, particularly the muscle. The most common symptom for early onset of the disease is intermittent claudication, or pain during walking [14]. The muscle atrophies and leads to extreme pain for individuals even at rest. This can result in eventual amputation or even mortality. Over a third of the patients diagnosed with late-staged PAD require major amputation [17]. Worse, a 1-year mortality rate of about 20% is observed for these late-staged patients [18].

1.4.1 Treatments and other investigated therapies

PAD treatments involve a two-front approach. The progression of the atherosclerosis must be impeded and interventions to increase blood flow to the limbs and improvement of quality-of-life must also be addressed. If the claudication is lifestyle-limiting and cannot be treated with improvement in the quality of life or with pharmacotherapy then catheter procedures or surgery is required by either surgical revascularization or endovascular interventions [14]. These procedures involve stents, atherectomy, bypass grafting, and angioplasty. Some of these techniques are highly invasive, require multiple follow-up procedures, and none are a full-proof solution. Unfortunately, few individuals diagnosed with PAD are even candidates for these treatments. The search for a solution has researchers extensively investigating cell delivery, gene delivery, growth factors, and biomaterials for increasing blood perfusion and subsequent muscle regeneration into the affected limbs.

1.4.2 Cell delivery treatments

Current and past clinical trials have utilized multiple cell types to treat PAD. These include, but are not limited to: mesenchymal stem cells, hematopoietic stem cells, mononuclear cells, endothelial progenitor cells, and skeletal myoblast progenitor cells [19, 20, 21, 22, 23, 24].

Bone marrow and peripheral blood mononuclear cells, also known as endothelial progenitor cells (EPCs) have been the most highly investigated cell type in the last decade. They have shown increased proliferation and differentiation in ischemic tissue with the potential to home to the damaged site [25, 26]. These cells express CD-34 and share other hematopoieitic stem cell protein moieties. In preclinical studies they have been shown to increase capillary density in hind limb ischemia. As of 2008 there have been over 25 reports of studies using EPCs in PAD clinical trials [27]. These have shown the best clinical phase 2 outcomes in terms of lowering amputation rate compared to placebo, though not significantly ($p=0.134$) [28].

Mesenchymal stromal cells (MSCs) are the most investigated pre-clinical cell type with the least amount of human clinical data thus far [29]. Most of the current and ongoing clinical trials for PAD or criticial limb ischemia are utilizing MSC delivery. Currently, 13 clinical trials inject MSCs either intramuscularly or intervenously for improving intermittent claudication symptoms and attenuating the innate immune response [29]. They can be used from an autologous cell source which is beneficial as it avoids potential immune rejection. These cells posses the capability to differentiate into multiple lineages such as bone, blood, and muscle. The hope for most of these studies is that they provide a stem-like, angiogenic potential upon delivery to the ischemic region. Once integrated into the host tissue, they will differentiate into the physiologically required cell type. MSCs appear promising as a therapeutic, however as mentioned there is little clinical data as to whether this cell type presents better outcomes compared to placebo groups.

A number of other clinical trials use multiple cell delivery as a mode of treatment [29]. In 2011, a phase 2 clinical trial completed involved the injection

of lymphoid cells and myeloid cells in tandem [30]. There were some significant results: the time of first occurrence to treatment failure was much greater in this cell group compared to the control [30]. This was a last measure readout indicating that it did not aid in improvement of the disease but rather prolonged the inevitable outcome of amputation. In general there was little difference in efficacy endpoints to treating the disease.

Skeletal myoblasts have been studied extensively as a therapeutic in many cardiovascular animal disease models, particularly in cell delivery into myocardial infarct and hindlimb ischemia models. In 2000, these cells were first realized to be potentially valuable for cell therapy in the infarcted heart [31]. These cells possess the capability of secreting important paracrine factors that are responsible for angiogenesis and increasing viability of other necessary cells. Harnessing this intrinsic ability and utilizing these cells as an in vivo therapeutic has obvious advantages. First, these cells are easily expandable, and culture well *in vitro*. Consequently, mass scale up is not a limiting factor unlike many other cell types. These cells also can be used as an autologous cell delivery option, which minimizes or eliminates any negative host response. They also have a "myogenic-restricted" lineage capacity. In other words they are unable to differentiate into any other (unwanted) cell type and thus avoids tumorogenecity [31]. Lastly, they integrate well into ischemic tissue to reform damaged muscle tissue by fusing with existing or regenerating myotubes.

Currently there are approximately 15-20 clinical trials that are in progress or have completed that utilize myoblasts as a cell delivery therapeutic for ischemia or muscle incontinence [32]. These clinical trials are not always successful, or if they are, they show marginal improvement [33, 34, 35, 20, 36, 37]. This is due to the inability for myoblasts to be delivered locally, stay at the site of injection, remain viable in ischemic environments, and engraft into the local tissue. Groups have shown that up to 90% myoblast cells will die over the first two days of implantation in both the heart and skeletal muscle [31]. Injecting larger numbers of cells as a compensatory mechanism can actually have a negative effect as a result of increased shear death through the syringe, over packing into the muscle

tissue and potential overgrowth. Groups have hypothesized that physical strain of the needle, inflammatory response, ischemia, and loss of the native extracellular matrix could all be contributing factors to the increased cell death [31]. Thus, there could be an improvement in the cell delivery vehicle by use of a gel/scaffold or addition of another cell type providing anti-apoptotic cues. For example groups have shown improvement in myoblast retention when co-injecting them with bone marrow stem cells [31].

Because retention and viability is a major hurdle for these cell types, investigators are looking elsewhere for strategies to repair muscle. For instance, many groups are studying the upstream muscle stem cells that have shown to be more plastic, can handle hypoxic environments, and engraft far better than myoblasts [38]. However, these cells are extremely difficult to isolate, culture, and expand to cell numbers that are therapeutically suitable for in vivo delivery [32].

1.5 Co-culture as an *in vitro* system to improve cell therapies

1.5.1 Evolution of co-culture

In order to improve current cell therapies for PAD, a larger knowledge base and further biological investigation at a cellular and molecular scale may be required to best utilize the cell type of interest. In recent years, tissue engineers have acknowledged the necessity to better model physiological environments *in vitro* by including multiple cell types, ECM proteins, substrate elastic moduli, and paracrine signals to a particular cell type of interest. Co-culture, a tool that has been used since the early 1980's, is a powerful method for understanding cellular interactions with their surrounding cell environment [39]. It has been continually gaining traction in the field as incredibly important in understanding many physiological processes.

Co-culture involves the study of two or more cell types and specifically the investigation of one cell type of interest, or the "target cell." The other cells, or

"assisting cells," are included in order to either mimic the native physiology of the *in vivo* environment by studying cell-cell interactions via gap junctions, adhesion molecules, signaling molecules and migration, or to guide the target cells toward a specific cellular behavior [39]. These behaviors can include but are not limited to proliferation, increased matrix production, migration, maintenance of "stemness," mechanical maturation, differentiation, electrical propagation, or metabolic changes. Co-cultures have been used to study natural interactions between multiple populations such as infection studies, creating biomimetic environments in vitro, tissue level drug effects, and improving overall culture success of the target cell with the help of the assisting cell [40].

Co-culture has previously been an unorganized mixture of multiple cell populations in direct contact with one another. This direct co-culture has evolved to include technologies that better parse out the signaling and readouts such that the user has a clearer understanding of why certain behaviors are observed. Indirect co-culture, such as conditioned media assays and transwell assays allow the user to observe changes in cell behavior due to only another cell type's autocrine and paracrine signaling respectively. These cultures do not allow cells to interact in contact. In other words, cell behavioral changes in these contexts cannot be attributed to cell adhesion between the cell types or linkage through the ECM.

In addition, there are a number of other technologies groups have developed to create organized co-cultures. Fluid channel connection between compartments, compartments separated by membranes, cells in droplets, colonies of cells in petri dishes, gaseous substance exchange, cells encased in gels, and cell layers on glass slides have all ben used and tested for various cell-cell interaction applications [40]. With so many various technologies that allows the user to explore cell behavior it is important to choose the technology that will allow a simple answer to a biological problem.

Variables that are involved in implementing a co-culture device depend on the degree of contact between populations and how the boundaries between the two populations exchange information [40]. For example, substance exchange between populations is an important influence on cell fate. As a result, diffusion rates

of the substance must be considered as this rate will vary through a membrane and as a function of cell population distance [41]. Changing separation distance between two distinct populations has also shown a vast behavioral change in cell phenotype [42]. Likewise, when controlling studies for cell-cell contact the type of micropattern or microfluidic device used will also play a role in the overall cell behavior(s) in culture [43, 44]. Most of these devices require finely tuning parameters such as flow rate, cell density, and cell passage number which makes the assay extremely sensitive and can greatly influence measured cell behaviors.

In recent years it has become of utmost importance to best mimic the in vivo environment by understanding cell-cell and cell-matrix interactions in 3D. 3D culture poses very difficult challenge for developing co-culture technologies that allow analysis of one cell type in a multiple-cell population in organized fashion. Currently, there are products that allow the user to seed cells in manfucatured scaffolds (Alvetex®, 3DKube™, etc) that are highly porous and claim to re-create organotypic tissues. Unfortunately, the scaffold porosity, stiffness, thickness, and biochemical ECM makeup greatly affects this behavior. Consequently, for a given application it is important for the user to finely tune the scaffold-cell microenvironment to allow for these cues and *in vivo* like characteristics. Even though no 3D device or co-culture scaffold is perfect, understanding cell-cell interactions on a three dimensional co-culture model has shown promise in the field by recapitulating the in vivo microenvironment [45].

Major advances in tissue engineering have been attributed to studying cells in co-culture. In the heart, cardiac fibroblasts have been shown to significantly drive embryoid bodies into beating cardiomyocyte-like 3D structures with indirect co-culture [46]. Cardiac progenitor cells, a cell type only recently discovered and investigated, has been shown to express more mature cardiac activity when co-cultured with cardiomyocytes [47]. Cardiac fibroblasts have also been shown to be integral in mature electrical propagation in beating cardiomyocytes *in vitro* and when injected in vivo [48].

Thus far there is less literature in the field on skeletal muscle cell engineering and the implications of adding multiple cell types to repair functional muscle.

Like cardiac muscle, skeletal muscle is highly organized, contains many ECM components and has limited regenerative capacity in vivo. There is thus a great deal of rationale in co-culturing other cell types to either push regeneration via endogeneous cells, engineer muscle ex vivo for implantation, or investigate other cell types for such repair.

1.5.2 Limitations of co-culture systems

As previously mentioned co-culture has gained the attention and respect of many scientists for understanding complex cell interactions. As a result, there has been a need to continually improve on the pre-existing technologies to make better, more useful tools [49]. The need for advanced tools is partially due to the limitations of co-culture in analyzing and studying cellular behavior. As mentioned, in direct co-culture cell-cell interactions can be observed for both contact and paracrine signaling. However, an observer is unable to parse out whether contact or paracrine are more important, analyze only one cell type of interest (without doing some sort of cell sorting), or understand mechanistic causation (i.e. is there a synergism, antagonism, no effect, etc) [50]. Autocrine signaling via conditioned media yields even less information regarding how cells interact since this culturing method does not allow heterotypic cell signaling [51]. Transwell, perhaps one of the most organized indirect co-culture methods, still does not allow for visualization of contact-dependent interactions and has a fixed large 1.35 mm distance between the cell types which may be potentially too far for certain paracrine signals to traverse in culture.

Lastly, there are a host of microfluidic devices and patterned co-culture devices being created [49]. However, these usually can only be utilized with small cell numbers and does not represent a population-scale cell behavior. Additionally, sample prep can be incredibly difficult and tedious for the user [52]. These still do not always accurately mimic the native microenvironment in the body. There is thus a pressing need in the field to improve on these technologies to accurately predict biological behavior *in vitro*. As mentioned in the previous section, the number of variables required to best model an in vivo environment is extensive,

but by providing the majority of these cues one can better model cell-cell behavior in vitro

1.6 Scope of dissertation

Myoblast differentiation for skeletal muscle repair is still not well understood. The intrinsic ability for these cells to repair muscle *in vivo* upon injury is a physiological work of art. Since this regeneration is limited, it is of interest in this thesis to understand the following. First, using a novel, improved co-culture technology we show how these cells act as target cells in response to skeletal fibroblasts. Then we advance this technology and demonstrate, as a proof-of-concept, how myoblasts along with a specific substrate stiffness can push myogenic differentiation of adult stem cells. Lastly, we translate of some of these findings into a markedly improved in vivo therapeutic for peripheral artery disease.

Chapter 1 gives an overview of skeletal muscle physiology, the current therapies in peripheral artery disease, and how myoblasts can aid in repair. It also expounds on the ways in which researchers can study cells in more physiologically relevant contexts or to achieve increased mature tissue formation by using co-culture.

Chapter 2 investigates the role of a mature fibroblast phenotype on a skeletal myoblast cell on a novel reconfigurable co-culture device. These experiments show an increase in alignment of myotube formation in direct contact with fibroblasts, but an overall inhibition of differentiation when fibroblasts are present at all.

Chapter 3 explains the method and results of advancing the co-culture technology to include a tunable stiffness such that the elastic modulus, contact/paracrine signaling, and protein attachment can be user-defined and well controlled. We show that adipose derived stem cells on a muscle-like stiffness and in co-culture with myoblasts pushes myogenic differentiation *in vitro*.

Chapter 4 uses rationale from results in Chapter 2 combined with a previously successful decellularized skeletal muscle matrix hydrogel to create a 3D co-culture system *in vitro*. This system increases viability and differentiation. Upon

implementation in vivo, this technology yields improved engraftment of myoblasts and perfusion in the hindlimbs of a murine peripheral artery disease model.

Chapter 5 summarizes the work and conclusions in this dissertation and addresses some potential limitations. It also provides suggestions for further avenues of investigation for improved skeletal muscle repair.

Chapter 2

Understanding the role of fibroblasts on myoblast differentiation by a novel co-culture technology

2.1 Introduction

As mentioned in Chapter 1, myoblasts fuse with one another upon skeletal muscle injury to create terminally differentiated myotubes, the building blocks of muscle fiber formation [11]. It is well established that most skeletal muscle has a large regenerative capacity due to satellite cell infiltration in response to injury [53]. However, in larger and more severe injuries, skeletal muscle may not regenerate completely, and fibrosis and scar tissue can cause decreased functionality of the tissue [54]. Additionally, in regions that are not associated with limbs, there is heterogeneity in the proliferation efficiency of these satellite cells due to injury response, and simultaneously there may be a lack of these cells to cause an appreciable difference in repair at the site of injury [55]. There is therefore a need to develop strategies for skeletal muscle repair. A number of other cell types may be potentially important in this repair and satellite cell differentiation process. In vivo, myogenic cells are also influenced by fibroblasts at the site of injury, particularly in establishing a stabilizing extracellular matrix [56]. These fibroblasts

sit in close proximity to muscle tissue and develop the basement membrane of this tissue. This relationship between fibroblasts and myocytes is well characterized in the heart. Cardiomyocytes undergo phenotypic and morphological changes when in the presence of cardiac fibroblasts *in vitro*, including increased contractility [57]. It has also been shown that merely the fibroblast paracrine signals are enough to attribute to these differences [57]. Other studies have shown that cardiomyocytes align, contract, and avoid apoptosis pathways when co-cultured with cardiac fibroblasts [58]. Extensive *in vitro* data has suggested that cardiac fibroblasts are necessary in repair, function, matrix synthesis/degradation, and important cytokine secretion [59, 60]. Moreover, producing functional cardiac tissue in vivo improves with the implantation of both fibroblast and cardiomyocyte cell types in organized cell sheets [61]. The requirement for these two cell types to be present and synergistically create a functional tissue could analogously have similar implications for skeletal muscle; however, the effect of fibroblasts on myoblast differentiation and alignment has not been well documented or studied. Interestingly, in diseased models such as arrhythmia and myocardial infarction, myofibroblasts actually have a negative effect on cardiac remodeling. They can undergo "fibrotic remodeling" which causes an overabundant secretion of ECM proteins that separates cardiomyocytes and inhibits electrical conduction [62]. These cells are unable to go through normal apoptosis in this state, and persist to create scar tissue [63, 64, 62]. From this data, there is a potential for skeletal fibroblasts to also have a negative effect on skeletal muscle formation in characteristic phenotypic states. Few groups have studied how fibroblasts influence skeletal myoblasts. The most extensive study to date involved plating C2C12 myoblasts on a fibroblast feeder layer, which resulted in myotubes that were highly adherent and contractile with functional electrical propagation as evidenced by calcium transients between cell types [65]. This study showed that fibroblasts play a beneficial role in maintaining mature myotube functionality. However, it did not examine how fibroblasts influence differentiation of myoblasts into mature myotubes. Another more recent study used a transwell assay to co-culture myoblasts and fibroblasts, and demonstrated that fibroblast paracrine factors protected myoblasts from apoptosis when

undergoing differentiation [66]. Understanding fibroblast influence on these muscle progenitor cells, as in the case with cardiac muscle cells, could have direct implications on cell therapies for repairing skeletal muscle, which have to date only utilized skeletal myoblasts or stem cell populations alone [67]. Those that have used myoblast or satellite cell therapies alone have shown some improvement, but demonstrate the need for more efficient delivery, inhibited apoptosis, and increased therapeutic response [68, 69, 70, 71, 67]. In this study, we investigated the role of fibroblasts on skeletal muscle progenitor differentiation and alignment using a microfabricated, reconfigurable co-culture device [50]. This setup allows for both contact and paracrine signals to be monitored independently and in tandem. It also provides the user with the ability to separate two cell populations and dynamically study and manipulate the co-culture configuration [50]. Furthermore, this technology can: 1) determine whether a cell type has an influence on another's differentiation, proliferation, etc., 2) conclude whether a paracrine signal or a contact dependency is needed, and 3) isolate only the cell type of interest for analysis. These advantages allow one to better understand the mechanisms of cross talk between two cell types of interest. Herein, we analyzed C2C12 murine myoblasts co-cultured with 3T3 murine fibroblasts on the reconfigurable co-culture device. We demonstrate that fibroblasts inhibited myoblast differentiation independent of contact, while cell-cell contact between the two cell types yielded more organized alignment of myotubes upon differentiation. Secretion of basic fibroblasts growth factor (FGF-2) is an important player in both regulating differentiation and, in conjunction with contact signals, improving myotube alignment. Lastly, these two cell types are required to be in the presence of one another to elicit such responses. It has been shown with multiple cell types, most commonly with tumor or cancer cell communication, that protein signaling is only turned on when two or more cells "cross-talk" with one another [51]. In this study we show that fibroblasts and myoblasts must be in close proximity with one another (as opposed to using conditioned media of one on the other) to show these differences.

2.2 Methods

2.2.1 Cell culture

Murine C2C12 myoblasts and 3T3 fibroblast cells (ATCC, Manassas, VA) were each cultured in growth media (GM) consisting of high glucose Dulbecco's Modified Eagle Medium (Gibco, Grand Island, NY) containing 10% fetal bovine serum (Hyclone), 100 units/mL penicillin, and 100 ţg/mL streptomycin (Gibco, Grand Island, NY). 3T3 and C2C12 cells were cultured at 37°C and 5% CO2 and split at 1:10 when 80% confluence was reached; media was changed every two days. For myoblast culture, tissue culture flasks were coated with 1 mg/mL collagen in 0.1 M acetic acid for 1 hour at 37°C and rinsed with 1X Dulbecco's Phosphate Buffer Saline (PBS) prior to seeding. Fibroblasts were cultured on uncoated tissue culture flasks.

2.2.2 Reconfigurable co-culture device

The silicon reconfigurable co-culture devices were fabricated according to previously established protocols [50]. Each half of the device, called "combs" were individually coated with 1 mg/mL collagen prior to seeding for 1 hour. The collagen was removed and the combs were rinsed with sterile PBS. For each comb pair, myoblasts were seeded on the male half; the female half was seeded with either fibroblasts or myoblasts. Each collagen coated comb half was placed in a 12-well plate. Approximately 1,000,000 C2C12 and 750,000 3T3 cells were added to each half to create complete confluence upon seeding. The plate was then placed in the incubator at 37°C. In order to achieve a complete monolayer on the devices, the plate was lightly shaken for 5 seconds by hand after 30 minutes and 1 hour after seeding. After six hours, the combs were each individually rinsed with 1X PBS and the parts were fit together with sterile tweezers (SPI, West Chester, PA). The combs were connected in the proper configuration and maintained in a new 12-well plate containing 2 mL of cell culture media. The combs were visualized via an upright microscope to ensure that the fingers fit properly (in either gap or contact) and no cellular debris was floating in the media. Media was changed every two

days. The following groups were examined: myoblasts cultured with myoblasts in gap, myoblasts cultured with myoblasts in contact, myoblasts cultured with fibroblasts in gap, and myoblasts cultured with fibroblasts in contact (4 groups). Each group contained two sets of comb pairs and every finger of the male combs (9 fingers per comb), containing the cells of interest, was individually analyzed (n = 18 per group). After six days the four groups were stained, mounted and analyzed by immunofluorescence as described below. For the FGF-2 neutralization experiments, 2 comb pairs (n=18) per group were cultured with anti-FGF-2 neutralizing antibody (Millipore, Temecula, CA) at 10 μg/uL for six days. This was well mixed in pre-warmed media and replenished every 2 days. 2 mL of this media was added to each comb in the same manner as stated previously.

2.2.3 Conditioned media assays

3T3 fibroblasts were cultured independently of C2C12 myoblasts prior to the experiment. Once the fibroblasts had reached confluence, myoblasts were seeded at 500,000 cells/well in eight wells of a collagen coated (1 mg/mL) 48-well plate. The wells were filled with a total volume of 1mL of GM. Once the myoblasts were confluent, media was removed from these wells and 500 μL of new GM was added with 500 μL of media from cultured fibroblasts. In the other four wells, this 50:50 ratio was composed of new GM and myoblast cultured media. 500 ţL of media was removed from these wells and 500 μL of fresh GM was added. These media changes were carried out from day 1 and continued every subsequent day until day 6. On day 6, the media was removed and cells were rinsed with PBS. They were fixed with 4% paraformaldehyde, stained, and imaged as described below. Three 200X images were taken for each well (n=12).

2.2.4 Transwell assays

Eight wells of a 24-well transwell plate (Corning, Union City, CA) were coated with 1 mg/mL collagen. Four of the wells contained 3T3 fibroblasts on a membrane over C2C12 myoblasts. The other four were myoblasts co-cultured

over myoblasts. All wells were seeded with 500,000 C2C12s and the membrane was seeded with either 100,000 myoblasts or fibroblasts. The cells on membranes were cultured separately until adherent, at which point they were placed on top of the myoblast wells. A total of 700 μL of GM covered each transwell. This media was changed every two days and on day 6, the membranes were removed and wells were fixed and stained according to the immunofluorescence procedures outlined below. Three 200X images were taken per well for analysis (n=12).

2.2.5 Immunofluorescence quantification

After 6 days, cells were fixed with 4% paraformaldehyde (Wako Chemicals, Richmond, VA) for ten minutes at room temperature. Once fixed, the cells were rinsed with PBS to remove any excess paraformaldehyde. The fixed cells were permeabilized, and blocked in "blocking buffer," containing .03% Triton-X 100 and 1% Bovine Serum Albumin in 1X PBS. Primary antibody, mouse anti-mouse myosin heavy chain (skeletal, fast, 1:200, SIGMA, St. Louis, MO), was incubated in the blocking buffer for 1 hour at room temperature. Secondary antibodies (Alex Fluor 588, 1:200, Invitrogen, Carlsbad, CA) were incubated for 30 minutes at room temperature in blocking buffer. Cells were stained with Phalloidin 468 (1:200, Millipore, Temecula, CA) in buffer for 30 additional minutes. Hoescht 33342 (0.1μg/ml in DI water, Invitrogen, Carlsbad, CA) staining was used to visualize the nuclei. Once stained, the combs were taken out of wells and mounted on slides with Fluoromount-G (Southern Biosciences, Birmingham, AL). A Zeiss Observer.D1 fluorescent Axio Observer scope was used for image acquisition, and Axiovision software was employed for image analysis. 100X images were taken at the free end of the finger of each male comb. Three 200X images were analyzed from each well of the conditioned media and transwell assays. Percent differentiation was calculated by manually counting the total number of nuclei within myotubes and dividing by total nuclei within the image. The total number of nuclei was quantified automatically via AxioVision software. Each myotube was identified and the angle deviation relative to the parallel of the comb finger was measured by AxioVision angle measurement tool.

2.3 Results

To study the effect of the presence of fibroblasts on myoblast differentiation and subsequent alignment, we employed a previously described microfabricated co-culture device [72]. This device has interlocking "combs" that can be positioned either to allow direct cell-cell contact or to separate the cell populations by a gap of 80 μm (Fig. 2.1). In this study, the male end contained the analyzed cell type (myoblasts only) and the female end contained either fibroblasts or myoblasts.

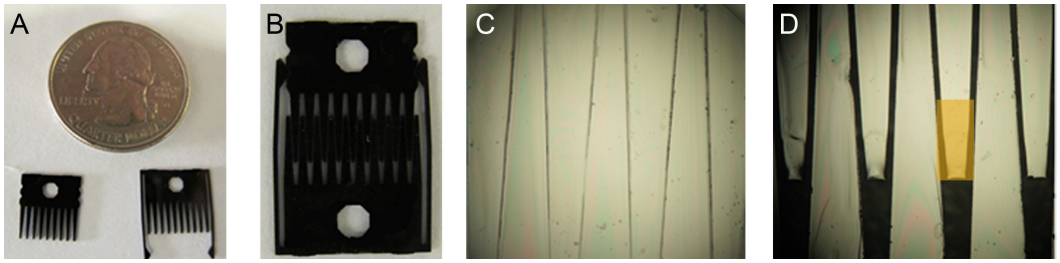

Figure 2.1: **Visual representation of the reconfigurable co-culture device.** **(a)** Both male and female pairs of "combs." The holes in the comb allow the user to move and manipulate the device with the use of forceps. **(b)** Photo of a comb pair in gap mode. **(c, d)** 40X brightfield images in both contact and gap mode respectively. Orange box represents area of interest for analysis in which we refer to as the "finger" of the comb. An 80 micron gap separates the fingers in gap mode. Cells are unable to traverse this gap, only secreted factors.

Each finger of every configuration (myoblasts co-cultured with myoblasts or myoblasts co-cultured with fibroblasts, in gap or contact) was imaged by the methods described above. Figure 2.2 demonstrates examples of comb images with staining for F-actin, myosin heavy chain, and nuclei, as shown in green, red, and blue respectively. Each of the four images represented are one of 18 fingers analyzed for each of the four groups. The 80 μm gap was clearly visible in these cultures and showed no positive staining. Myosin heavy chain, a marker for myotube formation, was used to determine percent differentiation of myoblasts. Fibroblast comb halves did not stain positive for myosin heavy chain as expected. This demonstrates that no cross-contamination had occurred in either gap or contact configurations. Percent differentiation, as reflected by myosin heavy chain positive cells and highly aligned myotubes are two phenotypic characteristics reflective of a mature muscle phenotype. To assess the effects of fibroblasts on myoblast maturation, we quantified both the percent differentiation and degree of alignment of myoblasts in myoblast-myoblast and myoblast-fibroblast co-cultures, when in contact and in gap.

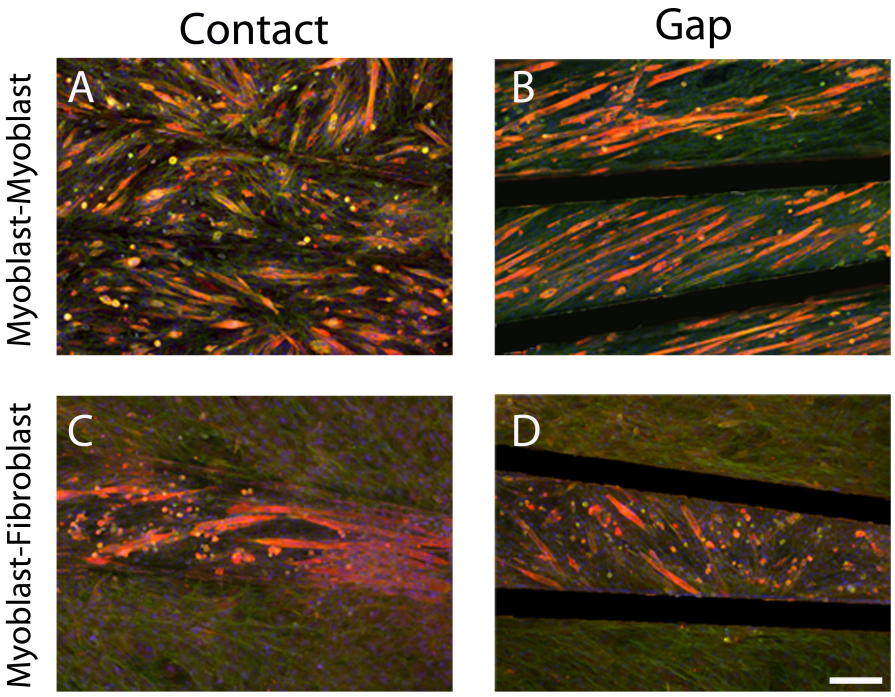

Figure 2.2: **Immunofluorescent images of a given myoblast finger in all culture configurations after 6 days in culture.** Nuclei, f-actin, and myosin heavy chain are stained in blue, green, and red respectively (scale bar = 200 μm.) **(a)** Myoblasts co-cultured with myoblasts in contact configuration. **(b)** Myoblasts co-cultured with myoblasts in gap mode. **(c, d)** Fibroblasts co-cultured with myoblasts in contact and gap mode respectively. Note: No myosin heavy chain staining is found on fibroblast fingers.

2.3.1 Myotube alignment is increased only when in contact with fibroblasts and percent differentiation is decreased in the presence of fibroblasts

Myotube alignment, as well as percent differentiation, is a desirable phenotype for myoblast differentiation into mature myotubes. More highly aligned myotubes recapitulates the more favorable mature muscle phenotype *in vitro*. We quantified the alignment of the myotubes on the fingers of each of the male combs (n=18). The alignment was calculated by averaging all of the angles between each myotube and that of the parallel of the finger of the comb. After six days in culture, the co-cultures containing fibroblasts in contact with myoblasts showed an increase in alignment with the finger parallel by approximately 10 degrees (Figure 2.3a), which is more evident when representing the data in a histogram format (Figure 2.3b).

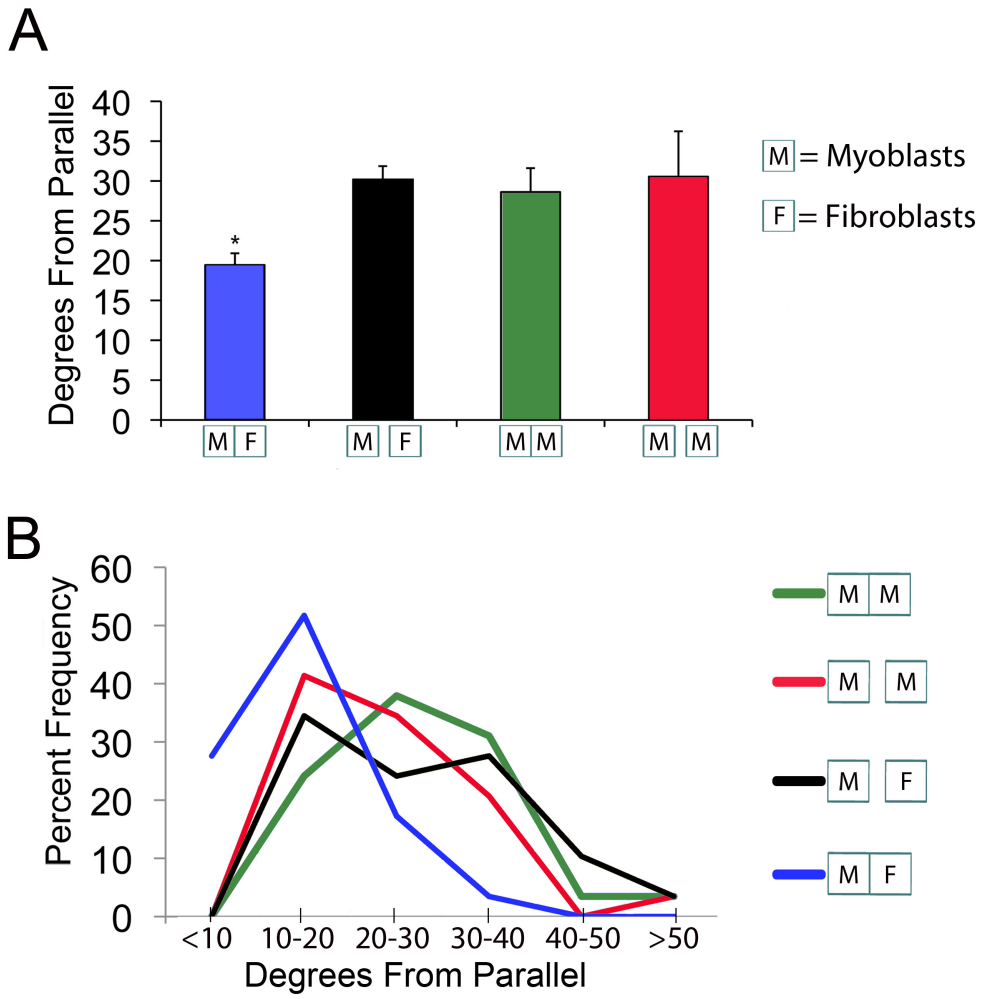

Figure 2.3: **Quantification of myotube alignment in the reconfigurable co-culture device after 6 days in culture.** "M" represents myoblasts; "F" represents fibroblasts in each figure. Contact mode is represented by adjacent boxes touching one another and gap is represented by a space between boxes. **(a)** Graphical representation of degrees from parallel versus culture type. Lower values indicate more aligned myotubes. The average degree from parallel of the finger of the comb in the myoblast- fibroblast contact co-culture was significantly less (*$p < 0.05$) compared to all other groups, indicating that the myoblasts were more aligned. **(b)** Histogram representation of myotube alignment. The data for degrees from parallel is grouped into 6 bins. Lower bin numbers represent more aligned myotubes with the comb finger. Graph shows a skewed distribution of myoblasts and fibroblasts in contact toward lower degree numbers.

Myoblast-fibroblast cultures in contact show a skewed distribution towards lower degree angles, suggesting that a larger number of myotubes are more highly aligned to the parallel in this culture type. All other co-culture settings showed no significant difference in alignment between each other. We show that regardless of configuration, contact or gap, fibroblasts caused a significant inhibition of myoblast differentiation (Figure 2.4). Since percent differentiation between gap and contact in myoblast-fibroblast co-cultures showed no differences, this further suggested that the inhibition of differentiation seen in fibroblast cultures is due to a paracrine signal and not a contact dependent signal. In myoblast-myoblast co-cultures, a higher percentage of nuclei were contained within myotubes than in co-cultures with fibroblasts. There were up to 50% more nuclei that co-stained positive with myosin heavy chain for these myoblast only cultures. No significant differences were observed between myoblasts in either contact or gap. This finding suggested that fibroblasts inhibited this myotube formation in culture on the male half of the comb. Unlike these differentiation studies, myotube alignment was only increased in contact with fibroblast cultures, suggesting contact dependent (alignment) and contact independent (differentiation) pathways underlying the effects of fibroblasts on myoblast differentiation.

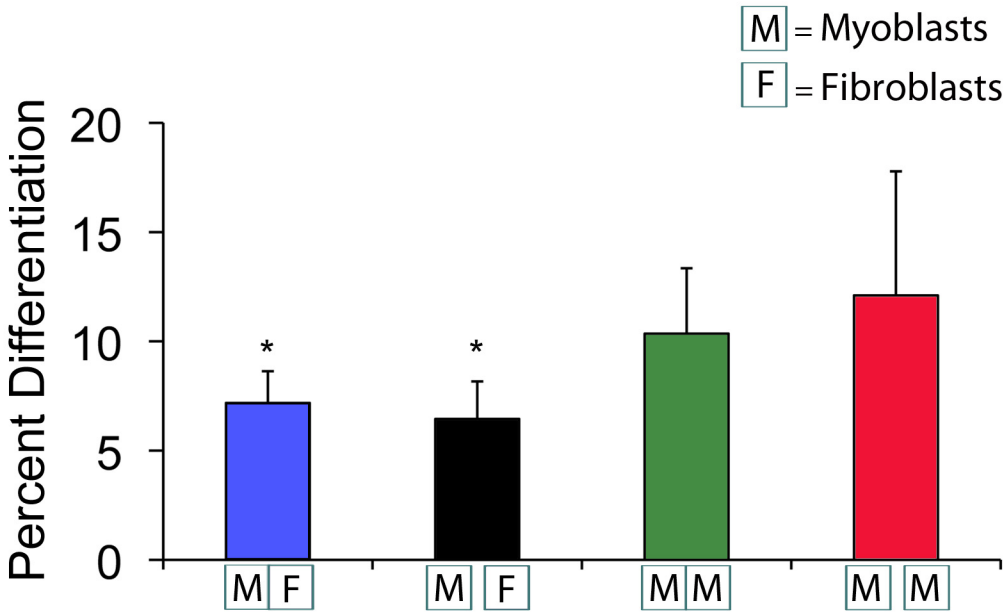

Figure 2.4: **Quantification of percent differentiation in the reconfigurable co-culture device.** Co-culture with fibroblasts reduced the percent differentiation on the myoblast comb compared to myoblast only cultures regardless of configuration after 6 days (*p $<$0.01), suggesting a paracrine factor is responsible.

2.3.2 Myotube differentiation is reduced and alignment is increased in fibroblast co-culture through an FGF-2-dependent mechanism

It is well documented that FGF-2 has a major influence on increasing skeletal muscle cell proliferation and prevents their terminal differentiation [73, 74, 75]. To determine whether FGF-2 could influence differentiation of myoblasts in contact with fibroblasts, we sought to assess percent myoblast differentiation in these co-cultures containing media, which includes or excludes neutralizing antibodies to FGF-2. Neutralizing antibodies to FGF-2 have been shown to bind and neutralize the effects of soluble FGF-2 to its receptors, and thus eliminate its functionality [76]. Unlike our previous observations, we show that fibroblasts do not significantly influence myoblast differentiation and alignment in myoblast-fibroblast co-cultures in the presence of FGF-2-neutralizing antibodies, when compared to other co-culture conditions (Figure 2.5). Interestingly, our results reveal that the percent of differentiated myoblasts in myoblast-fibroblast co-cultures increased to the level endogenously observed in myoblast-myoblast cultures. However, myotube alignment in these studies remained similar to what was previously observed in all other cell culture types.

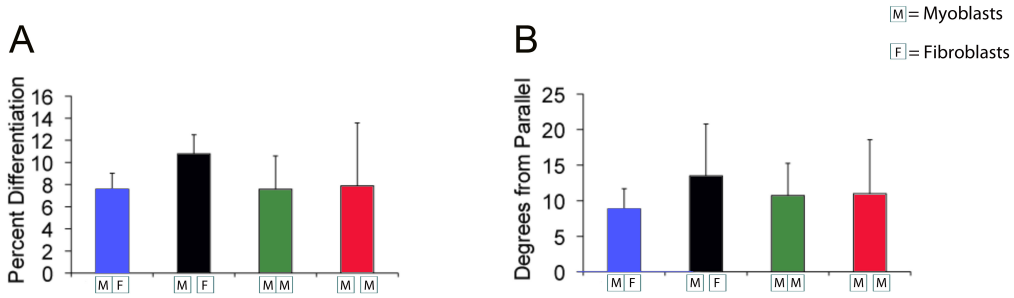

Figure 2.5: **FGF-2 blocking by anti-FGF-2 neutralizing antibody.** No significance is found between any groups for **(a)** percent differentiation or **(b)** quantification of alignment of myoblasts after 6 days in co-culture with an FGF-2 neutralizing antibody added into the media. Percent differentiation of both myoblast-fibroblast contact and gap cultures and alignment in the fibroblast-myoblast contact culture increased as a result of adding the neutralizing FGF-2 antibody.

2.3.3 Bi-direction signaling is critical in myoblast-fibroblast interactions

In this study we show that FGF-2 plays a major influential role in myoblast differentiation and alignment in myoblast-fibroblast co-cultures. We wanted to further explore whether fibroblast-secreted factors, independent of a myoblast signal, resulted in the same effect. We tested this scenario by growing myoblasts in media transferred from fibroblast cultures. By utilizing this conditioned media, we were able to determine whether fibroblast secreted factors were enough to maintain the phenotypic changes seen when the cells were in direct co-culture. We reproducibly show that there are no statistical differences in percent myoblast differentiation when myoblasts are cultured with fibroblast-conditioned media (Fig. 2.6). Percent differentiation in both groups lied between 13-15% after six days. Conditioned media experiments, therefore, did not produce the same result as the gap configuration from our previous co-culture experiments. One possible explanation of this phenomenon could be due to the secreted factors having only a short-range paracrine effect, which has previously been observed in gap co-culture [50]. To test the hypothesis whether paracrine factors were responsible in eliciting differentiation changes between co-culture types, we mimicked gap conditions of the comb by utilizing a transwell assay where fibroblasts were separated from myoblasts by a transwell membrane. The major differences between these assays and the gap conformation is 1) a larger distance separates the two cell types (1.35 mm rather than 80 μm), and 2) spatially the transwell has cells on top of one another (z-direction) rather than adjacent to one another on the same plane. The transwell assays recapitulated our findings from the reconfigurable co-culture device. We show that myoblast differentiation was inhibited by up to 10% in the presence of fibroblasts that were separated from myoblast-myoblast wells (Fig. 2.7). The difference in inhibition between culture types could be readily visualized by comparing the number of myotubes in 100X images of each culture type. The behaviors of Transwell and gap co-cultures were similar, which is not consistent with short-range paracrine signaling [76]. Instead, the data support a critical role for bi-directional signaling, or cross talk. Constitutively expressed fibroblast

paracrine factors captured in conditioned media do not produce the same behavior that occurs when feedback signaling between the two cell types is made possible. As mentioned previously many cells only secrete factors in the presence of another cell signal [77, 51]. For example, drug therapies for cancer are targeted to block the cross-talk between cancer cells and stromal cells to reverse detrimental effects [78]. These data strongly suggest that there is a need for the two cell types to be in close proximity to communicate with one another and allow for signaling between them to cause these phenotypic changes seen by the comb and transwell assays.

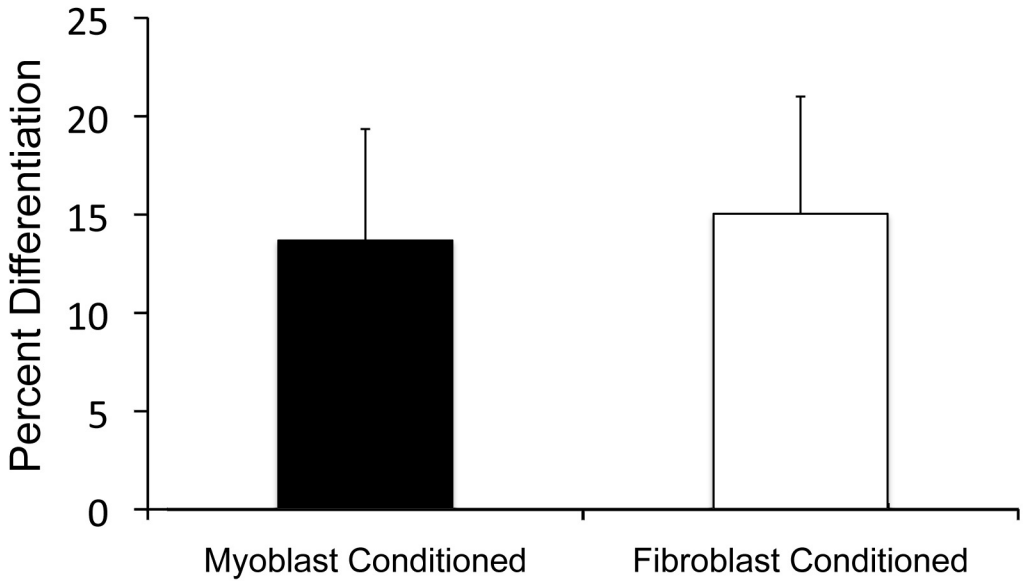

Figure 2.6: **Quantification of percent differentiation of conditioned media experiments.** Conditioned media from either fibroblast only cultures or myoblast only cultures was added to additional myoblasts cultures for 6 days. No significant difference in terms of differentiation was observed between cultures with fibroblast conditioned and myoblast conditioned media when staining with myosin heavy chain after 6 days.

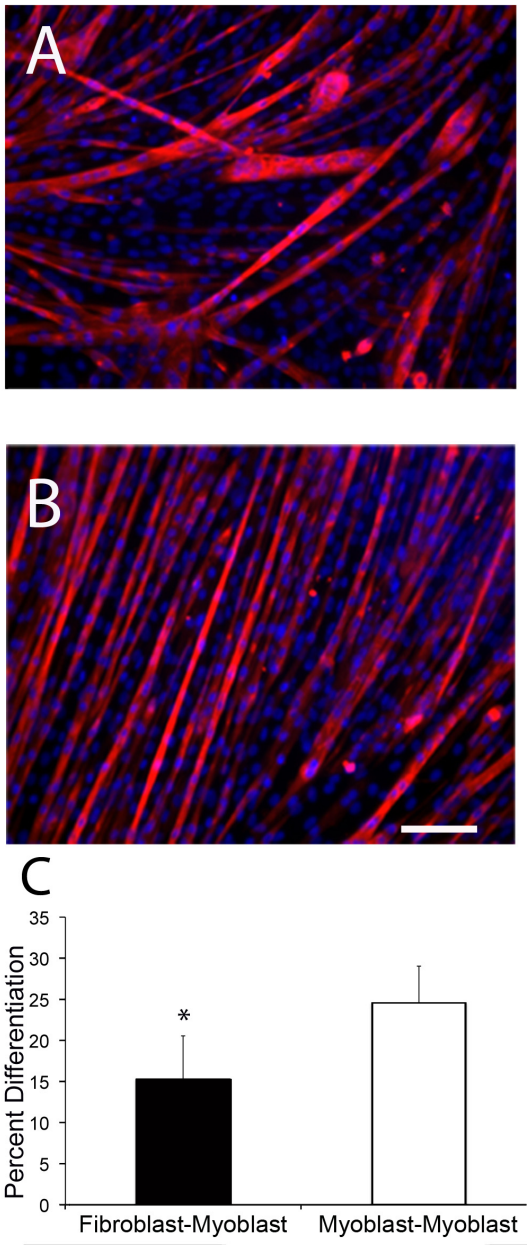

Figure 2.7: **Confirmation of inhibition of differentiation by use of a transwell assay.** **(a)** Immunofluorescence image of myoblasts when co- cultured with fibroblasts using a transwell setup. **(b)** Immunofluorescence image of myoblasts when co-cultured with myoblasts. The decrease in density of myotubes stained with myosin heavy chain in **(a)** shows the decrease in percent differentiation **(c)** Graphical representation of difference in percent differentiation between both groups after 6 days. Percent differentiation of the fibroblast co-culture is significantly decreased compared to myoblast (*p $<$0.01, scale bar = 100 μm)

2.4 Discussion

From the results of this study, we have reproducibly shown that myoblasts differentiate into myotubes at a slower rate when fibroblasts are present in culture. Whether the fibroblasts were in contact or in gap mode in the microfabricated co-culture devices, myoblast differentiation into myotubes was inhibited. This suggests that a paracrine signal from the fibroblasts caused these phenotypic changes. These cell types are needed to be in close proximity, in co-culture, to cause such changes. Fibroblast-secreted factors alone are not enough to show any significant changes in myoblast differentiation compared to standard myoblast culture. With the reconfigurable co-culture device we were also able to show that there were changes in myotube alignment when the cultures are in physical contact with one another. Myotubes aligned parallel to the comb finger direction when fibroblasts flanked the cells in contact. This implies that cell-cell signaling via junctional (gap, connexin, or cadherin) proteins between fibroblasts and myoblasts may be necessary in order to drive myotube directionality. We have also shown that without the reconfigurable co-culture device, these findings would not be easily observed. By modulating between gap and contact modes we are able to witness phenotypic changes. In addition, the desired readouts are more manageable on the fingers of these combs because of the spatial patterning. The ability to distinguish one cell type from another by direction and placement on each comb half was an advantage in immunofluorescence quantification. Every comb half also contains a great deal of information due to the individual "microenvironments" that every finger occupies, providing a larger sample size. Previous literature and standard primary myoblast cell-culture, has shown that FGF-2 is needed for *in vitro* control over myoblast cell cycle, proliferation, and differentiation [79, 80, 81, 74]. FGF-2 has also been used to engineer muscle cells *in vitro* to promote increased proliferation and regeneration in skeletal muscle [75]. By adding FGF-2, cells are stalled from differentiating in culture [79]. By inactivating this factor with large concentrations of neutralizing antibody as done previously by several groups [82, 83, 84], we observed an offset of this inhibition. Myoblasts were able to differentiate more readily even when fibroblasts were in culture with the anti-FGF-2 antibody present. We

show that FGF-2 is ultimately responsible for both the inhibition of differentiation and a player in myotube alignment. The FGF-2 pathway is well characterized and extensively studied in the context of myogenesis. FGF-2 activates RhoA thus blocking muscle differentiation [85]. When RhoA is inhibited, RhoE levels increase and muscle terminally differentiates. RhoE also increases myotube alignment by an m-cadherin dependent pathway [86]. Thus far, there was no evidence that solely fibroblast cells cause alignment of myoblast fusion when organized in contact with myoblasts. However, it has been demonstrated that myoblast alignment is dependent on a number of factors, including substrate geometries as shown by micropatterning [87]. Specific growth factors (some of which are secreted by fibroblasts) have been shown to play a regulatory role in both myogenesis and alignment [88, 89, 90, 75]. As mentioned, none of these studies attribute fibroblasts as causing such changes, only growth factors that can be secreted by a host of cell types and may be abundantly found in the extracellular matrix. The necessary cell contact of fibroblasts to myoblasts to show such changes in alignment is potentially due to the cell-cell contact signals that are created between cell types in addition to the FGF-2 secreted signal. The inhibition due to FGF-2 is only noticed when myoblasts are in communication with fibroblasts, as seen from the results of conditioned media and transwell assays. We hypothesize that this could be due to "bilateral signaling," meaning that the myoblasts are eliciting a signal(s) that in turn causes fibroblasts to signal back causing this change in differentiation. Alternatively, multiple paracrine signals could be responsible for this change but require FGF-2 to be present. This has potential implications for skeletal muscle engineering. First, it supports the case that cellular therapy may be a necessary option in order to elicit alignment and differentiation responses. It may require a number of cells in particular ratios to cause the highest percent differentiation and alignment to form a functional tissue. As shown with cardiomyocytes, cardiac fibroblasts are required for functional electrical conduction through the heart [91]. Likewise, adding fibroblasts or even other cell types found in vivo may be necessary in regulating skeletal muscle repair or regeneration. FGF-2 has been shown to increase proliferation in myoblasts that over express the growth factor in

muscle regeneration and reduces apoptosis [75]. Consequently, our results suggest that adding fibroblasts in tandem could elicit a similar effect; however, a balance between proliferation and differentiation will likely be necessary for proper regeneration. We demonstrate that the reconfigurable co-culture device is a useful tool in understanding changes in cell phenotype as a result of another cell type. We show that myotube formation is regulated and inhibited by FGF-2 secretion by fibroblast cells. Alignment of these myotubes is governed by a contact dependent mechanism between these two cell types. However, if FGF-2 is neutralized, improvement in alignment via contact signaling is eliminated. Lastly, these two cells must be in proximity with one another, implying that there is a more than one signal between the two causing such changes. These findings are important in understanding how these cells interact together and could provide potential avenues for skeletal muscle repair in vivo.

Chapter 2 in part is a reprint of the material *Rao N, Evans S, Stewart D, Spencer K, Sheikh F, Hui, E E, Christman K L. Fibroblasts influence muscle progenitor differentiation and alignment in contact independent and dependent manners in organized co-culture devices. Biomedical Microdevices, 2013; 15:161-9.* The dissertation author was the primary author.

Chapter 3

Development of a co-culture device with tunable stiffness to understand myoblast effects on adipose-derived stem cell myogenesis

3.1 Introduction

The microenvironment that surrounds cells in vivo consists of growth factors, interstitial fluid, and the extracellular matrix (ECM), a protein based scaffold that surrounds and supports cells. These components of the microenvironment provide cells with multiple types of signals that regulate intracellular signaling leading to a change in cell behavior or fate. These variables include but are not limited to paracrine/autocrine signals, cell-cell physical interactions, and ECM stiffness/composition. In the last decade, scientists have demonstrated that it is not accurate to mimic in vivo cell behavior using *in vitro* substrates which regulate just one of these variables. This is particularly true when attempting to mirror complex processes such as tumorigenesis, morphogenesis, stem cell differentiation and wound healing [92, 93, 94, 95, 96]. Embryonic, adult, and induced pluripotent stem cells have all been shown to differentiate based on substrate stiffness and

composition and/or cell-cell interactions *in vitro* [97, 98, 99, 100] which further emphasizes the importance of developing technologies that introduce diverse sets of variables for cell culture. In addition to more closely mimicking the microenvironment, these technologies must be easily fabricated, allow for simple readouts such as isolation of mRNA and protein, include the potential to image cell morphology and immunofluorescence (IF), and allow for facile co-culture of different cell types in a controlled manner.

As mentioned previously, co-culture is commonly performed when studying cell-cell interaction *in vitro*. Various co-culture technologies have been developed to monitor contact, paracrine, and autocrine effects. A number of devices use microfabrication, microfluidics, and flow chambers to study cell-cell interactions [101, 102, 103]. Others pattern cells in specific geometric configurations, use different ECM proteins, or utilize various substrate materials to regulate cell attachment and subsequent cell-cell interaction [92, 104, 105, 106, 107]. However, most of these approaches require single cell co-culture or low cell density in a complex, microfabricated device that is not always user-friendly [103]. Some of these devices cannot use specific proteins and require differential plating of different cell types to achieve a micropatterned co-culture [108]. Biochemical readouts can be difficult to produce because of minimal cell material from small cell numbers or involve complex interpretations from the presence of multiple cell populations that are not separable.

Shown in Chapter 2, the reconfigurable co-culture device has been shown to be a powerful tool to understand how cell interactions via direct contact or paracrine signaling causes changes in cell behavior [50, 109]. However, this device requires users to culture cells directly on the hard silicon dioxide comb surface (gigaPascal; gPa), which does not recapitulate the softer microenvironment seen in most tissues in vivo (kiloPascal; kPa). Not only does this stiffness not mimic the in vivo environment, but also recent evidence from a number of groups has demonstrated that substrate stiffness plays an important role in regulating cell behavior, including stem cell differentiation,[98, 110, 111, 112, 113, 114]. Thus far, no tool has been engineered to reproducibly and easily combine substrate stiffness

and co-culture to induce changes in a particular cell fate. In order to advance the understanding of cell behavior and better model in vivo environments in 2-D co-culture, we modified the reconfigurable co-culture device with an ECM protein-functionalized hydrogel of tunable stiffness. In this way, the user can monitor cell-cell interactions combined with any permutation of stiffness and ECM protein type. Groups have shown independently that myogenic stiffness (e.g. 10 kPa) and murine myoblast presence can induce myogenic differentiation of ASCs [100, 114, 115]. By using this new tool, we demonstrate that controlled myoblast co-culture on a substrate of myogenic stiffness can cause a synergistic upregulation in myogenic gene expression compared to either method alone.

3.2 Methods

3.2.1 Device preparation, polymerization, and protein functionalization

The silicon reconfigurable co-culture device (combs) was fabricated and developed by previously established methods [50]. This device is approximately 15 mm x 11.2 mm when fit into contact with a 350 μm thickness. The combs were initially cleaned by piranha treatment as described previously [109]. These combs were first paired together to ensure that they are completely flush in contact mode by visualization under an upright 40 X objective. Once paired, they were UVO treated for 10 minutes to activate the silicon surface. 3-(Trimethoxysilyl)propyl methacrylate (Sigma-Aldrich, St. Louis, MO) was used to further treat the surface in order to covalently attach the polyacrylamide gels to the silicon surface. 3-(Trimethoxysilyl)propyl methacrylate (0.1 mL) was diluted in 20 mL 100% ethanol and 0.6 mL of 1:10 glacial acetic acid was added to make a final methacrylate concentration of 20.3 mM. The solution was immediately mixed and added to the combs. The combs were incubated at room temperature in the solution for 3 minutes and the solution was removed. The combs were rinsed with 100% ethanol and allowed to air dry for 30 minutes to remove residual ethanol. The combs displayed

a visual color change that suggested successful methacrylate coating. Prior to functionalizing with polyacrylamide, 1 mm glass microscope slides (Fisher Scientific, Pittsburgh, PA) and 25mm circle coverslips were treated with dichlorodimethylsilane (DCDMS, Sigma-Aldrich, St. Louis, MO) to create hydrophobic surfaces [116]. Each comb pair was placed on a coated microscope slide. For the initial gap studies, acrylamide of 6% w/w of a 40% w/w stock (Fisher Scientific, Pittsburgh, PA), varying amounts of a 2% stock w/w bisacrylamide (Fisher Scientific, Pittsburgh, PA), and Milli-Q water were mixed together to create a total of 5 mL. Acrylamide monomer and bisacrylamide crosslinker concentrations had to be modified and tested in order to achieve similar z-axis heights with varying stiffness for contact scheme. This liquid was degassed by bubbling argon for 10 minutes to remove oxygen. These stocks were then aliquoted and stored at -20°C. 2,2'-Azobis(2-methylpropionamidine) dihydrochloride (0.5 wt%, Sigma-Aldrich, St. Louis, MO) was added to thawed aliquots of 1 mL of solution. The solution was mixed carefully by rotating the tube several times and sonicating for 5 seconds. 7.5 uL of the solution was added to the interface between the two comb halves in contact. The DCDMS coverslip was added on top of the solution. The comb-polymer solution-coverslip setup was then irradiated with 305 nm UV light 2 inches directly above the setup with a surface intensity of 0.85 mW/cm2 for 10 minutes. After 10 minutes, the DCDMS coverslips and glass were carefully removed from the comb. Peeling the coverslip off required gentle removal to ensure that the PA did not tear off the comb pair. Once the comb pair was separated, it was immediately added into 2 mL of 1X Dulbecco's Phosphate-Buffered Saline (DPBS, Invitrogen, Carlsbad, CA). These gels were allowed to swell by incubation in PBS at room temperature for 24 hrs. Polyacrylamide mixtures were characterized by atomic force microscopy (AFM) to assess stiffness of the gel [116]. 0.2 mg/ml of Sufosuccinimidyl-6-(4-azido-2-nitrophenylamino)-hexanoate (Sulfo-SANPAH, Pierce Biotechnology, Rockford, IL) diluted in 50 mM HEPES buffer at pH 8.5 was used to covalently link protein to the polyacrylamide via established methods [116]. The Sulfo-SANPAH was washed twice with the HEPES buffer. Next, 10 ug/mL fibronectin (Sigma-Aldrich, St. Louis, MO) diluted in HEPES

was added and allowed to attach to the surface overnight at 37°C. The solution was removed from the combs and combs were rinsed once more with DPBS. The combs were sterilized under UV light in the tissue culture hood for 45 minutes and then used for cell seeding and attachment.

3.2.2 Gel thickness and stiffness

Gels were prepared as above with the addition of 10μl/ml of 0.5 μm fluorescent 505/515-carboxylated microspheres (Invitrogen, Carlsbad, CA) and 0.1% v/v Tween-20. The gels were allowed to swell in DPBS overnight. A 600X CARV II confocal microscope (BD Biosciences) was used to visualize the spheres and determine thickness post-swelling by panning from the bottom of the gel to the top in the z-direction while gels were in PBS [117]. Five randomized points on the gel-comb device were taken from 6 comb halves (n=30) per stiffness to determine thickness. Stiffness was quantified via Atomic Force Microscopy (AFM). AFM data was collected by averaging 10 points per comb on 3 separate combs (n=30/group).

3.2.3 Cell culture

Adipose derived stem cells (ASCs) were harvested from 7 different donor patients. Two groups of three patients' cells were pooled together. These cells were isolated from donor ages between 20 - 31 years of age by methods described previously [114] with the approval of the UCSD human research protections program (Project 101878). All the following experiments were carried out with informed consent and compliance with UC San Diego's institutional guidelines. These cells were cultured in adipose cell growth media (AGM) made up of low glucose Dulbecco's modified Eagle's medium (low-glucose DMEM) (Invitrogen, Carlsbad, CA), containing 10% fetal bovine serum (FBS, Hyclone), and 100-units/mL penicillin/streptomycin (P/S, Invitrogen, Carlsbad, CA). Cells were passaged at 1:4 and were used for experiments up to passage number 6. Murine C2C12 myoblasts (ATCC, Manassas, VA) were grown as described previously in growth media (GM) with 4.5 g/L glucose-Dulbecco's modified Eagle's medium (DMEM), 10% FBS, and

1% P/S.

3.2.4 Monoculture differentiation assays

Each of the fibronectin coated PA comb pairs were placed in a 12-well plate. ASCs were seeded on 1, 10, and 34 kPa gels coated combs. Combs without a gel but with adsorbed fibronection at 10 μg/mL were used as a control. Each comb pair was seeded with 30,000-40,000 cells per well in 2 mL of media. The plate was shaken for 5 seconds after seeding for 30 minutes and 1 hour in order to promote even cell seeding on the surface. After cells were attached, combs were removed and placed into a new 12-well plate with the same AGM. Media was replaced every two days in culture. After 6 days, the cultures were washed with PBS and fixed with 4% paraformaldehyde for 10 minutes for staining. Duplicate stiffness combs were stained for βIII-Tubulin, MyoD, or CBFA1 to identify neuronal, myogenic and osteogenic differentiation, respectively, as previously demonstrated. Staining was carried out as described below.

3.2.5 Gap co-culture differentiation assays

Combs were prepared as mentioned above with or without PA and functionalized with fibronection. Comb halves were separated and male combs were used for ASC seeding and analysis whereas female halves were seeded with either ASCs or C2C12 myoblasts. The ASC halves were seeded with 30-40,000 cells in AGM and the myoblasts with 750,000 cells in GM per 12-well. The cells were allowed to attach and shaken as in the monoculture studies. Once attached, the cells were taken out of the 12-well, dipped and rinsed in PBS and added into a new 12-well with 2 mL AGM. Combs were fit together in the following configurations in duplicate (4 groups): 1) ASCs in co-culture with ASCs on silicon, 2) ASCs on 10 kPa gels in co-culture with ASCs on 10 kPa gels, 3) ASCs in co-culture with myoblasts on silicon, 4) ASCs on 10 kPa gels in co-culture with myoblasts on 10 kPa gels. All co-cultures were in the gap configuration so that cell contact interactions could not occur. Media was changed every two days. On day 6, the cultures were either fixed

with 4% paraformaldehyde for downstream staining or male halves were disengaged from the females and RNA was isolated for downstream qRT-PCR gene expression analysis. Staining was performed as in the monoculture assays with MyoD for the myogenic differentiation marker and with an anti-human mitochondrial DNA antibody (Millipore) that identifies only the human cells. RNA was isolated from only the male halves of the combs and pooled from triplicate cultures, converted to cDNA and analyzed with qPCR. Desmin and Myogenin were analyzed for gene expression in PCR. Fold expression was averaged from six separate experiments.

3.2.6 Migration studies

Myoblasts were seeded to confluence on comb halves of either 40 kPa or 1 kPa pairs. Once cells adhered, halves were placed into contact with another gel type without any cells in 2 mL of GM. Groups consisted of the following: cells on a 1 kPa gel in contact with a 40 kPa gel with no cells, cells on a 1 kPa gel in contact with a 1 kPa gel with no cells, and cells on a 40 kPa gel in contact with a 1 kPa gel with no cells. Other permutations using 10 kPa (instead of a 1 kPa) and 40 kPa were also tested. Once adhered after 3 hours, the halves were snapped with another corresponding half. After 4 days, the combs were stained with Desmin and Hoescht.

3.2.7 ASC differentiation on varying stiffness gels in either contact or gap mode

As with the gap co-culture studies, gels were generated on comb pairs fit into tight contact. In this case, all combs were modified with either 10 kPa or 40 kPa gels. Once polymerized, swollen, and protein functionalized with fibronectin, cells were seeded on comb halves. The cells were allowed to attach and shaken as in the gap co-culture studies. Once attached, the cells were taken out of the 12-well, dipped and rinsed in PBS and added into a new 12-well with 2 mL AGM. Some of the comb pairs were substituted such that groups with 40 kPa male halves and 10 kPa female halves were placed into contact. Because these gels post-swelling

measured 30 ţm in height, cells could be placed on both halves and maintain z-axis contact. Cells were seeded to confluence on individual halves to create the following groups: ASCs on 40 kPa in contact or gap with myoblasts on 10 kPa, ASCs on 10 kPa in contact or gap with myoblasts on 10 kPa, and ASCs on 40 kPa in contact with ASCs on 40 kPa as a control (5 groups, n=3/group). AGM media was replaced every other day. After 6 days, RNA was collected from the male ASC half of each culture group. qPCR was carried out with Desmin, Myogenin, and GAPDH to test myogenic gene expression.

3.2.8 Immunofluorescence staining

After fixing in 4% paraformaldehyde (Wako Chemicals, Richmond, VA) for 10 minutes, combs were rinsed with PBS. A solution of 1% Triton X-100 in PBS was added for 15 minutes at room temperature. The combs were then rinsed with a staining solution (SS) made with 1mM MgCl2 in 1X PBS. Primary antibodies: Desmin (1:200, Abcam, Cambridge, MA), neuronal βIII-Tubulin (1:100, Sigma, St. Louis, MO)), MyoD (1:100, Santa Cruz Biotechnologies, Santa Cruz, CA), CBFA1 (1:100, Alpha Diagnostic International, San Antonio, TX) and for some assays Human Mitochondrial DNA (1:200, Millipore, Temecula, CA) were added to 2% BSA in SS for 30 minutes at 37°C. The solution was removed and washed 3X with SS. Next, secondary antibodies, AlexFluor 488 or AlexaFluor 568 (1:200, Invitrogen, Carlsbad, CA) were added in 2% BSA in SS for 30 minutes at 37°C. The solution was removed and washed three times with SS. Hoescht 33342 (0.1 μg/ml in DI water, Invitrogen, Carlsbad, CA) was incubated for 10 minutes at room temperature. Finally, the samples were rinsed with PBS and combs were individually mounted on microscope slides with Fluoromount-G (Southern Biosciences, Birmingham, AL). Immunofluorescence was carried out using the CARV II Confocal Microscope (BD Biosciences). Images were taken with a Nikon Eclipse TE2000-U microscope with a Cool-Snap HQ Camera and were then analyzed by Metamorph 7.6.

3.2.9 Quantitative polymerase chain reaction (qPCR)

After 6 days, male combs were carefully removed from the female combs and transferred to a new plate. The RNEasy kit (Qiagen, Valencia, CA) was used to extract total RNA from cells. The lysis buffer was directly added to the comb surface and a cell scraper was used to remove and consolidate cells from the comb into the solution. The RNA from two male combs in the same group was pooled together to improve yield. cDNA was synthesized via Superscript III Reverse Transcriptase kit (Applied Biosystems). SYBR Green PCR Master Mix (Applied Biosystems) was used with a 10 μM final concentration of forward and reverse primer. Primers were designed to be human specific (e.g. did not cross-react with the mouse genome) using human and mouse BLAT genome software (genome.ucsc.edu). Myogenin (NM002479.4) F: 5'-GCCTTGATGTGCAGCAACAGCTTA-3', R: 5'-AACTGCTGGGTGCCATTTAAACCC-3'; Desmin (NM001927.3) F: 5'-CCGCGGGCGGGTTTCGGCTC-3', R: 5'-GGCCACTCGCGTCGGCTCGC-3'; and GAPDH (NM002046.4) F: 5'-TGAGCCCGCAGCCTCCCGCTT-3', R: 5' TCAGCGCCAGCATCGCCCCACT-3'.

Samples were done in technical triplicates on the ABI Prism 7900 HT Fast Real-Time PCR System (Applied Biosystems). The following thermal cycle settings were used: 2min at 50°C, 10 min at 95°C, followed by 40 cycles of 15 sec at 95°C and 1 min at 60°C. The SDS 2.3 Software (Applied Biosystems) was used to record and analyze cycle number and gene expression fold change. All data was normalized to GAPDH. Gap gene expression studies were then normalized to adipose stem cells seeded on non-polyacrylamide silicon combs or adipose stem cells on 40 kPa alone in the final experiment.

3.2.10 Statistical evaluation

Significance was tested for all experiments using a 1-way ANOVA with a two-tailed distribution followed by Tukey post-hoc t-test with a 95% confidence interval. Mean fold changes and standard deviations for gene expression measurements were calculated with at least experimental triplicates. AFM data is represented with averages and s.e.m.

3.3 Results

3.3.1 Gel polymerization and characterization on the surface of the device

Polyacrylamide (PA) gels have been previously functionalized to borosilicate glass coverslips and slides to control substrate stiffness [98, 107, 114, 116].These protocols were modified specifically for the co-culture device to ensure that complete coverage of each comb finger was achieved. Combs were cleaned, plasma treated with ultraviolet-ozone, and methacrylate functionalized. An azo-photoinitator was used to allow for temporal control of the PA polymerization. UV initiated acrylamide polymerization allows the solution to be carefully placed on the device and to evenly cover the surface of the fingers before the polymerization occurs.

To promote even and consistent polymerization, combs were pre-fit to ensure that there were no gaps in the comb fingers when in contact mode to prevent leakage of the acrylamide solution. Additionally, the combs were placed on dimethyldichlorosilane (DCDMS) coated microscope slides to prevent sticking of residual PA gel to the glass and to easily remove the polymerized comb from the glass surface (Fig. 3.1a). The solution was carefully added to the center of the comb-pair interface, and a DCDMS coated coverslip was placed on top of the liquid. The liquid spread via surface tension provided by the glass coverslip on the comb (Fig. 3.1b). Once the solution was applied evenly, the combs were placed (with minimal movement) under a 305 nM UV lamp for 10 minutes. Afterwards, the coverslip was carefully peeled off the comb. Comb pairs were separated from each other with the PA gel in a dehydrated state so that the gel features would be maintained on the comb fingers before swelling in PBS. Once in PBS, several rinses were performed to eliminate any free monomer. Proteins were then attached to the hydrogel surface via N-Sulfosuccinimidyl-6-[4'-azido-2'-nitrophenylamino] hexanoate (sulfo-SANPAH), which reacts with primary amines on the protein and links them to the PA gel. The overall process from comb preparation to cell seeding is depicted in Fig. 3.1c. All configurations of the device (separated, gap, and

contact) are shown in Fig. 3.1d-f.

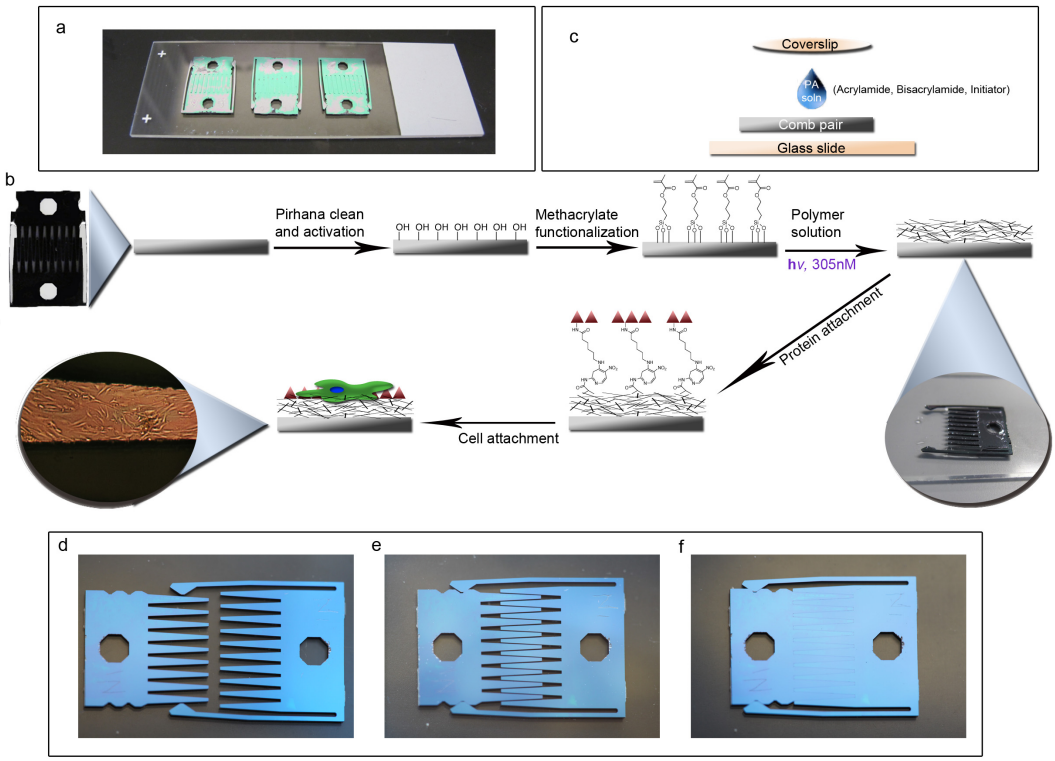

Figure 3.1: **Setup and scheme of device modification.** **(a)** Three cleaned and methacrylate functionalized combs are placed into contact onto a DCDMS coated glass slide to demonstrate the scale of the device. **(b)** The overall scheme of the device begins with pirhana cleaning and UVO treatment to first activate the device surface. Next, methacrylate groups are functionalized on the surface in order to covalently link polyacrylamide to the surface. The polyacrylamide solution consists of acrylamide monomer, bisacrylamide crosslinker, water, and the azo-photoinitiator. These are degassed, well mixed and added to the comb as shown in **(c)**. 7.5 μL of polyacrylamide (PA) solution is placed on the comb on the DCDMS coated glass slide. A DCDMS coated coverslip is carefully added to the top of the drop of PA solution to allow even solution spreading over the device. After 10 minutes of exposure to 305 nm UV light, the PA has gelled and the coverslip is carefully peeled off (see inset). The combs are separated and placed in PBS to swell. Then sulfo-SANPAH crosslinker in HEPES buffer is added for 10 minutes under 350 nm UV light. The protein is attached and the device is sterilized with UV. Cells are then added to the surface. The final inset shows a finger of a comb containing ASCs illuminated by a 40X upright microscope.

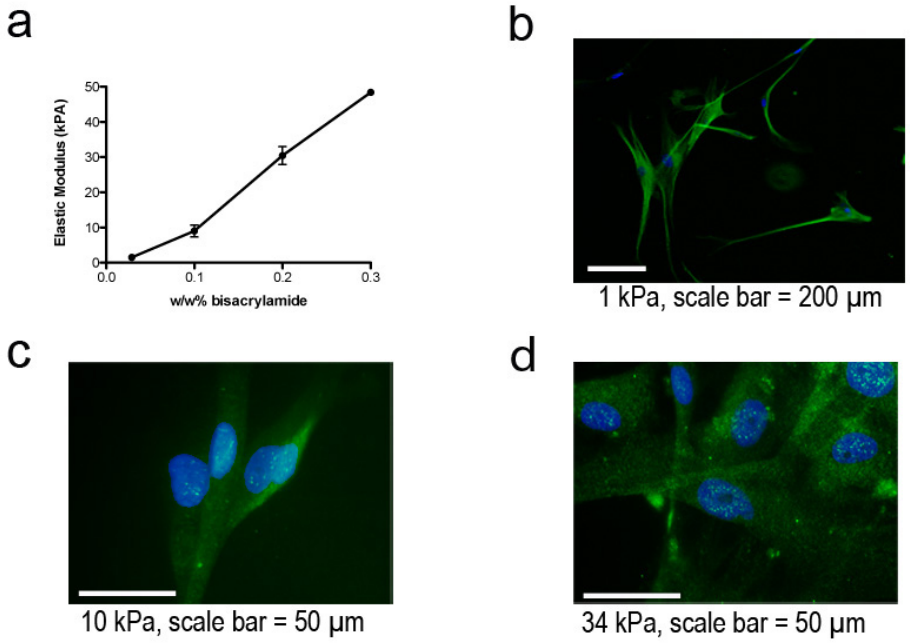

Figure 3.2: **Polyacrylamide stiffness on the device and ASC differentiation.** **(a)** The elastic modulus of the gel linked to the device in PBS at room temperature is determined by AFM. Monomer and initiator are fixed and bisacrylamide is varied. Positive staining for **(b)** βIII-tubulin on 1 kPa, **(c)** MyoD on 10 kPa, and **(d)** CBFA1 on 34 kPa represent differentiation in the appropriate lineages based on previous work with these substrate stiffnesses.

PA gels were polymerized from acrylamide solutions with bisacrylamide concentrations of 0.028 w/w%, 0.1 w/w%, and 0.2 w/w%, resulting in soft (1 kPa), intermediate (10 kPa), and stiff PA gels (34 kPa), respectively, as measured by atomic force microscopy (AFM) (Fig. 3.2a). 7.5 μL of the acrylamide solution was found to create a 30-50 μm tall PA gel, which is above the 20 μm thick threshold that ensures cells feel the gel and not the substrate below [118, 98]. Fluorescent microbeads in the polymerization mixture allowed us to determine with confocal microscopy that our gels consistently exceeded the minimum height requirement.

3.3.2 Myogenic differentiation of ASCs is increased by combining myogenic stiffness and paracrine interactions

Choi et al. recently showed that ASCs differentiate into neuronal, myogenic, and osteogenic lineages on 1, 11, and 34 kPa, respectively. We first tested whether these results could be reproduced on the combs because the monomer and crosslinker ratios, initiator, and substrate were different, though the stiffness values were similar. ASCs alone were cultured for six days in growth media and stained for βIII-Tubulin, MyoD, and CBFA1 as shown in Fig. 3.2b-d. While βIII-Tubulin was found in cells on all stiffnesses, cells on 1 kPa combs showed increased branching and a neuronal morphology compared to the two stiffer gels (Fig. 3.2b). MyoD and CBFA1, transcription factors that are indicative of myogenic and osteogenic differentiation, were present and punctuated in nuclei on the 10 and 34 kPa gels, respectively (Fig. 3.2c-d); positive staining was not present on gels of other stiffness (3.3). Monoculture results on individual combs supported the findings of Choi et al., demonstrating a higher propensity for neuronal, myogenic, and osteogenic differentiation on combs modified with 1 kPa, 10 kPa, and 34 kPa gels, respectively.

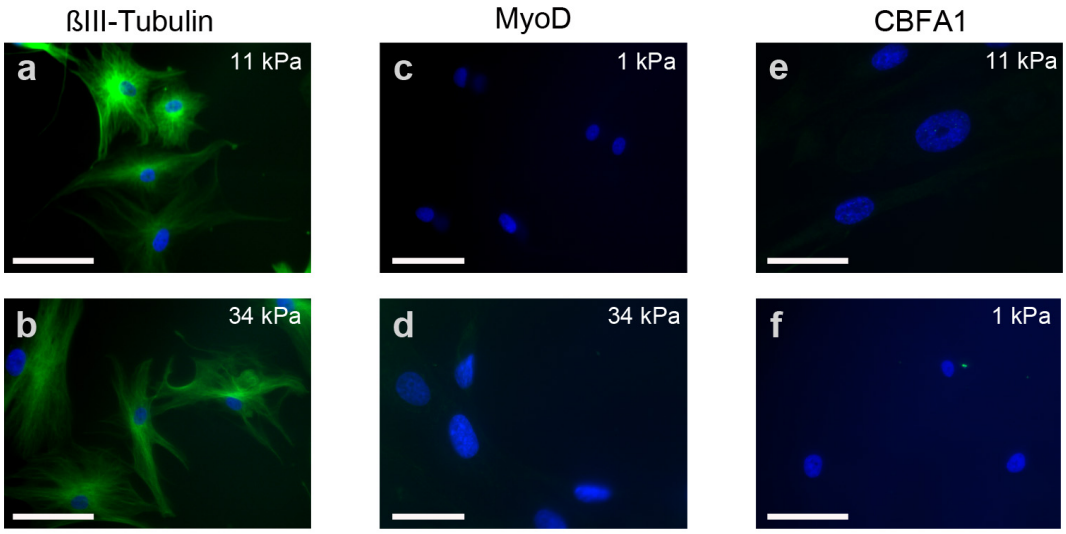

Figure 3.3: β**III-Tubulin, MyoD, and CBFA1 antibody staining on polyacrylamide linked silicon combs. (A)** βIII-Tubulin (green) and nuclei (blue) staining on 11 kPa gels in **(B)** on 34 kPa gels show a spread out, fibroblast-like morphology, scale bar = 200 μm. **(C, D)** Negative staining for MyoD (green) and nuclei (blue) on a 1 and 34 kPa gel respectively, scale bar = 200 μm, 50 μm. **(E, F)** Representative image of negative staining for CBFA1 (green) and nuclei (blue) on an 11 and 1 kPa gel (scale bar =50 μm, and 200 μm repsectively).

We then sought to demonstrate the utility of this device by studying the effect of substrate stiffness and skeletal myoblasts co-culture on ASC differentiation in three distinct configurations. First, combs with adsorbed fibronectin or with a fibronectin-coated myogenic stiffness (10kPa) gel were created. The male half of the comb was seeded with ASCs and the female half with either ASCs or myoblasts (Fig. 3.4a).

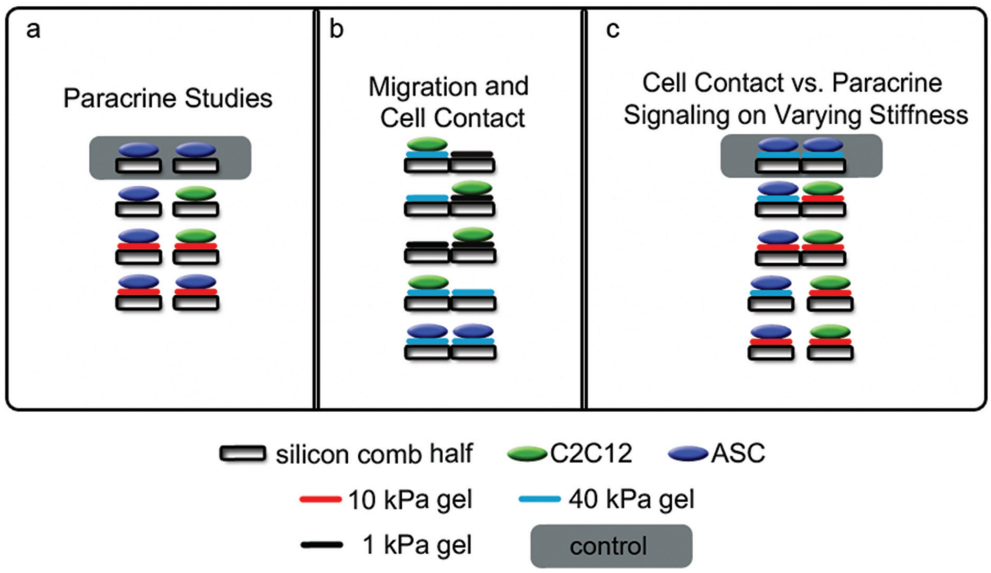

Figure 3.4: **Experimental setup. Schematics explaining all cell culture setups to demonstrate utility of the technology.** The gray shaded cultures are those to which the qPCR results are normalized. **(a)** Gap studies comparing 10 kPa gels to bare silicon on the combs with ASC's (blue) and myoblasts (green). The results are shown in Fig. 3.5. **(b)** Migration studies with myoblasts were used in the permutations described with various gel types in contact. ASC's on 40 kPa were also stained to show contact on the same plane on different comb halves. Results are shown in Fig. 3.7. **(c)** ASC differentiation on various gel stiffness in either contact or gap mode. Gene expression studies using a combination of 10 and 40 kPa gels in gap or contact were analyzed to show changes in myogenic gene expression. IF and qPCR results are shown in Fig. 3.9.

The device was kept in gap configuration so that the ASCs experience only the paracrine signals from cells across an 80 μm gap, and not the physical or contact cues from the other cell type. After 6 days, a subset of ASCs on 10 kPa gels in both the presence or absence of myoblasts showed punctate positive staining for MyoD on the comb fingers (Fig. 3.5a-b) whereas staining was undetectable in ASCs cultured on bare silicon. A human mitochondrial stain confirmed that the stained cells were human and not contaminating murine cells (Fig. 3.5c-d, Fig.3.6). This data suggests that both myoblast co-culture and myogenic stiffness were promoting ASC myogenesis. MyoD staining was used to confirm that myogenesis had occurred; however extent of myogenesis was quantified via gene expression measurements. RT-PCR gene expression was used to further assess myogenesis of ASCs on only the male halves (ASC halves) of the combs in the ASC-myoblast co-cultures. This was to ensure that only the ASC RNA was isolated and analyzed. Additionally, human specific primers were used as a second means of selecting for only human cells. ASCs were analyzed after six days for expression of Desmin, a later stage muscle-specific intermediate filament protein that proceeds fusion citePaulin:2004aa,Londhe:2011aa, and Myogenin, an early muscle regulatory factor (MRF) responsible for initiating the cascade of skeletal muscle gene activation [119]. Fig. 4e-f shows normalized gene expression changes from qPCR for these two genes; Desmin expression significantly increased when both myoblasts and myogenic stiffness were present (Fig. 4f). Myogenin levels showed a similar increase though not significant when both cells and myogenic stiffness were present (Fig. 3.5e).

Secondly, the device was used in contact mode to illustrate the influences of cell-cell contact. While gel height does not impact gap mode, contact mode requires gels that are in physical contact, share a border, and are on the same plane. In other words, the gels should have the capability to be seeded separately and once placed into contact allow for cell-cell physical contact across the interface. In our initial gap mode experiments, differential gel swelling as a result of two dissimilar polymer concentrations resulted in different gel heights. For contact mode, it was essential to create gels that maintained near identical heights to ensure only

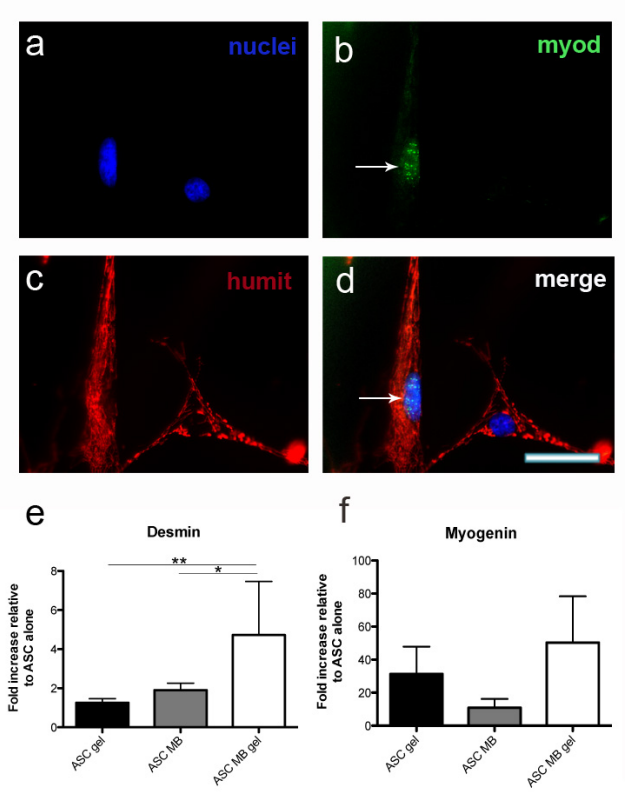

Figure 3.5: **Myoblasts in co-culture with ASCs on 10 kPa gels demonstrate increased myogenesis.** ASC's and myoblasts were co-cultured in the following groups: ASC-ASC (silicon), ASC-ASC (10 kPa), ASC-myoblast (silicon), ASC-myoblast (10 kPa) for 6 days in growth medium. **(a-d)** A representative image of myogenic differentiation demonstrates positive staining for MyoD (green) in adipose derived stem cells on 10 kPa gels. The arrow emphasizes the positive green staining. Note the lack of MyoD in the adjacent cell on the right half of the image. MyoD staining was scarcely observed in all cultures except for ASC-ASC (silicon). A Human mitochondrial DNA antibody (red) was used to distinguish the human ASCs from the murine myoblasts. Hoechst stained the nuclei (blue), scale bar = 50 μm. **(e)** qPCR results for Desmin shows an increase in gene expression when ASCs are plated on either 10 kPa alone or co-cultured with myoblasts on silicon compared to ASCs on bare silicon alone. A synergistic increase is observed when both 10 kPa gels and myoblasts are present in gap compared to 10 kPa monoculture or co-culture on bare silicon (*$p < 0.05$, **$p < 0.01$). **(f)** The same trend is observed for Myogenin gene expression when both cells and gel are present in culture. Data represents the mean and standard deviation for 6 replicates.

lateral cell-cell contact. As a result, contact mode experiments utilized different acrylamide and bisacrylamide formulations to yield a consistent 30 μm gel height post swelling as graphed in Fig. 3.7a. The heights were not statistically different (Fig. 3.7b), and averaged 30.4, 28.2, and 28 μm for the 40, 10 and 1 kPa gels, respectively. The heights of contact formulations were further characterized with AFM topographical maps (3.8a-b) to further emphasize that the two disparate gels are on the same plane and in contact with each other. With a contiguous surface, we then asked whether cells migrated from one comb half to another. Myoblasts were grown to confluence on 1 and 40 kPa comb halves, and once adhered, the half was put into contact with another fibronectin functionalized 1 or 40 kPa half without cells (Fig. 3.2b). Note that myoblasts had not fused into myotubes. All permutations were tested to determine whether migration across the comb would occur; after 4 days, no directed migration, or "durotaxis [120]," was seen in any of the configurations including mismatched ones. Fig. 3.7c-e demonstrates that these cells do not migrate to the other half regardless of stiffness pairing. When cells were seeded on both halves, ASCs were seen extending projections across the gel interface but still did not exhibit durotaxis (Fig. 3.7f).

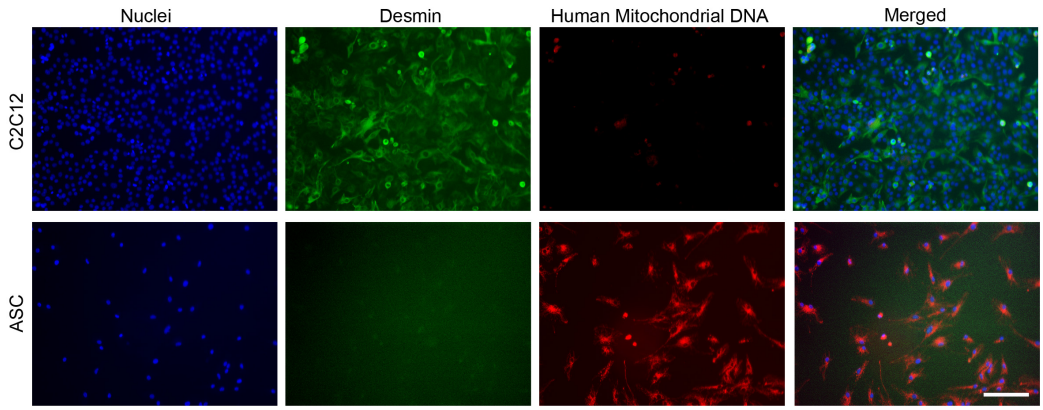

Figure 3.6: **Human mitochondrial DNA and Desmin antibody staining on C2C12s and ASCs.** C2C12s and ASCs in top and bottom rows respectively were plated in separate wells and once adhered, stained with desmin (green), human mitochondrial DNA (red), and Hoescht (blue). Exposure times for each channel were kept constant for both cell types to show specificity of each antibody, scale bar = 200 μm.

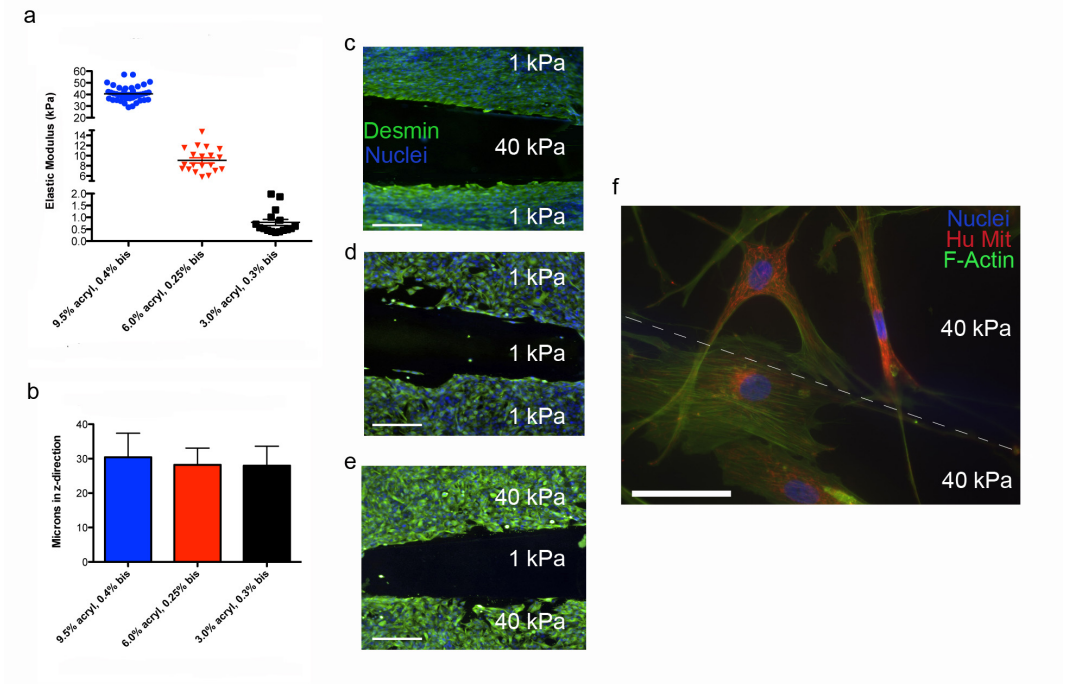

Figure 3.7: **AFM height map of contiguous gels in contact.** Two representative AFM height maps of the interface between two fingers of a 10 kPa and 40 kPa pair placed into contact and submerged in PBS. AFM topographical maps were generated to show that the gels were i) disparate or non continuous and ii) on similar enough heights in regard to the scale of a cell 10 μm. Height maps with a z-axis scale from 0-3 μm. In a) the interface between the combs shows a valley, in b) the gels are closer on the surface and do not display a valley, but a shift in height. Note the 2-D nature of these graphs show that variation in the z-axis is small (3 μm) and that cells can physically touch on the z-axis plane from one comb to another.

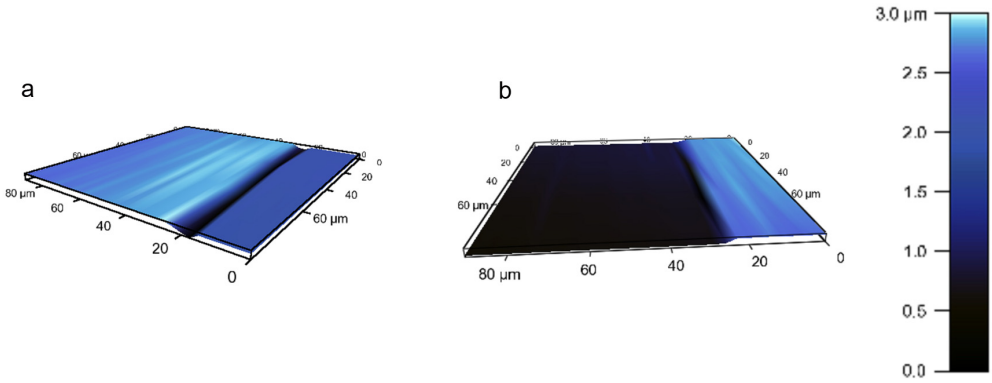

Figure 3.8: **Confirmation of contact formulations and cell-cell contact.** For contact studies, the gels required same heights between soft, medium and stiff moduli in order for cells to experience physical contacts on heterotypic gel stiffness. **(a)** The elastic modulus determined by AFM for stiff (blue, 40 kPa), medium (red, 10 kPa), and soft (black, 1 kPa) gels. Each gel is created with varying formulations of monomer and crosslinker. **(b)** The corresponding heights of each of the gel types show an approximate 30 micron height on the surface of the comb when swollen in PBS. Myoblasts were added to the 1 or 40 kPa gels prior to putting them in contact with a gel that contained only a fibronectin functionalized gel and no cells. These cells were stained for Desmin (green) and Hoechst (blue) for myoblast identification and nuclei, respectively. **(c)** Cells on a 1 kPa gel in contact with a 40 kPa gel with no cells, **(d)** cells on a 1 kPa gel in contact with a 1 kPa gel with no cells, **(e)** cells on a 40 kPa gel in contact with a 1 kPa gel with no cells (scale bars = 200 μm). No significant migration was observed after four days in culture for each of these formulations. **(f)** ASC's were plated on different 40 kPa gels and placed into contact for 6 days. Cells were stained with phalloidin (green) and human mitochondrial DNA (red), and nuclei (blue). The dashed line in **(f)** represents the interface between the cells, scale bar = 25 μm.

Finally, we examined the interplay of stiffness, paracrine, and cell-cell contact signals on ASC myogenesis by intentionally mismatching 10 and 40 kPa substrates for given cell types to examine cell fate.. The following groups were cultured (Fig. 3.4c): ASC (40 kPa) - ASC (40 kPa) in contact, ASC (40kPa) - Myoblasts (10 kPa), and ASC (10 kPa) - Myoblasts (10 kPa) in either gap or contact (5 groups, n=3/group). These cultures (both in gap and contact) were created using the polyacrylamide formulations as previously characterized in Fig. 5a to ensure equal heights between gels in contact. IF images show the two cell types plated in contact on the different gels (Fig. 3.9a). Desmin positive cells were found when ASCs were cultured on 10kPa gels (Fig.3.9b , Fig. 3.10). This staining was not localized to a specific region on the fingers of the comb. Sparse Desmin positive staining was found on ASCs seeded on 40 kPa gels co-cultured with myoblasts (Fig. 3.10b). To confirm myogenesis, qPCR was also carried out to determine how disparate gel stiffnesses and configurations affected myogenic gene expression (Fig. 3.9c). Myogenin was significantly upregulated in all groups co-cultured with myoblasts compared to ASCs on 40 kPa alone. While a similar trend was observed with Desmin, only ASCs on a 10 kPa gel were significantly increased compared to ASCs on 40 kPa alone. Both Desmin and Myogenin were significantly upregulated with ASCs on 10 kPa in contact with myoblasts compared to ASCs on 40 kPa in gap with myoblasts. This suggests that a 10 kPa substrate and contact with myoblasts increases myogenic gene expression.

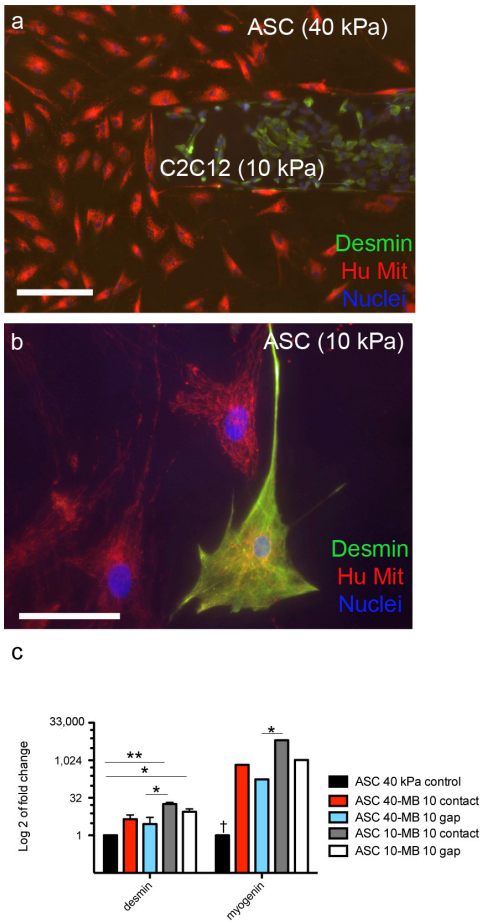

Figure 3.9: **Differentiation of ASCs in co-cultures on 40 or 10 kPa gels in contact or gap.** Co-cultures were setup with the following groups: ASC (40 kPa)-ASC (40 kPa) contact, ASC (40 kPa)-myoblast (10 kPa) contact and gap, and ASC (10 kPa)-myoblasts (10 kPa) contact and gap (5 groups, n = 3 per group). (a) Myoblasts stained positive for Desmin (green) on a 10 kPa gel and ASC's stained for human mitochondrial DNA (red) on a 40 kPa gel are placed in contact, scale bar = 200 μm. (b) A representative image of a positively stained Desmin cell on an ASC half of a comb on 10 kPa gel, scale bar = 25 μm. (c) qPCR results showing all groups normalized to ASC's on 40 kPa gels. Fold change on a log 2 scale is used to clearly represent the data in graphical form (*$p < 0.05$, **$p < 0.01$). Myogenin in the ASC 40 kPa control is significantly downregulated compared to all other groups (†$p < 0.01$). Error bars have been included in all data contained in the graphs.

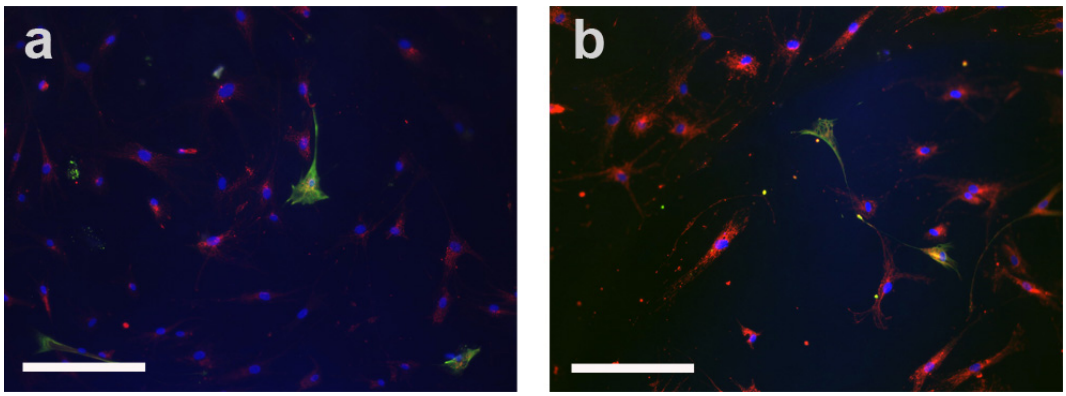

Figure 3.10: **Desmin positive staining on ASCs 6 days in co-culture with myoblasts (10X resolution).** Two representative images of positive desmin staining (green) co-stained with human mitochondrial DNA stain (red) on ASC halves on a (A) 10 kPa gel and (B) 40 kPa gel after 6 days in culture, scale bar = 200 μm. These images were taken in the middle of the finger of each ASC half.

3.4 Discussion

There is a need to develop novel technologies for 2-D *in vitro* cell culture, which can examine the different variables that cells experience in vivo such as substrate stiffness, paracrine/autocrine signals, cell-cell physical interactions, and cell-matrix interactions. The technology we have developed has many advantages over traditional co-culture. The reconfigurable co-culture device allows for two cell types to be individually examined in pure populations. This has already been demonstrated previously as a more useful co-culture tool as one can observe contact, paracrine, and temporal changes independently [50, 109].Yet as mentioned, many groups have studied cell behavior on substrates of varying stiffness in the context of stem cell differentiation, wound healing, cancer metastasis, and aging [92, 93, 94, 95, 96].

Currently, the field lacks methods to examine cell substrate and cell interactions in an organized, independent way. No existing cell culture methods allow one to independently examine substrate stiffness and co-culture with separable cell populations. By covalently linking a polyacrylamide gel on the silicon surface of the reconfigurable co-culture device, we developed a platform to independently vary substrate stiffness of two cell populations, which can be cultured in either contact with each other or with a gap, which only allows paracrine signals between the populations. Moreover, each comb half can be functionalize with different ECM proteins, thereby also allowing one to examine additional cell-matrix interactions. We show that cells on one comb half will interact with cells on the other when placed in contact, yet will remain on their respective half, which allows cell populations to be examined individually. With this system in place, the user can examine: 1) cell contact interactions, 2) cell paracrine interactions, 3) substrate stiffness, 4) cell-ECM protein interactions, and 4) temporal changes by removing one comb half and inserting another. With any co-culture tool it is important that the user can make easy readouts. We have shown that RNA can easily be isolated from polyacrylamide gels on the silicon surface and immunofluorescence can be carried out directly on the device. Cell lysates can be collected in similar fashion though were not shown here.

Adipose derived stem cells (ASCs) have been shown to differentiate into neuronal, myogenic and osteogenic lineages by culturing them on approximately 1, 11, and 30-40 kPa polyacrylamide (PA) gels respectively [114]. These gels were previously synthesized by free radical initiation using ammonium persulfate and N,N,N',N'-Tetramethylethylenediamine covalently linked to amino-silanated glass coverslips [114, 116]. In order to functionalize this polymer on the silicon reconfigurable co-culture device, we adapted alternative methods to covalently link the polymer to the substrate and UV initiate the polymerization. In this way, the user can prepare and pipette the solution on the surface carefully and control the initiation of the polymerization. AFM was used to characterize these new gel formulations on the device. We repeated the studies of Choi et al. on these gels by plating ASCs on 1, 10, and 34 kPa gels functionalized on the combs. Positive immunofluorescence staining for neuronal, myogenic, and osteogenic markers on 1, 10, and 34 kPa gels respectively was consistent with previous findings and thus we moved forward to with additional studies to examine the potential of this technology.

Groups have previously shown that paracrine signaling by myoblasts cause spontaneous differentiation of ASCs [121, 100]. However, no groups had previously shown the combination of substrate and cell signaling influence on ASC myogenesis. It was hypothesized that by adding myoblasts in culture combined with a myogenic stiffness, ASC myogenesis would increase. We took advantage of the gap configuration of the device to model this paracrine effect and functionalized a 10 kPa PA gel to its surface. Co-culture with myoblasts in combination with a substrate of myogenic stiffness showed a synergistic increase of myogenic differentiation relative to ASC's on silicon alone, as shown by increased expression of Desmin and Myogenin.

Previous studies have shown myogenic differentiation of ASCs and MSCs with myoblasts in direct co-culture [122, 123, 115]. However, it is often unclear as to whether these cells are merely fusing with one another or inducing myogenesis via contact dependent mechanisms. One advantage of the modified reconfigurable co-culture device is that it allows the user to maintain, examine, and perform

qPCR/IF readouts on only one population, even when cells are in contact. This cannot be achieved in standard culture setups unless harsh separation methods such as flow cytometry are used. Previous gel formulations in our initial studies performed in the gap configuration varied in height between the different stiffnesses. In order to carry out cultures in contact with disparate stiffnesses, new gel formulations were used to ensure cell-cell contact on the same plane. Advantageously, these cells also were maintained on their respective comb half regardless of gel substrate stiffness. This is most likely due to the fact that the two gels are discrete, or non-continuous, even though they are in physical contact and on the same plane. Choi et al. demonstrates that on gels with gradient stiffness, cells "sense" the stiffer environment and thus move towards stiffer areas [124]. However, in our co-culture regime, this cue is eliminated. Though the gels are physically touching on the same plane, they are discontinuous and not physically crosslinked across the interface of the fingers of the comb. Consequently as the cells contract their local matrix, deformations within one gel do not propagate to the other; thus cells cannot sense the other gel via typical mechanotransduction mechanisms [125]. Further evidence of this discontinuity can be seen in the representative AFM topographical map, which shows a very slight, 3 μm change in the z-plane. The cells would not be able to physically sense the other gel half without cell-cell interaction between the interfaces. This is important in regard to maintaining populations of cells on their respective halves; cells are prevented from migrating to the other gel interface, but can establish physical contacts across the fingers of the comb.

We thus examined the effect of contact of ASCs with myoblasts and observed whether this would increase myogenesis over paracrine signaling alone. Simultaneously, to further show utility of this device, we compared ASCs seeded on 40 kPa to those seeded on 10 kPa. Desmin staining was detected on all cultures with 10 kPa gels and less commonly on 40 kPa gels when myoblasts were present in culture. As mentioned previously, we did not quantify staining due to the rarity of the MyoD/Desmin staining in cultures. However, it is important to note that immunofluorescence quantification can be carried out on this device [109]. It has been shown previously that gene expression quantification (RT-PCR

and qRT-PCR) for myogenesis of ASCs is an accurate correlation for myogenic protein expression [126, 122, 114, 100]. Desmin and Myogenin gene expression of ASCs showed a consistent trend. In general, myoblasts in contact increased gene expression relative to gap alone. However, gene expression for both genes was significantly higher when ASCs were plated on 10 kPa and in contact with myoblasts versus ASCs on 40 kPa in gap with myoblasts. It should be noted, however, that only the cells at the interface of the comb fingers experience direct cell-cell contact. These reasons could explain why contact only marginally increased gene expression relative to gap. ASCs cultured on 10 kPa gels caused an increase of myogenic gene expression relative to those plated on 40 kPa gels. This supports previous findings that 10 kPa gels are in the stiffness regime that is ideal for increased myogenesis, and that this substrate stiffness in combination with myoblast co-culture synergistically upregulates ASC myogenesis.

This device has allowed us to probe differences between cell contact and paracrine effects on cells cultured on varying substrate stiffness for this first time. The cells are cultured on separable, spatially organized substrates that achieve a large surface area for cell interaction in 2-D. The culture setup restricts cell migration to allow for gene and protein expression analysis on solely one cell type. This system is not only useful for examining changes in stem cell differentiation but can be applied to study more complex systems in which controlling co-culture and cell microenvironment can elucidate basic mechanisms in cell biology. With numerous potential applications, this device can span multiple disciplines as a useful tool to understanding basic cell-cell and cell-matrix interactions.

Chapter 3 in part is a reprint of the material *Rao N, Grover G N, Vincent L G, Evans S, Choi Y S, Spencer K, Hui E E, Engler A J, Christman K L. A co-culture device with a tunable stiffness to understand combinatorial cell-cell and cell-matrix interactions. Integrative Biology. 2013; 5: 1344-54. Inside cover article.* The dissertation author was the primary author.

Chapter 4

Utilization of a skeletal muscle matrix hydrogel and multiple cell delivery approach to treating hind limb ischemia

4.1 Introduction

As mentioned in Chapter 1, peripheral artery disease (PAD) affects millions of people globally [13]. Because of the prevalence and the lack of a viable therapy, there is a pressing need to create treatments for this disease. In early stages of PAD onset, blood vessels are partially occluded by either calcification or atherosclerotic plaques. This leads to decreased blood flow in the legs. Over time, this lack of blood flow causes a scarcity of nutrients to the surrounding muscle tissue.

Cell delivery is a potentially viable option for treating PAD. Studies in rodents and large animal models have proven very promising and have progressed to clinical trials. As previously mentioned, a number of cell types have been used to treat PAD [19, 20, 21, 22, 23, 24]. However, it is unclear whether one cell type or multiple co-delivered are necessary to effectively treat the disease. Additionally, it is unclear whether there are more specific subsets of cells or untested types that

could be more beneficial. To emphasize, the primary goal for treating PAD is to improve vascularization in the ischemic limb. Secondarily, it is important to regenerate the damaged and atrophied muscle. Skeletal myoblast progenitor cells have been shown to increase angiogenesis by paracrine effects and, in tandem, can fuse with one another in damaged muscle to regenerate the tissue [127, 128, 31]. They are advantageous because they can handle ischemic environments, be isolated from an autologous cell source, and expanded *in vitro* rapidly and easily [31].

As much as this seems to be a viable therapeutic there are some limitations to delivering skeletal myoblasts. First, within the first few hours after injection into ischemic muscle tissue, approximately 90% of the cells die [31]. This is could be due to the following: low pH, apoptoic paracrine signals, negative effects of inflammatory cells, and the lack of healthy extracellular matrix [38]. As a result, groups inject high payloads, which also comes with a price. Injecting dense concentrations of cells through a syringe causes issues with death due to shearing through the needle [129]. Additionally high payloads can also cause over-packing in the host tissue leading to further apoptosis [130]. Lastly, of the cells that make it to the site of injection, and remain viable, only a few are actually maintained and integrated into the host tissue. This is most likely due to the fact that injected myoblasts potentially "wash out" of the location of injection due to limited anchorage points in damaged tissue [31, 131, 132, 133]. They do not produce much of their own ECM themselves and thus must rely on production of other cells or the host environment to attach to.

Addition of a biomaterial in order to mitigate the negative effects of *in vivo* myoblast delivery could prove to be an effective therapeutic [134, 135, 136]. In particular, we are interested in the addition of a decellularized skeletal muscle matrix hydrogel (SkECM) which itself has shown positive results *in vivo*. Upon *in vivo* injection into a rat hindlimb ischemia model, we have shown that the gel increases neovascularization and recruits endogenous muscle cells [37]. This naturally derived biomaterial is initially an injectable shear-thinning viscous fluid that when subjected to physiological pH and temperature becomes a hydrogel [37]. An important factor in injecting material or cells into a patient is the gauge size of the

syringe used to administer the treatment. Clinical trials have used needle gauge sizes from 21G up to 30G depending on the cell type and delivery method. It is preferable to use larger gauge sizes (smaller needles) to decrease pain associated with cell injections. However, by decreasing needle size, one increases shear death of the cells upon injection. Previous work using alginate [129] shows a protective effect on myoblast viability when injected together through the syringe. It is hypothesized that the SkECM could also provide this protective buffering and consequently could be a promising technology to combine in tandem with cell injections. Another possible way to help myoblast viability *in vivo* would be to add other cell types that stimulate growth or protect them from harsh ischemic conditions. In the heart, groups have shown that the addition of cardiac fibroblasts is necessary to increase cardiomyocyte viability and promote electrical propagation, function, and engraftment [48, 137]. *In vitro* studies suggest that skeletal fibroblasts could also aid in myoblast viability and increase myotube maturation as previously mentioned in Chapter 2 [109]. In this study, we investigate the potential for the SkECM to protect myoblasts in 3D culture, push myogenic differentiation *in vitro*, and protect the cells during and after injection into the tibialis anterior of mice with or without the addition of skeletal fibroblasts. Lastly, we translate these findings to a mouse hindlimb ischemia model to determine whether the SkECM and/or skeletal fibroblasts can improve engraftment and/or blood perfusion.

4.2 Methods

4.2.1 Skeletal muscle decellularization, neutralization, and preparation

Porcine lion muscle tissue was harvested from Yorkshire pigs and decellularized following a modified version of a previously reported protocol [37]. Briefly, the skeletal muscle was cut into small pieces and decellularized in a solution of 1% (wt/vol) sodium dodecyl sulfate (SDS), phosphate buffered saline (PBS), and 0.5% penicillin/streptomycin. After 5 days in SDS solution, the tissue was then

rinsed in isopropyl alcohol for an additional 24 hours to remove residual fat. The tissue was rinsed repeatedly with water and frozen at -80°C. The material was then lyophilized, milled and collected for long-term storage. The material was digested with sterile pepsin and hydrochloric acid as previously demonstrated for 2 days [37]. The solution was neutralized on ice in sterile conditions such that the solution had a final sodium chloride concentration of 8 mg/mL and a pH of 7.4. The gel was aliquoted and frozen at -80°C then lyophilized for future cell experiments. The Picogreen Assay (Life Technologies, Carlsbad, CA) and 1,9-dimethylmethylene blue (DMMB, Sigma-Aldrich) assays were used to determine amount of DNA isolated (DNEasy Kit, Qiagen, Valencia, CA) from the material and sulfated GAG content respectively. Gelation was determined when the gel no longer flowed (i.e. stuck to the bottom of a vial) by previously documented methods [37].

4.2.2 Rheological and viscosity measurements

To evaluate the storage modulus of the skeletal muscle matrix, lyophilized protein aliquots were resuspended to create 500 μL of either 6 or 8 mg/mL solutions. These solutions were allowed to gel at 37°C overnight (n = 3). Gels were placed on a TA Instruments ARG2 Rheometer with a 37°C preheated 20 mm parallel plate geometry and a 1.2 mm gap distance. Storage modulus was recorded at frequencies from 0.4 -16 Hz, and plotted at 1 Hz. For viscosity measurements, 200 μL of liquid SkECM was used with a gap height of 500 μm. Data was generated for frequencies from 0.1-50 Hz.

4.2.3 Isolation of primary GFP myoblasts and mCherry fibroblasts

EGFP primary skeletal myoblasts and mCherry skeletal fibroblasts were isolated from transgenic mice, C57BL/6-Tg(UBC-GFP)30Scha/J and B6(Cg)-Tyrc-2J Tg(UBC-mCherry)1Phbs/J respectively (Jackson Laboratory). The muscle tissue was harvested from the hind limbs of the mice, minced, and cultured on

collagen-adsorbed plates. Fibroblasts were removed from the myoblast population per previously established protocols [68]. Subsequent rounds of preplating for approximately 15 passages separated the fibroblast population from the myoblasts.

4.2.4 Cell culture

Mouse primary eGFP myoblasts and primary mCherry fibroblasts were cultured in growth media (GM) consisting of 45% low glucose Dulbecco's Modified Eagle Medium (Life Technologies, Carlsbad, CA), 40% HAMS F-10 (Life Technologies, Carlsbad, CA), 15% fetal bovine serum (FBS, Thermo Scientific), and 0.5% penicillin/streptomycin (Life Technologies, Carlsbad, CA). bFGF at 2.5 ng/mL (Life Technologies, Carlsbad, CA) was added to myoblast cultures. For both the myoblast and the fibroblast cultures, tissue culture flasks were coated with 1 mg/mL collagen in 0.1 M acetic acid for 1 hour at 37°C and rinsed with 1X Dulbecco's Phosphate Buffer Saline prior to seeding. The cells were culture at 37°C and 5% CO_2 and split 1:3 when 90% confluence was reached; media was changed every two days.

4.2.5 Cell encapsulation

The lyophilized protein was resuspended with 500 μL of sterile water that was supplemented with 0.49 mM magnesium chloride and 0.9 mM of calcium chloride. These suspensions were vortexed to form a homogeneous liquid and kept on ice. Total cell number and ratio was varied depending on the experiment. The liquid mixture (25 μL) was added to a 24 well plate preheated to 40°C. The plate was incubated at 37°C and 5% CO_2 for 20 minutes. Another 25 μL of the mixture was added directly above the previous 25 μL and then incubated for 20 minutes again. 1 mL of GM was added to each well after gelation. After one day the GM was replaced to differentiation media (DM) that consisted low glucose Dulbecco's Modified Eagle Medium containing 2% Horse Serum (Thermo Scientific) and 0.5% penicillin/streptomycin. The encapsulations were cultured at 37°C and 5% CO_2; the media was changed every two days.

4.2.6 Metabolic activity assays

Cells were encapsulated at 300,000 cells/25 μL of ECM (50 μL total, n=6) in 24-well plates. 1 mL of GM was added to the cells. 100 μL of Alamar Blue reagent (Life Technologies, Carlsbad, CA) was added to the media and allowed to incubate for at least 4 hours until fluorescent readings were taken by removing 100 μL of supernatant and added into a black 96-well plate. A BioTEK fluorescent plate reader was used to detect Alamar Blue at 560 Ex/590 Em. For assays containing reactive oxygen species, 2.5 mM H_2O_2 was premixed with the media prior to addition to the encapsulated gel. Peroxide treated groups were compared to non-treated groups to account for small variability such as cell number and cell-type differences.

4.2.7 Differentiation experiments

Cell-gel encapsulations were created as previously described with 300,000 cells/25 μL, 600,0000 total cells. For monoculture assays, myoblasts were either re-suspended in 2.5 mg/mL rat-tail collagen, 6 mg/mL or 8 mg/mL SkECM. Myoblast cell number was fixed at 600,000 cells for co-culture groups with an additional 10% increase in total cell number (660,000) due to added mCherry skeletal fibroblasts. RNA was isolated with an RNEasy kit (Qiagen, Valencia, CA) from these gels at 0, 3, and 7 days upon adding DM. Cultures were pooled to generate enough RNA with a final 3 experimental samples per group. cDNA was generated by the SuperScript III Reverse Transcriptase kit (Applied Biosystems). Primers for MyoD (F: 5'-AGGACACGACTGCTTTCTTCA-3', R: 5'-TTAACTTTCTGCCACTCCGGA-3'), GAPDH (F: 5'-CATCAAGAAGGTGGTGAAGC-3', R: 5'-GTTGTCATACCAGGAAATGAGC-3'), Myosin Heavy Chain (F:5'-GCAGAGACCGAGAAGGAG-3', R: 5'-CTTTCAAGAGGGACACCATC), and GFP (F: 5'-AAGCTGACCCTGAAGTTCATCTGC-3', R: 5'-CTTGTAGTTGCCGTCGTCCTTGAA-3'), were used to detect mRNA expression levels using SYBR Green PCR Master Mix (Applied Biosystems). Samples were run on the BioRad CFX96 Real-Time PCR Detection System. The following thermal cycle settings were used: 2 min at 50°C, 10 min at 95°C,

followed by 40 cycles of 15 s at 95°C and 1min at 60°C. In monoculture assays, the gene expression was normalized to GAPDH. In co-culture assays, gene expression was normalized to GFP. To visualize the SkECM, an Alexa Fluor 568 NHS Ester (Life Tech) was added at 1 μL/500 μL of liquid SkECM and vortexed on ice.

4.2.8 Syringe needle flow viability

Cells were resuspended in PBS, 6 mg/mL SkECM, or 8 mg/mL SkECM on ice at 40,000 cells/μL. 50 μL of the solution was loaded into a 1mL syringe (Becton Dickinson). The syringe was fitted with either a 25G, 27G, or 30G needle and mounted on a syringe pump. The liquid was ejected into microcentrifuge tubes containing PBS at 1 mL/min by a syringe pump. The cells were immediately stained with Trypan Blue (Life Technologies, Carlsbad, CA). Percent viability was calculated by counting the number of dead cells and total cells using a hemocytometer across multiple gel formulations (n=10/group).

4.2.9 Cell injections and non-invasive imaging in naïve murine hindlimbs

All animal procedures were performed in accordance with the guidelines established by the Committee on Animal Research at the University of California, San Diego and the American Association for Accreditation of Laboratory Animal Care. Myoblasts were stained with Xenolight DiR (Caliper, Hopkinton, MA) fluorescence dye at 320 mM for 30 min at 37°C. This concentration provided easily resolvable signal without cell toxicity. The cells were washed twice with PBS, trypsinized and spun down. 1 million myoblasts in a 25 μL suspension of PBS, 6 mg/mL SkECM, or 8 mg/mL SkECM was kept on ice prior to animal injections. Four to six week old female albino C57BL/6 mice were used as cell delivery donors (Jackson Laboratory). The suspensions were injected via Hamilton syringe using a 27G needle directly into the tibialis anterior (TA) of the mouse. The mice were immediately imaged under the In Vivo Imaging System (IVIS, Perkin Elmer) Spectrum 200 using the Perkin Elmer Living Image Software and thereafter each

day for one week. ROIs were created and total radiant efficiency at 710 ex/760 em wavelengths was recorded each day for every mouse hindlimb. After one week of noninvasive monitoring, the mice were euthanized and the TA was excised. Once excised, the muscle was placed into the IVIS for one final end-point reading to verify the cells were localized in the TA muscle. Further histological analysis was used to quantify percent GFP-positive staining per area of muscle section.

4.2.10 Hindlimb ischemia surgery and laser speckle imaging

Albino C57BL/6J mice were anesthetized with 5% isofluorane and lowered to 2.5% during surgery. The femoral artery and vein were ligated and removed from the right limb of the mouse. The other limb was used as an untreated control for all perfusion measurements. Immediately after surgery, perfusion measurements using the Perimed laser speckle contrast analysis system were recorded while under 2.5% isofluorane anesthesia. Images were recorded approximately 20 cm above the subject with a 5x5 cm area. Twenty-one images were recorded per second at a 0.17 mm resolution. Blood perfusion in the feet of the mice was recorded over time until perfusion leveled to a stable measurement (at least 20 minutes on a heated deck). Animals were required to have less than 30% blood perfusion immediately post-surgery compared to the control leg or they were not included in the study.

4.2.11 Myoblast injections into ischemic TAs

Seven days post-surgery, animal perfusion levels were recorded once more (pre-treatment). Cells were prepared as explained previously with Xenolight-DiR, and were either injected with 1 million myoblasts and 100,000 fibroblasts in 8mg/mL SkECM, 1 million myoblasts in 8mg/mL SkECM, or 1 million myoblasts in PBS (n=10/group, 25 μL volumes). The animals were then imaged under the IVIS, 0, 3 and 7 days after injection. Laser speckle recordings were taken 17, 28, and 42 days post-surgery. On day 42, the limbs were excised and frozen for immunofluorescence analysis.

4.2.12 Immunofluorescence analysis

The excised TAs were placed in 0.5% paraformaldehyde for 2 hours at 4°C, then transferred to a 20% sucrose solution at 4°C overnight. The tissue was placed in TissueTek OCT and frozen with liquid nitrogen cooled 2-methylbutane for sectioning. Ten micron tissue was sectioned in eight areas throughout the TA approximately 200-250 μm apart. In order to visualize eGFP, the sections were fixed again with 0.5% paraformaldehyde at room temperature for 10 minutes. The sections were blocked with 20% goat serum, and 0.3% Triton X-100 in PBS for one hour. Primary rabbit anti-GFP (1:200 Life Technologies), alpha smooth-muscle actin (1:100, Abcam), or CD-31 (1:200, Abcam) were diluted in blocking buffer and added to sections for one hour. The slides were rinsed 3 times in PBS for 5 minutes. Secondary antibody (Alexa Fluor 488/568, 1:200 Life Technologies, Carlsbad, CA) was added for 30 minutes in the blocking buffer. The slides were rinsed again and Hoescht 33342 (0.1 μg/mL in DI water, Life Technologies, Carlsbad, CA) was added for 10 minutes. Slides were scanned using the Leica Ariol slide scanner and imaged using Ariol Software. The GFP positive areas using a fixed threshold and exposure time for all slides were normalized to total muscle section area and summed for each limb. Vessels were counted in a similar fashion with number of capillaries and arterioles normalized to total muscle area.

4.2.13 Statistical evaluation

Significance was tested for all experiments using a 1-way ANOVA with a two-tailed distribution followed by Tukey post-hoc t-test with a 95% confidence interval. Mean fold changes and standard deviations for gene expression measurements were calculated with experimental triplicates. Syringe data was compared to a PBS control within a respective gauge size by Dunnet's post-hoc test.

4.3 Results

4.3.1 Hydrogel characterization

Porcine skeletal muscle was decellularized and quantified for remaining DNA content (0.255 ng DNA/mg ECM) by the PicoGreen Assay and verified via PAGE to contain a complex makeup of proteins at varying molecular weights as previously done for other decellularized matrices [138, 139, 37]. Sulfated glycosaminoglycan content was calculated from the DMMB assay at 2.9 μg GAG/mg ECM. The 6 mg/mL and 8 mg/mL SkECM solutions gelled between 10-15 minutes after resuspending lyophilized aliquots at 37°C. Rheometry measurements showed a concentration dependent increase in storage modulus from 16.58 $\pm$0.54 Pa to 37.41 $\pm$1.8 Pa at 1 Hz for the 6 mg/mL and 8 mg/mL gels respectively (Fig. 4.1a). A 2.5 mg/mL collagen suspension exhibited similar viscosity measurements to 6mg/mL SkECM but both were significantly lower in complex viscosity to 8 mg/mL SkECM for shear rates from 3 to 50 Hz (Fig. 4.1b).

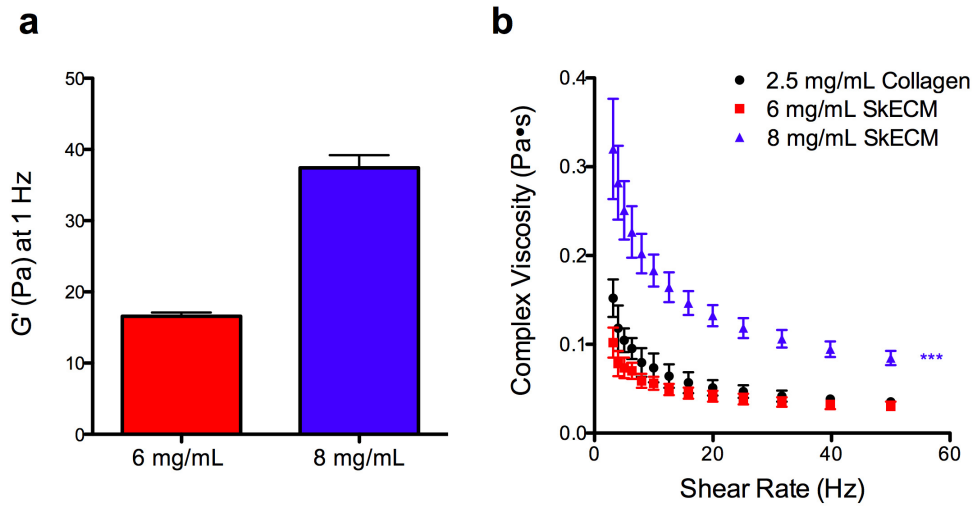

Figure 4.1: **Material properties of the SkECM vs. Collagen.** **(a)** The storage modulus was calculated by parallel plate rheometry for 6 and 8 mg/mL formulations of the SkECM post-gelation after 24 hours at 37°C (n=3/group). **(b)** Viscosity in the liquid form was measured by parallel plate rheometry at 4°C. 2.5 mg/mL collagen was used as the control and as verified here is similar to the 6 mg/mL SkECM formulation. The 8 mg/mL liquid suspension was significantly more viscous at every shear rate compared to the 2.5 mg/mL collagen and 6 mg/mL SkECM (***$p<0.001$, n=3/group). Values represent mean ±SD in all graphs.

4.3.2 Decellularized skeletal muscle matrix hydrogel (SkECM) protects myoblasts from reactive oxygen species and increases myogenic differentiation

The SkECM was used to encapsulate primary eGFP labeled myoblasts at 6mg/mL. Rat tail collagen at 2.5 mg/mL was used as a control because it was previously demonstrated that this gel has similar mechanical properties as other 6 mg/mL decellularized matrix hydrogel formulations [140]. Metabolic activity by the Alamar Blue assay showed that 24 hours post-encapsulation, viability in either matrix or collagen was not different (Fig. 4.2a). Once cells were encapsulated, they were either subjected to growth media (GM) or GM containing H_2O_2 (n=6/group). Alamar blue was added a day later and fluorescence readings were taken 12-24 hours thereafter. Fig. 4.2b shows the metabolic activity after 24 hours of the treatment group compared to control. Metabolic activity in the SkECM is reduced by only 60% of the nontreated control compared to 30-40% for TC plastic and collagen. The SkECM shows significant R.O.S. protection.

When encapsulated for 3 days, the SkECM significantly increases MyoD expression compared to collagen (Fig 4.2c-f). MyoD, as expected, drops as a function of differentiation shown by the decrease at 7 days. Myosin heavy chain expression increases as differentiation proceeds and is significantly higher in both 6 and 8 mg/mL SkECM compared to collagen by day 7 for both formulations. Myotubes were observed as early as 5 days in differentiation media in the SkECM. Very sparse numbers of fused myotubes were observed in the collagen group. Overall, the SkECM outperformed collagen in terms of protection from R.O.S. and differentiation.

Figure 4.2: **Metabolic activity and differentiation of myoblasts in SkECM (a)** Metabolic activity by Alamar blue assay of myoblasts and fibroblasts at 1 million cells and 100,000 cells respectively showed no significant difference between groups when encapsulated in 6mg/mL SkECM or 2.5 mg/mL collagen (n=6/group). **(b)** 2.5 mM H_2O_2 was added to the media and metabolic activity was measured after 12 hours and compared to an untreated control in each respective group (n=6/group). **(c-f)** RT-PCR gene expression measurement of myoblasts encapsulated in either 2.5 mg/mL collagen, 6mg/mL or 8mg/mL SkECM for myosin heavy chain (MHC) and MyoD at 3 and 7 days in differentiation media (DM). In (c,d) all values were normalized to collagen. In (e,f) All values were normalized to day 0 time-point (n=3/group, *$p<0.05$, **$p<0.01$, ***$p<0.001$). Values represent mean ±SD in all graphs.

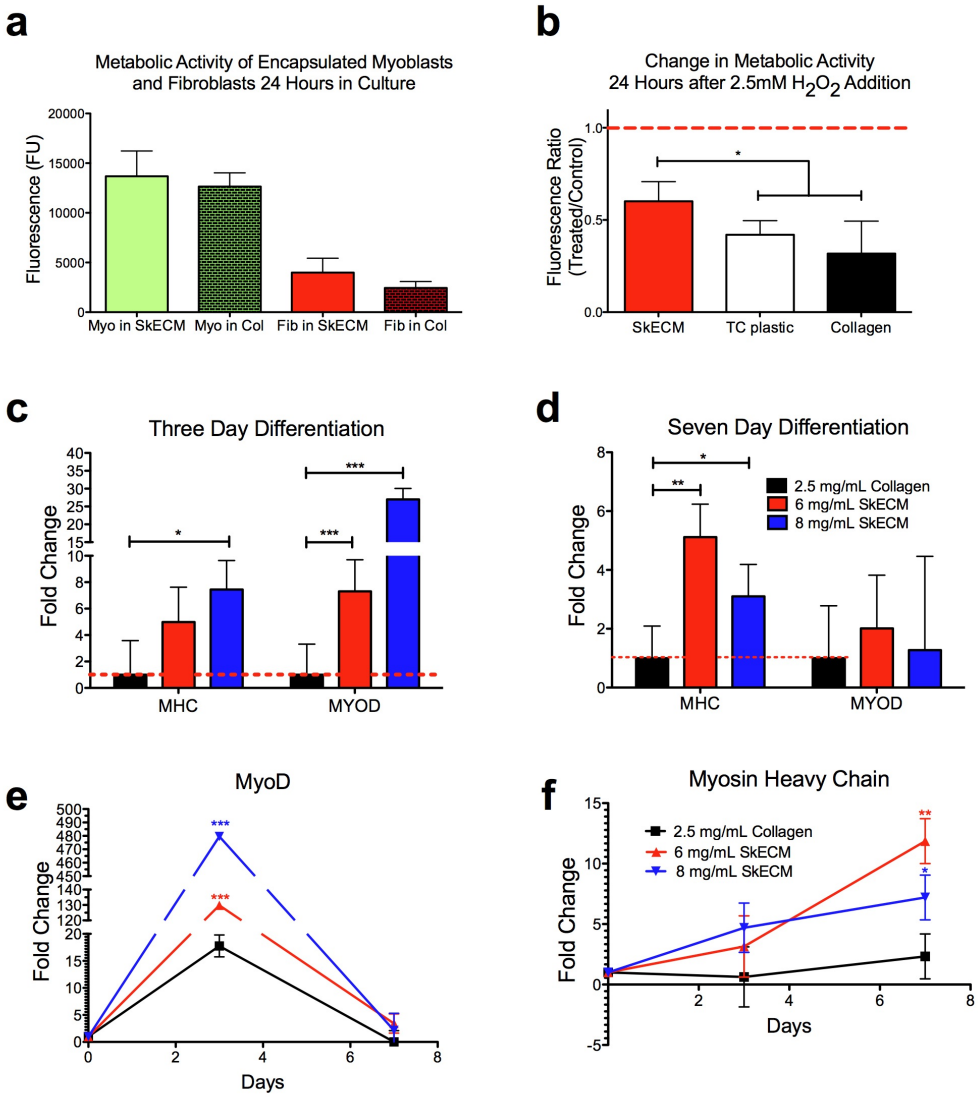
a
Metabolic Activity of Encapsulated Myoblasts and Fibroblasts 24 Hours in Culture
Fluorescence (FU)
20000
15000
10000
5000
0
Myo in SkECM
Myo in Col
Fib in SkECM
Fib in Col
b
Change in Metabolic Activity 24 Hours after 2.5mM H_2O_2 Addition
Fluorescence Ratio (Treated/Control)
1.0
0.5
0.0
*
SkECM
TC plastic
Collagen
c
Three Day Differentiation
Fold Change
40
35
30
25
20
15
10
8
6
4
2
0
*
***
***
MHC
MYOD
d
Seven Day Differentiation
Fold Change
8
6
4
2
0
*
**
2.5 mg/mL Collagen
6 mg/mL SkECM
8 mg/mL SkECM
MHC
MYOD
e
MyoD
Fold Change
500
490
480
470
460
450
140
130
120
20
15
10
5
0
***
***
0
2
4
6
8
Days
f
Myosin Heavy Chain
Fold Change
15
10
5
0
-5
2.5 mg/mL Collagen
6 mg/mL SkECM
8 mg/mL SkECM
**
*
2
4
6
8
Days

4.3.3 The SkECM protects myoblast viability through syringe injections

In order to evaluate whether delivery of this material and cells was feasible via injection, myoblast viability was evaluated after passing through the syringe. As previously mentioned, cell shearing can be a substantial cause for cell death. Upon resuspension, cells were approximately 99% viable after resuspension in PBS or SkECM at 6 or 8 mg/mL at 4 million cells/μL. Increasing the concentration to 10 mg/mL SkECM was not tested because the material was too viscous to flow through a 27G needle. The cell-material solution after passing through the syringe was evaluated via Trypan Blue for gauge sizes 25, 27, and 30. Viability of the cells decreased as gauge size increased in PBS as expected. Viability at all gauge sizes in the SkECM groups was significantly increased compared to the respective gauge for the PBS group (Fig. 4.3).

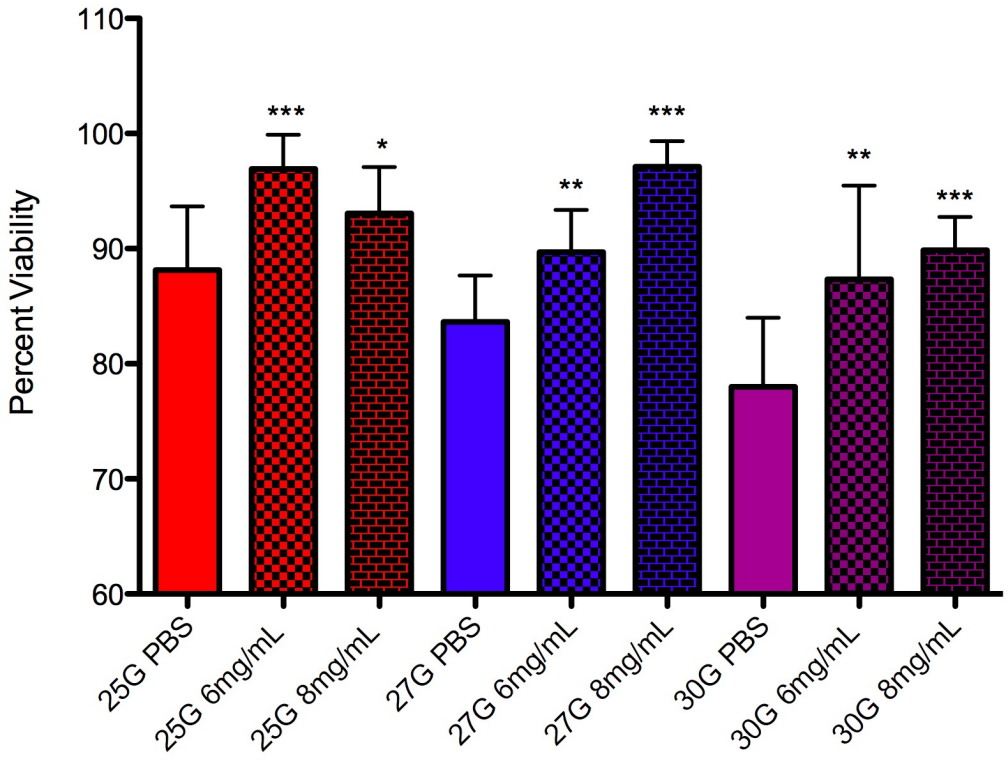

Figure 4.3: **Myoblast viability post-injection through 25, 27, and 30G needle sizes in the SkECM vs. PBS** Two million myoblasts were injected in 50uL of 6mg/mL, 8mg/mL SkECM solution or PBS in 25G, 27G, and 30G needle sizes. Trypan blue was used to measure the viability of these cells post-syringe injection by a syringe pump (n=10/group, *$p<0.05$, **$p<0.01$, ***$p<0.001$ compared to PBS control for each respective gauge size). Values represent mean ±SD.

4.3.4 Injection into naïve mouse tibialis anterior (TA)

Healthy mouse hindlimbs were injected with either myoblasts in PBS, 6 mg/mL SkECM, or 8 mg/mL SkECM. Noninvasive imaging of cells (IVIS) injected into the TAs of mice was recorded every day for one week and relative radiant efficiency was measured. The 8 mg/mL SkECM showed significant increases in DiR fluorescent signal compared to PBS (Fig. 4.4a) when normalized to the signal immediately after injection. After one week, the TAs were excised and re-imaged for total radiant efficiency on the IVIS to confirm that the cells were localized to the specific muscle of interest (Fig. 4.4b). The 8 mg/mL gels showed increased myoblast cell retention within the TAs compared to PBS and the 6 mg/mL group. Immunofluorescence of the limbs confirmed this finding by quantifying amount of GFP positive tissue area compared to total area in excised tissue (Fig. 4.4c). Colocalization with myosin heavy chain showed that not only were these cells present, but also engrafted into the muscle. The SkECM groups again demonstrated that there were more cells engrafted in the TA after 7 days.

Figure 4.4: **Myoblast cell viability and engraftment measurements in healthy tibialis anterior.** Mice hindlimbs were injected with 1 million DiR labeled GFP-myoblasts in 25 μL of either 6 mg/mL, 8 mg/mL SkECM or PBS (n=10/group). **(a)** IVIS measurements show change in fluorescence over seven days relative to the day 0 time-point. **(b)** Tissue was excised to confirm that these cells remained in the TA under IVIS measurements. **(c)** GFP engraftment was measured by histology using an anti-GFP antibody stain (green) and myosin heavy chain (red). GFP engraftment was calculated by measuring percent of area GFP+ in each group. (*$p<0.05$, **$p<0.01$, ***$p<0.001$). Values represent mean $\pm$SEM in all graphs.

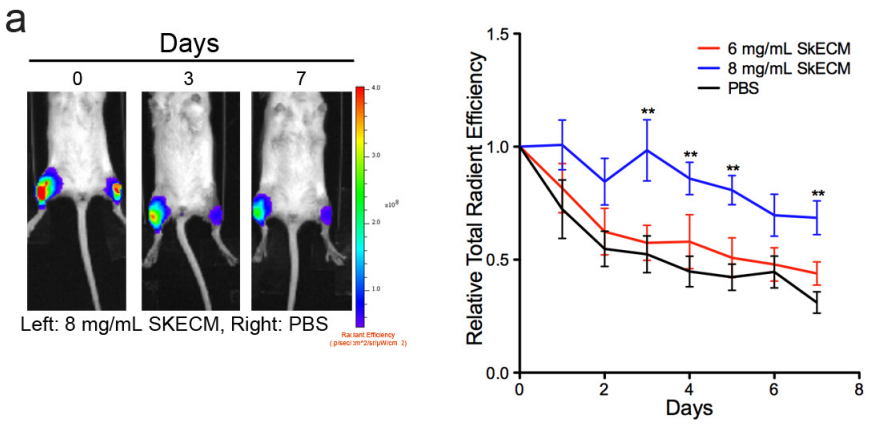
a
Days
0
3
7
Left: 8 mg/mL SKECM, Right: PBS
6 mg/mL SkECM
8 mg/mL SkECM
PBS
Relative Total Radient Efficiency
Days

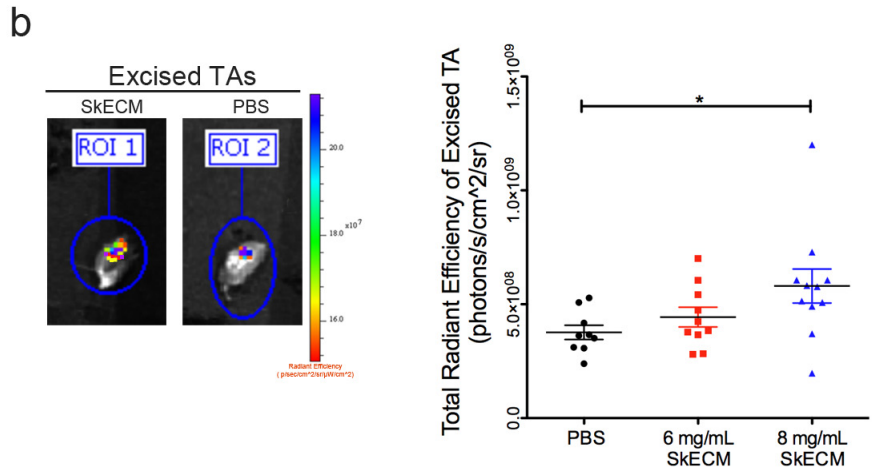
b
Excised TAs
SkECM
PBS
ROI 1
ROI 2
Total Radiant Efficiency of Excised TA
(photons/s/cm^2/sr)
PBS
6 mg/mL SkECM
8 mg/mL SkECM

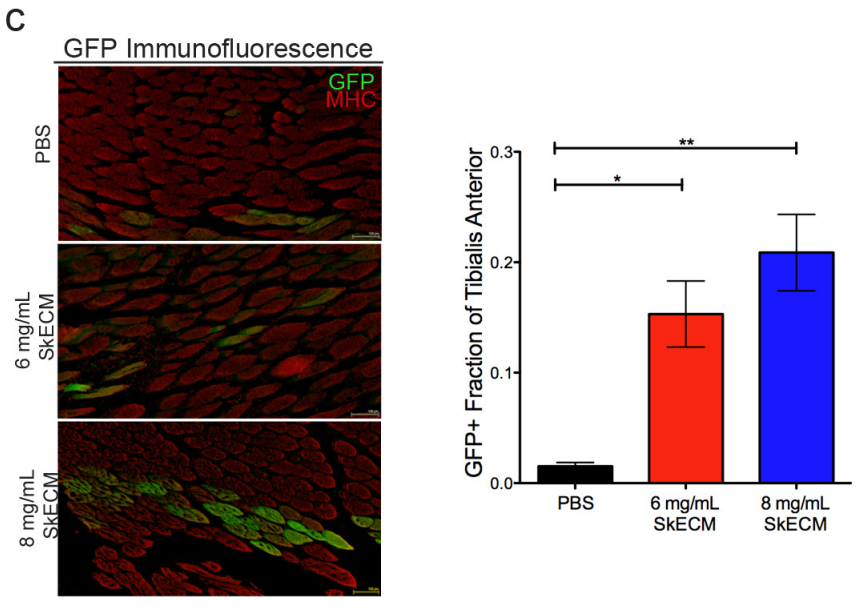
c
GFP Immunofluorescence
GFP
MHC
PBS
6 mg/mL SkECM
8 mg/mL SkECM
GFP+ Fraction of Tibialis Anterior
PBS
6 mg/mL SkECM
8 mg/mL SkECM

4.3.5 Fibroblasts protect myoblasts in SkECM co-culture and increase differentiation after one week

For the following studies we only used the 8 mg/mL SkECM formulation as the delivery vehicle because it outperformed PBS and 6 mg/mL in retaining cells in the TA. We sought to investigate whether adding 10% mCherry fibroblasts into the encapsulation in SkECM would improve viability and differentiation based on previous work demonstrating a 9:1 myoblast to fibroblast ratio to be important in *ex vivo* muscle formation [141]. eGFP myoblasts were encapsulated the same way as in monoculture studies in an 8 mg/mL SkECM hydrogel.

For the first experiment they were encapsulated in a well of a transwell with or without skeletal fibroblasts in the upper chamber. The fibroblast group increased encapsulated myoblast metabolic activity after seven days in a transwell, indicating that paracrine activity alone of the fibroblasts positively influences myoblast behavior in the 3D matrix (Fig.4.5a). Next, myoblasts were either encapsulated with or without 10% skeletal fibroblasts in 8 mg/mL gels and subjected to GM with or without H_2O_2 to simulate R.O.S. *in vitro*. The co-culture of myoblasts and fibroblasts had significantly higher metabolic activity under R.O.S. conditions when normalized to their untreated control compared to encapsulated monocultures of myoblasts or fibroblasts subjected to the same conditions (Fig. 4.5b).

We assessed extent of myogenic differentiation by culturing a monoculture or co-culture of encapsulated SkECM constructs in DM for 3-7 days. There was a noticeable increase in both MyoD expression on Day 3 and MHC expression on Day 7 for the myoblast-fibroblast co-culture (Fig 4.5c-d). Myotubes were visually confirmed in the co-culture and were much more elongated and multi-nucleated compared to myoblast alone (Fig. 4.5e-f). Unlike the monocultures, the co-cultures further visually reduced the size of the entire cel-gel construct. By 9 days, myotubes in co-culture spontaneously contracted indicating an increased maturation towards a muscle-like construct. It was hypothesized that the fibroblasts were further remodeling the matrix and thus allowing myotube formation and contraction. Matrix remodeling in the co-culture group was confirmed upon tethering

the SkECM with an Alexa Fluor 568 NHS, labeling the primary amines on the matrix. After 7 days, the co-culture group showed a substantial reorganization of the matrix compared to the monoculture, which had no apparent effect on matrix structure (Fig. 4.6).

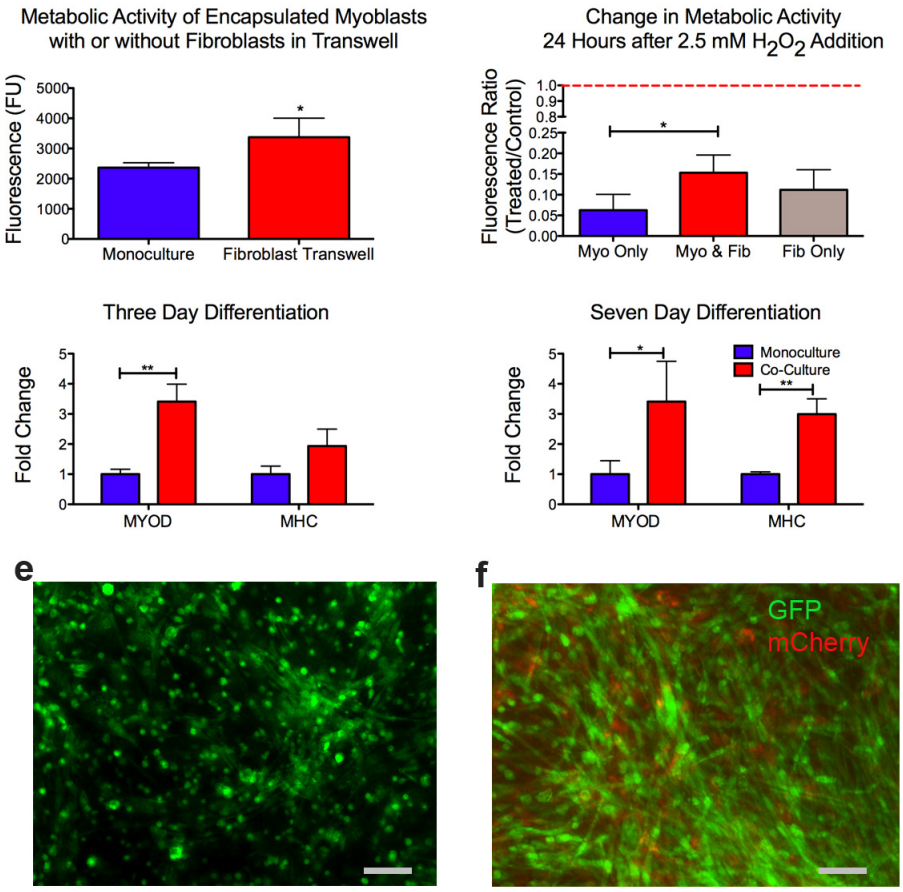

Figure 4.5: **Monoculture vs. Co-culture *in vitro* comparison encapsulated in 8 mg/mL SkECM. (a)** 600,000 Myoblasts were encapsulated in 50 μL of 8 mg/mL SkECM in transwell plates. Once seeded either 60,000 fibroblasts were placed on top with media or no cells as a control (n=6/group). Fluorescence signal by Alamar Blue was compared after one week in culture. **(b)** Myoblasts were encapsulated similarly as before with or without 10% mCherry fibroblasts. 2.5 mM H_2O_2 was added to the media and metabolic activity was measured after 12 hours and compared to an untreated control in each respective group (n=6/group). **(c, d)** RT-PCR gene expression measurement of monoculture or co-culture encapsulated in 8mg/mL SkECM for myosin heavy chain (MHC) and MyoD at 3 and 7 days in DM. All values are normalized to day 0 time-point. . **(e-f)** eGFP myoblasts and mCherry fibroblasts were imaged under a fluorescent microscope (Scale bar = 100 μm). Far more myotubes were observed in the co-culture group (f) compared to the monoculture (e). Values represent mean ±SD in all graphs (*p<0.05, ***p<0.001).

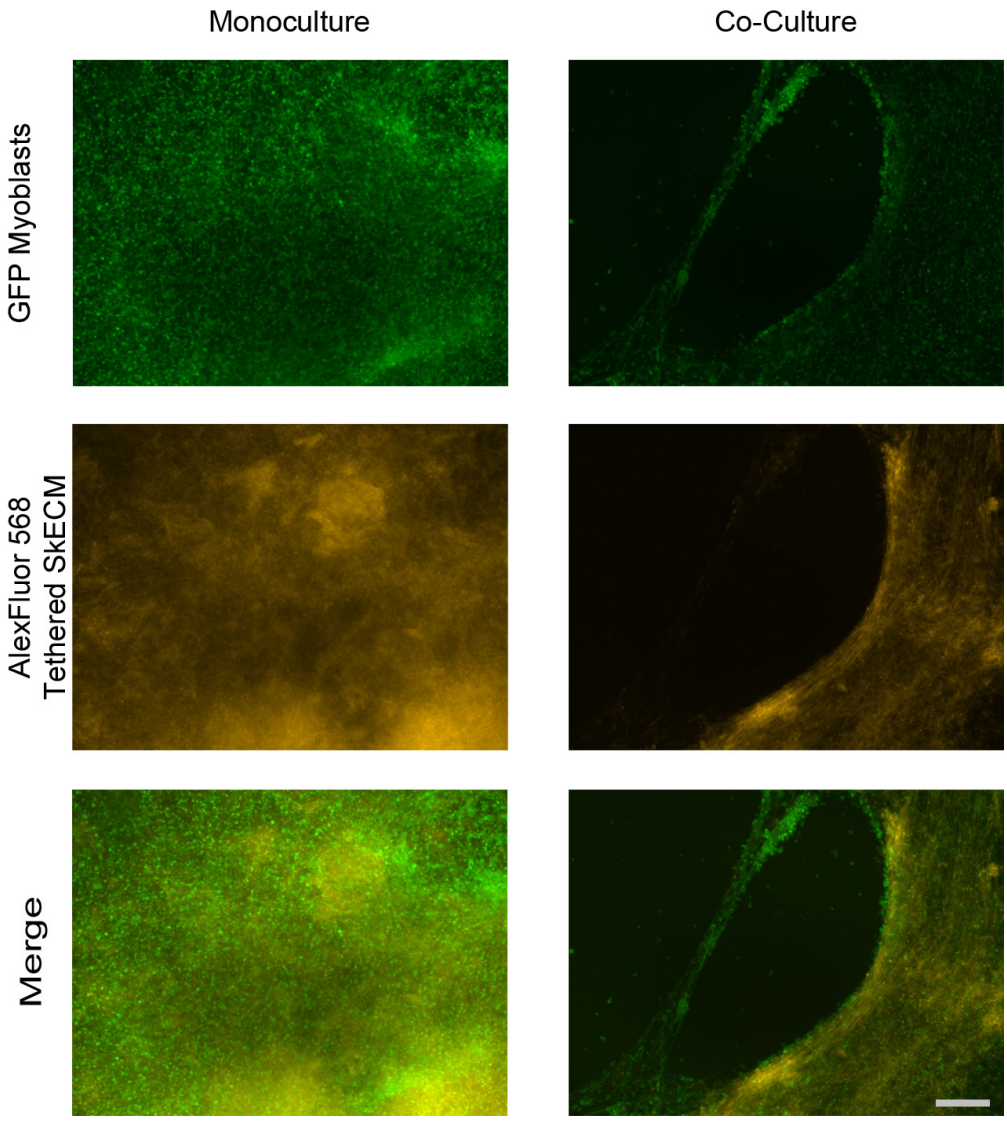

Figure 4.6: **Encapsulated GFP myoblasts with or without skeletal fiboroblasts in NHS-tethered SkECM *in vitro*.** NHS-568 alexa fluor was added to 8 mg/mL SkECM solution and vortexed prior to gelation. Cells were resuspended and encapsulated in this gel. The ECM in the monoculture groups did not reorganize or change over the course of one week. However in the co-culture groups the ECM showed increased organization and remodeling. Notice the elongated and highly organized fibrous strands of ECM in the co-culture group (n =6/group, scale bar = 100 μm).

4.3.6 Cell retention is increased in ischemic mice TAs with SkECM and fibroblasts

Extent of cell retention and viability *in vivo* is greatly influenced by the pathogenic state of the muscle. As previously demonstrated, the 8 mg/mL SkECM increases cell retention in healthy limbs compared to PBS. We sought to test whether this same outcome is achieved in a peripheral artery disease model. Additionally, from the encouraging *in vitro* data, we also included one group containing 10% of the total cell number to be fibroblasts. The femoral artery and vein were removed from the right leg of the mice. Myoblasts in saline, 8 mg/mL SkECM, or 8 mg/mL SkECM with 10% fibroblasts were used in this study (n=10/group). All groups were injected 7 days post-surgery and IVIS measurements were taken on day 0, 3, and 7. Cell retention by DiR-labelled myoblasts recorded by the IVIS was increased in the groups containing SkECM compared to saline at day 3, and significantly increased in co-culture groups on day 7 compared to saline (Fig. 4.7a,b). The limbs were excised 42 days post surgery, and anti-GFP antibody was used to quantify amount of GFP engraftment in each TA. Immunofluorescence shows an increase in GFP fluroescence in co-culture groups compared to saline and SkECM with myoblasts alone (Fig. 4.7c).

4.3.7 Perfusion is significantly increased in SkECM groups after 42 days

PERIMED laser Doppler speckle contrast analysis measurements showed an increasing trend in perfusion on day 17 and 28 for the groups containing the SkECM vs. myoblasts injected in only saline. Day 42 showed a significant difference between both groups containing SkECM vs. saline (Fig. 4.7d). The group containing fibroblasts showed a higher mean perfusion compared to all other groups but was not significantly compared to myoblasts in SkECM (Fig. 4.7e). On day 42, each animal's perfusion was subtracted from the initial measurement at 7 days post-surgery (pre-injection). The SkECM groups significantly increased perfusion compared to saline injected groups (**$p<0.01$, *$p<0.05$) (Fig. 4.7e). The average

perfusion in the saline groups did not change significantly from day 7 to day 42-post surgery (Fig. 4.7f). This indicates that the SkECM not only helped facilitate engraftment but also most likely had some increased vascular potential since no improvement was observed when myoblasts were injected alone. To confirm, TAs were excised, sectioned and stained with CD-31 and alpha-SMA to detect capillaries and arterioles (Fig. 4.7g). Capillaries, arterioles over 10 μm and over 25 μm were, in general, significantly higher than myoblasts delivered in saline (Fig. 4.7h-j). This further demonstrates that the SkECM delivered with myoblasts has the potential to increase vessel formation in the ischemic limb.

Figure 4.7: **Injection of skeletal myoblasts in a hindlimb ischemia model in either saline, SkECM, or SkECM with fibroblasts.** Mice were subjected to femoral artery and vein ligation (n=10/group). Perfusion was measured post surgery and on day 7 pre-treatment. On day 7, mice TAs were injected with 1 million myoblasts in either saline, 8 mg/mL SkECM, or with 100,000 fibroblasts and 8 mg/mL SkECM. **(a)** DiR-labelled myoblasts imaged under IVIS. Representative transillumination images showing myoblast cell retention in each group by IVIS on day 0, 3, and 7. The saline group signal visually reduces by day 3. **(b)** IVIS epifluorescence measurements were recorded on day 0, 3, and 7 and all data normalized to day 0 (**$p<0.01$, n=10/group compared to saline control). **(c)** Percentage of TA that stained GFP+ in each TA is calculated per total tibialis anterior cross section analyzed. Co-culture groups had significantly more GFP fluorescence (*$p<0.05$, n=9/group). **(d)** Representative laser speckle images of each group on day 42. Healthy limbs are on the left and ischemic/treated limbs are on the right. Areas of increased perfusion are indicated by yellow-red color. **(e)** Perfusion was measured for the ischemic leg relative to the healthy limb for each animal over the course of the study on day 7, 17, 21, and 42 days post-surgery. Gray dashed line represents administration of treatment. Significant differences were observed on day 42 for SkECM groups compared to saline (*$p<0.05$, **$p<0.01$ compared to saline control). Overall change for each animal from time of treatment to day 42 is plotted in **(f)** (*$p<0.05$, **$p<0.01$). **(g)** Representative images for CD31 (green) and alpha-smooth muscle actin (red) staining for capillaries and arterioles respectively (Scale bar = 200 μm). Quantification of **(h)** capillaries, **(i)** arterioles greater than 10 μm and **(j)** 25 μm. In **(h-j)** number of each were significantly greater in general in the SkECM groups (*$p<0.05$, **$p<0.01$, n=8/group). Values represent mean $\pm$SEM in all graphs.

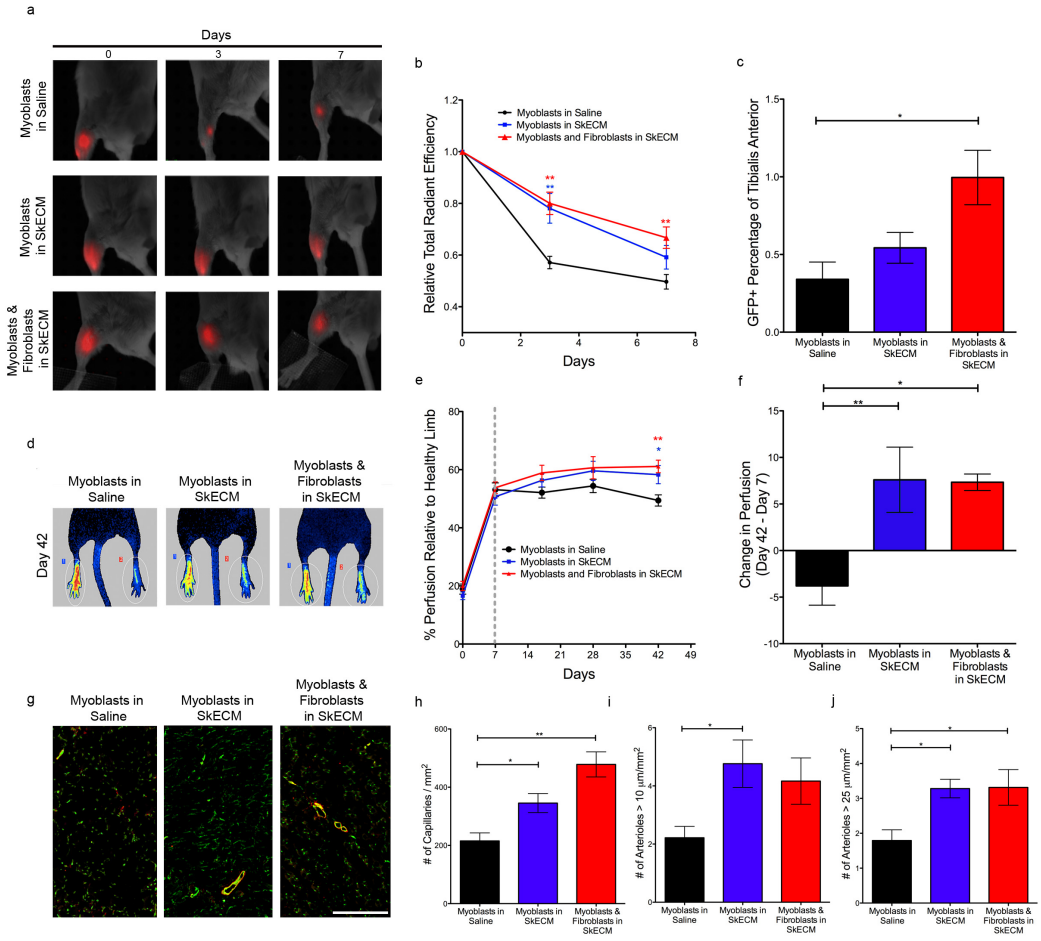
a
Days
0
3
7
Myoblasts in Saline
Myoblasts in SkECM
Myoblasts & Fibroblasts in SkECM
b
Relative Total Radiant Efficiency
Myoblasts in Saline
Myoblasts in SkECM
Myoblasts and Fibroblasts in SkECM
Days
c
GFP+ Percentage of Tibialis Anterior
Myoblasts in Saline
Myoblasts in SkECM
Myoblasts & Fibroblasts in SkECM
d
Myoblasts in Saline
Myoblasts in SkECM
Myoblasts & Fibroblasts in SkECM
Day 42
e
% Perfusion Relative to Healthy Limb
Myoblasts in Saline
Myoblasts in SkECM
Myoblasts and Fibroblasts in SkECM
Days
f
Change in Perfusion (Day 42 - Day 7)
Myoblasts in Saline
Myoblasts in SkECM
Myoblasts & Fibroblasts in SkECM
g
Myoblasts in Saline
Myoblasts in SkECM
Myoblasts & Fibroblasts in SkECM
h
# of Capillaries / mm2
i
# of Arterioles > 10 µm/mm2
j
# of Arterioles > 25 µm/mm2

4.4 Discussion

We successfully developed an encapsulation method *in vitro* that allows for myoblasts to be cultured in a three dimensional decellularized skeletal matrix hydrogel (SkECM). Thus far no groups have been successfully able to encapsulate cells *in vitro* using purely decellularized matrix hydrogels. From the *in vitro* experiments it is clear that the skeletal muscle matrix not only restores metabolic activity of myoblasts (suggesting increased viability of myoblasts) in culture better than collagen when subjected to reactive oxygen species, but also promotes differentiation of the myoblasts over the course of seven days. R.O.S. have been demonstrated as a significant contributor in cell apoptosis upon delivery to ischemic tissue [142, 143, 144]. The complex microenvironment (glycoasaminoglycans, proteoglycans, multiple structural proteins, and potentially various growth factor binding sites) of the SkECM could be contributing to an overall increase in cell viability under these stressed conditions. The differentiation process is easily observed via enhanced myogenic gene expression by qRT-PCR and increased myotube formation in the SkECM over collagen. This has been previously shown to be true with C2C12 myoblasts on a SkECM 2-D coating but never as a 3-D hydrogel [37]. Recapitulating this 3-D environment *in vitro* mimics a more physiologically accurate model for understanding cell-ECM interactions.

The hydrogel itself is not solely biochemically protective but acts as a mechanical buffer, decreasing the impact of shear stress between large loading densities of cells and the syringe needle. The needle topography has been shown to be inhomogeneous causing imperfect laminar flow upon ejection [145]. There is data to suggest that there are multiple materials that can be tuned to promote this resistance to shear death effect [129]. However, the material need not be modified like other materials to improve the viability through the needle, regardless of the gauge size (25, 27, and 30G). This potentially provides support for the use of smaller needle sizes to deliver cells to decrease pain for the patient.

Upon injection in healthy TAs, we monitored DiR signal from pre-labeled myoblasts by IVIS epifluorescent measurements. It is important to note the limitations of this DiR dye. For short-term studies, 0-10 days, it has been shown to

be useful for cell tracking and quantification [146, 147, 148, 149, 150, 151]. The DiR dye is extremely advantageous because it allows fluorescent quantifications in the far infrared channel which has little to no background signal from the animal itself. However, because the dye has a short half-life, we did not track the cells 7 days post-injection as the resolution of the dye substantially decreased and thus no further quantification was made. Over the course of 7 days, the 8 mg/mL SkECM formulation showed higher overall signal than the other groups. This indicates and was confirmed upon excision and histological analysis for anti-GFP that retention, viability, and engraftment were markedly increased in this group compared to injections with saline or the 6mg/mL SkECM group. It is believed that this is most likely due to increased matrix density for cell anchorage, faster gelling time, and a stiffer microenvironment which promotes a favorable cell niche. As mentioned previously, higher concentrations could perform even better than those tested here. However, concentrations higher than 10 mg/mL liquid SkECM would not flow through a 27G needle consistently. Thus for translational purposes, it was excluded from the study. Since the 8 mg/mL SkECM outperformed saline and 6 mg/mL in retention and engraftment and higher concentrations were not feasible, the remainder of the study relied solely on 8 mg/mL SkECM as the vehicle for *in vitro* and *in vivo* cell studies.

As mentioned, we hypothesized that addition of fibroblasts with myoblasts would aid in myoblast viability and myotube maturation encapsulated in the SkECM. When fibroblasts were added to the myoblasts in the SkECM at 10% of the total cell number, an even more enhanced protective effect was observed in a H_2O_2 stressed environment. Fibroblasts potentially withstood these conditions better, but more likely they are sharing positive anti-apoptotic paracrine/contact mediated signals with the myoblasts. This is hypothesized to be the case because we demonstrate that fibroblasts on their own encapsulated in SkECM do not recover as well as the co-culture in these conditions compared to the untreated control. Similar synergistic effects have been previously demonstrated, and that a positive bi-directional signaling cascade is observed when the two cell types are cultured together [109]. Differentiation of the myoblasts when encapsulated with

fibroblasts is markedly enhanced both visually with contracting myotubes by day 9 and with increased gene expression for MyoD and MHC over 7 days. This is most likely due to the fibroblasts reorganizing the matrix, aligning the SkECM and promoting a stiffer environment for the myoblasts to fuse, align and eventually contract. This phenomena has been supported by other groups showing that myoblast differentiation is significantly increased on stiffer, "muscle-like" substrates [152, 153]. This is suggested by an obvious shrinkage of the construct in co-culture compared to monoculture, a reorganization of the SkECM, and alignment of an NHS-568 alexa fluor tethered SkECM hydrogel when fibroblasts were present.

We sought to test whether the addition of SkECM with or without fibroblasts for myoblast delivery would increase retention and blood perfusion in a PAD model. The ischemia model used in this study attempts to recapitulate the decreased perfusion in the hind limbs. By injecting one-week post trauma, we allow the majority of the body's natural immune response to to repair the damage before administration of other treatments. This is more representative of what occurs in humans as a result of PAD onset. The natural ability by collateral formatin of the rodent to recover from this surgery is highlighted by the increase in perfusion from 20-50% of the healthy limb from day 0 to 7 [154, 155].

DiR-labeled myoblasts injected in the ischemic TA were measured noninvasively by IVIS on day 0, 3 and 7 post-treatment. Retention in the SkECM groups was significantly greater than saline at day 3. The co-culture group showed marked improvement on day 7 compared to the other groups. We hypothesize that this phenomena is due to the SkECM protecting cells from apoptosis in early onset into ischemic environment (0-3 days). After the cells are in place, the fibroblasts are required to keep myoblasts viable via positive cell signaling between fibroblasts and myoblasts (3-7 days). Interestingly perfusion measurements were equivalent between monoculture and co-culture groups in the SkECM, but both showed far more improvement than myoblasts in saline by day 42. This suggests that the SkECM is essential to promote increased blood flow. Myoblasts without a material carrier are ineffective at both retention and did not improve blood perfusion when injected into the TA. This data supports that the SkECM as pre-

viously demonstrated promotes vessel formation [37]. It is acknowledged that in order to increase muscle repair these myoblasts are required to fuse and engraft. The IVIS data suggests that this is promoted with both matrix and fibroblasts by increased myoblast retention. Compared to the standard of care treatment, this shows that a combined therapy can potentially increase muscle engraftment while also increasing blood perfusion into the ischemic limb.

Overall this data suggests broadly that delivery of myoblasts in saline is not enough to create a therapy that both improves muscle repair and increases blood flow in a PAD model after 5 weeks post-administration. The SkECM is needed to aid in the initial deliver of cells, protecting them from shear and a harsh ischemic microenvironment. The SkECM further improves blood flow to the damaged region. The addition of skeletal fibroblasts appears to maintain myoblast retention and viability at 7 days, indicating perhaps a long-term affect on myoblast cell survival. Multiple cell therapy in combination with biomaterial delivery may be the next step in a feasible therapeutic for a disease that causes multiple issues of lack of perfusion and extreme muscle damage.

Chapter 4 is in part currently being prepared for submission for publication of the material: Rao N, Agmon G, Tierney M, Braden R, Sacco A, Christman KL. Improving myoblast cell viability by co-delivery of an injectable skeletal-muscle specific microenvironment for treatment of peripheral artery disease. The dissertation author was the primary author.

Chapter 5

Conclusion and Future Directions in Skeletal Muscle Engineering

5.1 Summary of Dissertation

Throughout this dissertation we have stressed the need for newer, more advanced technologies. These technologies are required to understand mechanistically what is occurring at a basic biology level. In order to do so, they need to mimic the native *in vivo* microenvironment *in vitro*, allow for easy control and interfacing, and provide user-defined tunable parameters for customization of any co-culture system. The more these technologies advance, the more likely they are better at predicting behavior *in vivo* and thus *in vitro* to *in vivo* translation becomes more powerful.

We show that a novel technology, the reconfigurable co-culture device is a powerful tool that parses out the paracrine vs. contact effects of two cell types interacting with one another. The two populations are easily manipulated and separated for in-depth analysis on one population alone. With this technology we learned that myoblasts at a protein level experience specific differences in cell behavior when fibroblasts are in contact, in gap, or not present at all. We show that fibroblasts inhibit myoblast differentiation. However, when in contact this inhibition increases myotube alignment, which we acknowledge can undoubtedly

be a beneficial criteria in creating functional muscle tissue.

Next, we acknowledge the limitations of this device and realize the direction that would be required for this technology to advance and become more useful and relevant for *in vitro* studies. We develop a method for integrating a substrate with a tunable stiffness on the device based on the recent cell-substrate findings in the field - that cell behavior is greatly affected by substrate modulus. More importantly, stem cell fate is greatly governed by a very specific stiffness range that is representative of that found *in vivo*. We show that combining an organized co-culture device with variable stiffnesses can lead to increased differentiation. In this particular model system we show adipose derived stem cells differentiate towards an increased myogenic phenotype when co-cultured in contact with myoblasts on a 10 kPa gel.

Further, we take what we have learned from co-culture studies on this device in hopes of increasing efficacy of a currently investigated clinical therapy - myoblast cell injections for the treatment of peripheral artery disease. These cells have limited engraftment potential due to low cell viability immediately after transplantation and the harsh ischemic environment. However, groups continue to investigate these cells because they have several advantages and serve a dual role of increasing angiogenesis via paracrine signaling, and repairing damaged muscle tissue. We investigate the potential of these primary cells to interact with primary fibroblasts *in vitro* in a decellularized skeletal muscle matrix hydrogel (SkECM). We show that we can encapsulate myoblasts in the SkECM with fibroblasts. This setup improves cell viability, protects cells from R.O.S., and dramatically increases differentiation compared to controls. Upon injection through a syringe prior to gelation we see preserved viability of myoblasts in SkECM post-injection versus injecting in saline. Lastly, we inject myoblasts with SkECM in the TAs of mice and show increases in engraftment in 8 mg/mL formulations. When injecting fibroblasts, myoblasts and SkECM in a hindlimb ischemia model we observe increased engraftment. Hindlimb perfusion and arteriole generation is increased six weeks post surgery when the SkECM is present.

Scientists in the last few years are just now on the cusp of discovering how

multiple cell therapy, biomaterials and the combination of the two impacts a relevant disease. In an ideal world, only one of these therapies be required. However, to substantially improve and create viable treatments for not only restoration of overall physiological function, but further improving the *quality* of treatment to a re-establishment of a **normal** physiological state is an added challenge. We show that both multiple cells and biomaterial are required to add in a combinatorial way to address both muscle repair and restoration of blood perfusion.

5.2 Future Directions

We have shown a very bottom-up approach to understanding and developing a treatment for PAD. We acknowledge the clinical need and problem, and work from understanding cell behavior in a dish to translation towards an improved therapy. One of the major issues, as we have previously eluded to throughout the thesis, is in developing *in vitro* models that can actually model *in vivo* systems, in this case muscle damage. Our *in vitro* models are limited and even though we have demonstrated a novel device that has been advanced even further to systematically probe multiple variables, there is still a great deal of work to be done in more accurately defining these variables in the context of physiologically relevant systems. Advancing systems may want to consider the following: 3D vs. 2D culture, tri-culture or more cell types present, recapitulating the immune response to be a constant variable to any damaged state *in vitro*, addition of physical forces such as strain or shear forces, using hypoxic or low-pH conditions, stiffness as well as specific protein composition, and even various media types that would not only be more accurate of the body but also temporally variable as the body repairs in time.

There are multiple next steps and future directions for both improving the technology to study in vitro and develop an even better therapeutic in vivo. There are still other changes that can be made to make the reconfigurable co-culture device more useful for co-culture studies. The material as it stands is made of silicon. If the material was plastic or glass, the user could image directly through

the device rather than invert. This may also allow for cheaper, less damage-prone analysis of the device. Instead of a binary change from contact to 80 microns gap, one could make a continuous, user-defined distance between the two populations. Since soluble proteins can have short half-lives and in vivo distances between cell populations may be even closer than 80 microns but not touching, it is important to be able to model these interactions in a dish. Not only are the distance between interactions important, but also the 3D orientation of cells and ECM. Developing an organized co-culture device that models cell behavior in 3D and still allows for dynamic cell manipulation and analysis of one single population.

As shown in this thesis, the advanced reconfigurable co-culture device with a tunable stiffness is very useful in understanding complex cell-matrix interactions. It would be useful to further investigate the role that various matrix proteins tethered to the polyacrylamide surface does in driving stem cell differentiation. The SkECM tethered to a myogenic (10 kPa) stiffness could further push adipose derived stem cells towards muscle lineage. It is important to understand the implications for priming these ASCs toward a muscle lineage and potentially using these primed cells to treat PAD. Their angiogenic potential as well as myogenic fate could be more advantageous than myoblasts in repairing muscle while promoting blood flow in the ischemic limb.

In order to continue to make the PAD cell therapy better there are a number of other considerations to be made in the future. First, the myoblast cell type still may not be the ideal candidate therapy for PAD. As mentioned previously, mononuclear cells and mesenchymal stromal cells have shown a great deal of promise in increasing perfusion to the limbs. That being said, potentially a multiple cell approach with skeletal myoblasts could be useful in increasing muscle repair in the ischemic limb. Proper controls such as a sham without cells and a myoblast/fibroblast in saline group would be useful in understanding the efficacy of each alone. That way, the role of the cells vs. ECM vs. the combination of the two could be parsed out more accurately. This would help us understand whether tweaking the amount of ECM or the type/ratio/dosage/number of cells is the next step to address in therapeutic efficacy. In general, a more in depth analysis of

specific cell types and how they interact with the ECM for improved limb function would be the ideal next step in this process.

We have addressed some of these variables in the systems we have used and created, however, there are limitations to all these systems. Even if one could achieve an *in vitro* assay that accounts for all these variables, this is only half the battle. There is still a problem of analysis. In order to parse out which factor is generating some desired output, the user must find a way to systematically probe each input and isolate the one output. This creates an extensive matrix of potential solutions that are not as easily solvable as computational models because cellular empirical data is difficult to reproduce. We also may not clearly understand what the desired outcome is because we do not know the effect that will actually take place when introduce *in vivo*. For example in the case of muscle repair, are we interested in keeping myoblasts alive, or are we more interested in maturing them as quickly as possible? It is most likely a combination of the two but the answer is not binary.

Improvement in the way animal models are carried out and standardized is a direction that is critical in understanding how muscle repair can be achieved. Most animal models, in particular for PAD, consist of acute surgeries that ultimately not indicative of what happens when humans experience the pathogenesis. These acute surgeries drastically decrease blood flow as opposed to a gradual onset that takes place in humans. This is further complicated by the timing of treatment. Many groups will create the surgery and issue the treatment immediately thereafter. However, this is not at all what occurs in PAD patients. Treatment only occurs when the PAD patient actually has some relevant medical symptom such as hypertension, athlerosclerosis, cardiovascular issues, high blood pressure, increased pain in the legs or inability to walk, etc.

In order to advance the treatments demonstrated in this thesis an increasing level of complexity is most likely required. This involves either investigating another cell type, changing cell number and/or ratio, and potentially modulating the material properties of the SkECM. This thesis takes steps into the advancement of the state-of-the-art technologies and gives promise for a future, consistent,

and effective therapeutic for PAD.

Bibliography

[1] Hescheler J, Hauskeller C (2008) From basic research to the clinic. obstacles and options for stem cell therapies. Bundesgesundheitsblatt, Gesundheitsforschung, Gesundheitsschutz 51: 1014-1020.

[2] Hopkins PM (2006) Skeletal muscle physiology. Continuing Education in Anaesthesia, Critical Care amp; Pain 6: 1-6.

[3] Bendall JR (1967) The elastin content of various muscles of beef animals. Journal of the Science of Food and Agriculture 18: 553–558.

[4] Gillies AR, Lieber RL (2011) Structure and function of the skeletal muscle extracellular matrix. Muscle amp; Nerve 44: 318–331.

[5] Kherif S, Lafuma C, Fardeau M, Alameddine HS (1999) Expression of matrix metalloproteinases 2 and 9 in regenerating skeletal muscle: A study in experimentally injured andmdxmuscles. Developmental Biology 205: 158 - 170.

[6] Meyer GA, Lieber RL (2011) Elucidation of extracellular matrix mechanics from muscle fibers and fiber bundles. Journal of Biomechanics 44: 771 - 773.

[7] Turner N (2010) Fibroblast growth factor signalling: from development to cancer. Nat Rev Cancer 10: 116-129.

[8] Porter KE, Turner NA (2009) Cardiac fibroblasts: at the heart of myocardial remodeling. Pharmacol Ther 123: 255-78.

[9] Hawke TJ, Garry DJ (2001) Myogenic satellite cells: physiology to molecular biology. Journal of Applied Physiology 91: 534–551.

[10] Schultz E, Lipton BH (1982) Skeletal muscle satellite cells: Changes in proliferation potential as a function of age. Mechanisms of Ageing and Development 20: 377 - 383.

[11] Sharples AP, Al-Shanti N, Stewart CE (2010) C2 and c2c12 murine skeletal myoblast models of atrophic and hypertrophic potential: relevance to disease and ageing? Journal of cellular physiology 225: 240–250.

[12] CF Bentzinger MR YX Wang (2012) Building muscle: molecular regulation of myogenesis. Cold Spring Harb Perspect Biol 1;4.

[13] Norgren L, Hiatt WR, Dormandy JA, Hirsch AT, Jaff MR, Diehm C, Baumgartner I, Belch JJF (2010) The next 10 years in the management of peripheral artery disease: Perspectives from the 'pad 2009' conference. European Journal of Vascular and Endovascular Surgery 40: 375-380.

[14] Ouriel K (2001) Peripheral arterial disease. The lancet 358: 1257–1264.

[15] Kannel W, McGee D (1985) Update on some epidemiologic features of intermittent claudication: the framingham study. Journal of the American Geriatrics Society 33: 13–18.

[16] Zimmerman B, Palumbo P, O'fallon W, Ellefson R, Osmundson P, Kazmier F (1981) A prospective study of peripheral occlusive arterial disease in diabetes. iii. initial lipid and lipoprotein findings. In: Mayo Clinic proceedings. Mayo Clinic. volume 56, pp. 233–242.

[17] Luther M, Lepäntalo M, Albäck A, Matzke S (1996) Amputation rates as a measure of vascular surgical results. British journal of surgery 83: 241–244.

[18] Wolfe J (1986) Defining the outcome of critical ischemia-a one year prospective-study. In: British Journal of Surgery. Blackwell Science LTD, Oxford, England, volume 73, pp. 321–321.

[19] Iwase T, Nagaya N, Fujii T, Itoh T, Murakami S, Matsumoto T, Kangawa K, Kitamura S (2005) Comparison of angiogenic potency between mesenchymal stem cells and mononuclear cells in a rat model of hindlimb ischemia. Cardiovascular research 66: 543–551.

[20] Alev C, Ii M, Asahara T (2011) Endothelial progenitor cells: A novel tool for the therapy of ischemic diseases. Antioxidants Redox Signaling 15: 949-965.

[21] Lawall H, Bramlage P, Amann B (2011) Treatment of peripheral arterial disease using stem and progenitor cell therapy. J Vasc Surg 53: 445-53.

[22] Lawall H, Bramlage P, Amann B (2010) Stem cell and progenitor cell therapy in peripheral artery disease. Thromb Haemost 103: 696–709.

[23] Gupta R, Rao N, Kumar V (2011) Discovery of error-tolerant biclusters from noisy gene expression data. BMC Bioinformatics 12 Suppl 12: S1.

[24] Li Y, Zhang D, Zhang Y, He G, Zhang F (2010) Augmentation of neovascularization in murine hindlimb ischemia by combined therapy with simvastatin and bone marrow-derived mesenchymal stem cells transplantation. J Biomed Sci 17: 75.

[25] Asahara T, Masuda H, Takahashi T, Kalka C, Pastore C, Silver M, Kearne M, Magner M, Isner JM (1999) Bone marrow origin of endothelial progenitor cells responsible for postnatal vasculogenesis in physiological and pathological neovascularization. Circulation research 85: 221–228.

[26] Shi Q, Rafii S, Hong-De Wu M, Wijelath ES, Yu C, Ishida A, Fujita Y, Kothari S, Mohle R, Sauvage LR (1998) Evidence for circulating bone marrow-derived endothelial cells. Blood 92: 362–367.

[27] Sprengers RW, Lips DJ, Moll FL, Verhaar MC (2008) Progenitor cell therapy in patients with critical limb ischemia without surgical options. Annals of surgery 247: 411–420.

[28] Benoit E, O'Donnell Jr TF, Iafrati MD, Asher E, Bandyk DF, Hallett JW, Lumsden AB, Pearl GJ, Roddy SP, Vijayaraghavan K (2011) The role of amputation as an outcome measure in cellular therapy for critical limb ischemia: implications for clinical trial design. J Transl Med 9: 165.

[29] Bartel RL, Booth E, Cramer C, Ledford K, Watling S, Zeigler F (2013) From bench to bedside: review of gene and cell-based therapies and the slow advancement into phase 3 clinical trials, with a focus on aastrom's ixmyelocel-t. Stem Cell Reviews and Reports 9: 373–383.

[30] Powell RJ, Marston WA, Berceli SA, Guzman R, Henry TD, Longcore AT, Stern TP, Watling S, Bartel RL (2012) Cellular therapy with ixmyelocel-t to treat critical limb ischemia: the randomized, double-blind, placebo-controlled restore-cli trial. Molecular Therapy 20: 1280–1286.

[31] Menasché P (2005) Skeletal myoblast for cell therapy. Coronary artery disease 16: 105–110.

[32] Tedesco FS, Dellavalle A, Diaz-Manera J, Messina G, Cossu G (2010) Repairing skeletal muscle: regenerative potential of skeletal muscle stem cells. The Journal of clinical investigation 120: 11.

[33] Siminiak T, Kalawski R, Fiszer D, Jerzykowska O, Rzeźniczak J, Rozwadowska N, Kurpisz M (2004) Autologous skeletal myoblast transplantation for the treatment of postinfarction myocardial injury: phase i clinical study with 12 months of follow-up. American heart journal 148: 531–537.

[34] Hagège AA, Marolleau JP, Vilquin JT, Alhéritière A, Peyrard S, Duboc D, Abergel E, Messas E, Mousseaux E, Schwartz K (2006) Skeletal myoblast transplantation in ischemic heart failure long-term follow-up of the first phase i cohort of patients. Circulation 114: I–108.

[35] Menasché P, Hagège AA, Vilquin JT, Desnos M, Abergel E, Pouzet B, Bel A, Sarateanu S, Scorsin M, Schwartz K (2003) Autologous skeletal myoblast transplantation for severe postinfarction left ventricular dysfunction. Journal of the American College of Cardiology 41: 1078–1083.

[36] Gupta R, Losordo DW (2011) Cell therapy for critical limb ischemia moving forward one step at a time. Circulation-Cardiovascular Interventions 4: 2-5.

[37] Dequach JA, Lin JE, Cam C, Hu D, Salvatore MA, Sheikh F, Christman KL (2012) Injectable skeletal muscle matrix hydrogel promotes neovascularization and muscle cell infiltration in a hindlimb ischemia model. Eur Cell Mater 23: 400-12.

[38] Sacco A, Doyonnas R, Kraft P, Vitorovic S, Blau HM (2008) Self-renewal and expansion of single transplanted muscle stem cells. Nature 456: 502–506.

[39] Paschos NK, Brown WE, Eswaramoorthy R, Hu JC, Athanasiou KA (2014) Advances in tissue engineering through stem cell-based co-culture. Journal of tissue engineering and regenerative medicine .

[40] Goers L, Freemont P, Polizzi KM (2014) Co-culture systems and technologies: taking synthetic biology. Interface .

[41] Weber W, Daoud-El Baba M, Fussenegger M (2007) Synthetic ecosystems based on airborne inter-and intrakingdom communication. Proceedings of the National Academy of Sciences 104: 10435–10440.

[42] Basu S, Gerchman Y, Collins CH, Arnold FH, Weiss R (2005) A synthetic multicellular system for programmed pattern formation. Nature 434: 1130–1134.

[43] Zinchenko YS, Schrum LW, Clemens M, Coger RN (2006) Hepatocyte and kupffer cells co-cultured on micropatterned surfaces to optimize hepatocyte function. Tissue engineering 12: 751–761.

[44] Bhatia S, Balis U, Yarmush M, Toner M (1998) Microfabrication of hepatocyte/fibroblast co-cultures: Role of homotypic cell interactions. Biotechnology progress 14: 378–387.

[45] Wang R, Xu J, Juliette L, Castilleja A, Love J, Sung SY, Zhau HE, Goodwin TJ, Chung LW (2005) Three-dimensional co-culture models to study prostate cancer growth, progression, and metastasis to bone. In: Seminars in cancer biology. Elsevier, volume 15, pp. 353–364.

[46] Ou DB, Zeng D, Jin Y, Liu XT, Teng JW, Guo WG, Wang HT, Su FF, He Y, Zheng QS (2013) The long-term differentiation of embryonic stem cells into cardiomyocytes: an indirect co-culture model. PloS one 8: e55233.

[47] Laugwitz KL, Moretti A, Lam J, Gruber P, Chen Y, Woodard S, Lin LZ, Cai CL, Lu MM, Reth M (2005) Postnatal isl1+ cardioblasts enter fully differentiated cardiomyocyte lineages. Nature 433: 647–653.

[48] Camelliti P, McCulloch AD, Kohl P (2005) Microstructured cocultures of cardiac myocytes and fibroblasts: a two-dimensional in vitro model of cardiac tissue. Microscopy and Microanalysis 11: 249–259.

[49] Kim SM, Fukuda J, Khademhosseini A (2008) Patterned cocultures for controlling cell-cell interactions. Micro and Nanoengineering of the Cell Microenvironment Technologies and Applications .

[50] Hui EE, Bhatia SN (2007) Micromechanical control of cell-cell interactions. Proc Natl Acad Sci U S A 104: 5722-6.

[51] Buchanan CF, Szot CS, Wilson TD, Akman S, Metheny-Barlow LJ, Robertson JL, Freeman JW, Rylander MN (2011) Cross-talk between endothelial and breast cancer cells regulates reciprocal expression of angiogenic factors in vitro. J Cell Biochem .

[52] Sugiura S, Cha JM, Yanagawa F, Zorlutuna P, Bae H, Khademhosseini A (2013) Dynamic three-dimensional micropatterned cell co-cultures within photocurable and chemically degradable hydrogels. Journal of tissue engineering and regenerative medicine .

[53] Grounds MD, Yablonka-Reuveni Z (1993) Molecular and cell biology of skeletal muscle regeneration. Mol Cell Biol Hum Dis Ser 3: 210-56.

[54] McKeon-Fischer KD, Flagg DH, Freeman JW (2011) Coaxial electrospun poly(epsilon-caprolactone), multiwalled carbon nanotubes, and polyacrylic acid/polyvinyl alcohol scaffold for skeletal muscle tissue engineering. Journal of Biomedical Materials Research Part A 99: 493-9.

[55] Pavlath GK, Thaloor D, Rando TA, Cheong M, English AW, Zheng B (1998) Heterogeneity among muscle precursor cells in adult skeletal muscles with differing regenerative capacities. Developmental Dynamics 212: 495-508.

[56] Mann CJ, Perdiguero E, Kharraz Y, Aguilar S, Pessina P, Serrano AL, Munoz-Canoves P (2011) Aberrant repair and fibrosis development in skeletal muscle. Skelet Muscle 1: 21.

[57] LaFramboise WA, Scalise D, Stoodley P, Graner SR, Guthrie RD, Magovern JA, Becich MJ (2007) Cardiac fibroblasts influence cardiomyocyte phenotype in vitro. Am J Physiol Cell Physiol 292: C1799-808.

[58] Nichol JW, Engelmayr J G C, Cheng M, Freed LE (2008) Co-culture induces alignment in engineered cardiac constructs via mmp-2 expression. Biochem Biophys Res Commun 373: 360-5.

[59] Pirskanen A, Jaaskelainen T, Maenpaa PH (1994) Effects of transforming growth factor beta 1 on the regulation of osteocalcin synthesis in human mg-63 osteosarcoma cells. J Bone Miner Res 9: 1635-42.

[60] Porter KE, Turner NA (2009) Cardiac fibroblasts: At the heart of myocardial remodeling. Pharmacology Therapeutics 123: 255-278.

[61] Kobayashi H, Shimizu T, Yamato M, Tono K, Masuda H, Asahara T, Kasanuki H, Okano T (2008) Fibroblast sheets co-cultured with endothelial progenitor cells improve cardiac function of infarcted hearts. J Artif Organs 11: 141-7.

[62] Rohr S (2009) Myofibroblasts in diseased hearts: new players in cardiac arrhythmias? Heart Rhythm 6: 848-56.

[63] Peterson DJ, Ju H, Hao J, Panagia M, Chapman DC, Dixon IM (1999) Expression of gi-2 alpha and gs alpha in myofibroblasts localized to the infarct scar in heart failure due to myocardial infarction. Cardiovasc Res 41: 575-85.

[64] Sun Y, Kiani MF, Postlethwaite AE, Weber KT (2002) Infarct scar as living tissue. Basic Research in Cardiology 97: 343-347.

[65] Cooper ST, Maxwell AL, Kizana E, Ghoddusi M, Hardeman EC, Alexander IE, Allen DG, North KN (2004) C2c12 co-culture on a fibroblast substratum enables sustained survival of contractile, highly differentiated myotubes with peripheral nuclei and adult fast myosin expression. Cell Motil Cytoskeleton 58: 200-11.

[66] Zhang L, Yun H, Murray F, Lu R, Wang L, Hook V, Insel PA (2011) Cytotoxic t lymphocyte antigen-2 alpha induces apoptosis of murine t-lymphoma cells and cardiac fibroblasts and is regulated by camp/pka. Cell Signal 23: 1611-6.

[67] Otto A, Collins-Hooper H, Patel K (2009) The origin, molecular regulation and therapeutic potential of myogenic stem cell populations. J Anat 215: 477-97.

[68] Rando TA, Blau HM (1994) Primary mouse myoblast purification, characterization, and transplantation for cell-mediated gene therapy. Journal of Cell Biology 125: 1275-87.

[69] Fan Y, Maley M, Beilharz M, Grounds M (1996) Rapid death of injected myoblasts in myoblast transfer therapy. Muscle Nerve 19: 853-60.

[70] Beauchamp JR, Morgan JE, Pagel CN, Partridge TA (1999) Dynamics of myoblast transplantation reveal a discrete minority of precursors with stem cell-like properties as the myogenic source. Journal of Cell Biology 144: 1113-22.

[71] Peault B, Rudnicki M, Torrente Y, Cossu G, Tremblay JP, Partridge T, Gussoni E, Kunkel LM, Huard J (2007) Stem and progenitor cells in skeletal muscle development, maintenance, and therapy. Mol Ther 15: 867-77.

[72] Hui EE, Bhatia SN (2007) Micromechanical control of cell-cell interactions. Proc Natl Acad Sci U S A 104: 5722-6.

[73] Cook DR, Doumit ME, Merkel RA (1993) Transforming growth factor-beta, basic fibroblast growth factor, and platelet-derived growth factor-bb interact to affect proliferation of clonally derived porcine satellite cells. J Cell Physiol 157: 307-12.

[74] Wiedlocha A, Sorensen V (2004) Signaling, internalization, and intracellular activity of fibroblast growth factor. Curr Top Microbiol Immunol 286: 45-79.

[75] Stratos I, Madry H, Rotter R, Weimer A, Graff J, Cucchiarini M, Mittlmeier T, Vollmar B (2011) Fibroblast growth factor-2-overexpressing myoblasts encapsulated in alginate spheres increase proliferation, reduce apoptosis, induce adipogenesis, and enhance regeneration following skeletal muscle injury in rats. Tissue Eng Part A .

[76] Sheikh F, Fandrich RR, Kardami E, Cattini PA (1999) Overexpression of long or short fgfr-1 results in fgf-2-mediated proliferation in neonatal cardiac myocyte cultures. Cardiovasc Res 42: 696-705.

[77] Decker NK, Abdelmoneim SS, Yaqoob U, Hendrickson H, Hormes J, Bentley M, Pitot H, Urrutia R, Gores GJ, Shah VH (2008) Nitric oxide regulates tumor cell cross-talk with stromal cells in the tumor microenvironment of the liver. Am J Pathol 173: 1002-12.

[78] Said N, Smith S, Sanchez-Carbayo M, Theodorescu D (2011) Tumor endothelin-1 enhances metastatic colonization of the lung in mouse xenograft models of bladder cancer. J Clin Invest 121: 132-47.

[79] Hannon K, Kudla AJ, McAvoy MJ, Clase KL, Olwin BB (1996) Differentially expressed fibroblast growth factors regulate skeletal muscle development through autocrine and paracrine mechanisms. Journal of Cell Biology 132: 1151-1159.

[80] Flanagan-Steet H, Hannon K, McAvoy MJ, Hullinger R, Olwin BB (2000) Loss of fgf receptor 1 signaling reduces skeletal muscle mass and disrupts myofiber organization in the developing limb. Dev Biol 218: 21-37.

[81] Neuhaus P, Oustanina S, Loch T, Kruger M, Bober E, Dono R, Zeller R, Braun T (2003) Reduced mobility of fibroblast growth factor (fgf)-deficient myoblasts might contribute to dystrophic changes in the musculature of fgf2/fgf6/mdx triple-mutant mice. Molecular and Cellular Biology 23: 6037-48.

[82] Santiago JJ, Ma X, McNaughton LJ, Nickel BE, Bestvater BP, Yu L, Fandrich RR, Netticadan T, Kardami E (2011) Preferential accumulation and export of high molecular weight fgf-2 by rat cardiac non-myocytes. Cardiovasc Res 89: 139-47.

[83] Savage MP, Hart CE, Riley BB, Sasse J, Olwin BB, Fallon JF (1993) Distribution of fgf-2 suggests it has a role in chick limb bud growth. Dev Dyn 198: 159-70.

[84] Seghezzi G, Patel S, Ren CJ, Gualandris A, Pintucci G, Robbins ES, Shapiro RL, Galloway AC, Rifkin DB, Mignatti P (1998) Fibroblast growth factor-2 (fgf-2) induces vascular endothelial growth factor (vegf) expression in the endothelial cells of forming capillaries: an autocrine mechanism contributing to angiogenesis. J Cell Biol 141: 1659-73.

[85] Lim MJ, Choi KJ, Ding Y, Kim JH, Kim BS, Kim YH, Lee J, Choe W, Kang I, Ha J, Yoon KS, Kim SS (2007) Rhoa/rho kinase blocks muscle differentiation via serine phosphorylation of insulin receptor substrate-1 and -2. Mol Endocrinol 21: 2282-93.

[86] Fortier M, Comunale F, Kucharczak J, Blangy A, Charrasse S, Gauthier-Rouviere C (2008) Rhoe controls myoblast alignment prior fusion through rhoa and rock. Cell Death Differ 15: 1221-31.

[87] Bajaj P, Reddy J B, Millet L, Wei C, Zorlutuna P, Bao G, Bashir R (2011) Patterning the differentiation of c2c12 skeletal myoblasts. Integr Biol (Camb) 3: 897-909.

[88] Peng H, Wen TC, Igase K, Tanaka J, Matsuda S, Aburaya J, Sakanaka M (1997) Suppression by platelet factor 4 of the myogenic activity of basic fibroblast growth factor. Arch Histol Cytol 60: 163-74.

[89] Pirskanen A, Kiefer JC, Hauschka SD (2000) Igfs, insulin, shh, bfgf, and tgf-beta1 interact synergistically to promote somite myogenesis in vitro. Dev Biol 224: 189-203.

[90] Ogawa A, Firth AL, Smith KA, Maliakal MV, Yuan JX (2011) Pdgf enhances store-operated ca2+ entry by upregulating stim1/orai1 via activation of akt/mtor in human pulmonary arterial smooth muscle cells. Am J Physiol Cell Physiol .

[91] Baudino TA, Carver W, Giles W, Borg TK (2006) Cardiac fibroblasts: friend or foe? Am J Physiol Heart Circ Physiol 291: H1015-26.

[92] Goubko CA, Cao XD (2009) Patterning multiple cell types in co-cultures: A review. Materials Science Engineering C-Materials for Biological Applications 29: 1855-1868.

[93] Calvo F, Sahai E (2011) Cell communication networks in cancer invasion. Curr Opin Cell Biol 23: 621-9.

[94] Duell BL, Cripps AW, Schembri MA, Ulett GC (2011) Epithelial cell co-culture models for studying infectious diseases: benefits and limitations. J Biomed Biotechnol 2011: 852419.

[95] Salameh TS, Le TT, Nichols MB, Bauer E, Cheng J, Camarillo IG (2013) An ex vivo co-culture model system to evaluate stromal-epithelial interactions in breast cancer. Int J Cancer 132: 288-96.

[96] Canseco JA, Kojima K, Penvose AR, Ross JD, Obokata H, Gomoll AH, Vacanti CA (2012) Effect on ligament marker expression by direct-contact co-culture of mesenchymal stem cells and anterior cruciate ligament cells. Tissue Eng Part A 18: 2549-58.

[97] Keung AJ, Asuri P, Kumar S, Schaffer DV (2012) Soft microenvironments promote the early neurogenic differentiation but not self-renewal of human pluripotent stem cells. Integrative Biology 4: 1049-1058.

[98] Engler AJ, Sen S, Sweeney HL, Discher DE (2006) Matrix elasticity directs stem cell lineage specification. Cell 126: 677-89.

[99] Zouani OF, Kalisky J, Ibarboure E, Durrieu MC (2013) Effect of bmp-2 from matrices of different stiffnesses for the modulation of stem cell fate. Biomaterials 34: 2157-66.

[100] Di Rocco G, Iachininoto MG, Tritarelli A, Straino S, Zacheo A, Germani A, Crea F, Capogrossi MC (2006) Myogenic potential of adipose-tissue-derived cells. J Cell Sci 119: 2945-52.

[101] Khademhosseini A, Yeh J, Eng G, Karp J, Kaji H, Borenstein J, Farokhzad OC, Langer R (2005) Cell docking inside microwells within reversibly sealed microfluidic channels for fabricating multiphenotype cell arrays. Lab on a Chip 5: 1380-1386.

[102] Hong S, Pan Q, Lee LP (2012) Single-cell level co-culture platform for intercellular communication. Integr Biol (Camb) 4: 374-80.

[103] Takayama S, McDonald JC, Ostuni E, Liang MN, Kenis PJA, Ismagilov RF, Whitesides GM (1999) Patterning cells and their environments using multiple laminar fluid flows in capillary networks. Proceedings of the National Academy of Sciences of the United States of America 96: 5545-5548.

[104] Fukuda J, Khademhosseini A, Yeh J, Eng G, Cheng JJ, Farokhzad OC, Langer R (2006) Micropatterned cell co-cultures using layer-by-layer deposition of extracellular matrix components. Biomaterials 27: 1479-1486.

[105] Kaji H, Camci-Unal G, Langer R, Khademhosseini A (2011) Engineering systems for the generation of patterned co-cultures for controlling cell-cell interactions. Biochimica Et Biophysica Acta-General Subjects 1810: 239-250.

[106] Christman KL, Enriquez-Rios VD, Maynard HD (2006) Nanopatterning proteins and peptides. Soft Matter 2: 928-939.

[107] Brafman DA, Chien S, Willert K (2012) Arrayed cellular microenvironments for identifying culture and differentiation conditions for stem, primary and rare cell populations. Nat Protoc 7: 703-17.

[108] Bhatia SN, Balis UJ, Yarmush ML, Toner M (1999) Effect of cell-cell interactions in preservation of cellular phenotype: cocultivation of hepatocytes and nonparenchymal cells. FASEB J 13: 1883-900.

[109] Rao N, Evans S, Stewart D, Spencer KH, Sheikh F, Hui EE, Christman KL (2013) Fibroblasts influence muscle progenitor differentiation and alignment in contact independent and dependent manners in organized co-culture devices. Biomedical Microdevices 15: 161-169.

[110] Baker EL, Bonnecaze RT, Zamao MH (2009) Extracellular matrix stiffness and architecture govern intracellular rheology in cancer. Biophysical Journal 97: 1013-1021.

[111] Bavister BD (1995) Culture of preimplantation embryos: Facts and artifacts. Human Reproduction Update 1: 91-148.

[112] Wells RG (2008) The role of matrix stiffness in regulating cell behavior. Hepatology 47: 1394-1400.

[113] Brandl F, Sommer F, Goepferich A (2007) Rational design of hydrogels for tissue engineering: Impact of physical factors on cell behavior. Biomaterials 28: 134-146.

[114] Choi YS, Vincent LG, Lee AR, Dobke MK, Engler AJ (2012) Mechanical derivation of functional myotubes from adipose-derived stem cells. Biomaterials 33: 2482-91.

[115] Vieira NM, Brandalise V, Zucconi E, Jazedje T, Secco M, Nunes VA, Strauss BE, Vainzof M, Zatz M (2008) Human multipotent adipose-derived stem cells restore dystrophin expression of duchenne skeletal-muscle cells in vitro. Biol Cell 100: 231-41.

[116] Tse JR, Engler AJ (2010) Preparation of hydrogel substrates with tunable mechanical properties. Curr Protoc Cell Biol Chapter 10: Unit 10 16.

[117] Leng L, McAllister A, Zhang BY, Radisic M, Gunther A (2012) Mosaic hydrogels: One-step formation of multiscale soft materials. Advanced Materials 24: 3650-3658.

[118] Maloney JM, Walton EB, Bruce CM, Van Vliet KJ (2008) Influence of finite thickness and stiffness on cellular adhesion-induced deformation of compliant substrata. Physical Review E 78.

[119] Black BL, Olson EN (1998) Transcriptional control of muscle development by myocyte enhancer factor-2 (mef2) proteins. Annu Rev Cell Dev Biol 14: 167-96.

[120] Tse JR, Engler AJ (2011) Stiffness gradients mimicking in vivo tissue variation regulate mesenchymal stem cell fate. PLoS One 6: e15978.

[121] Pecanha R, Bagno LL, Ribeiro MB, Robottom Ferreira AB, Moraes MO, Zapata-Sudo G, Kasai-Brunswick TH, Campos-de Carvalho AC, Goldenberg RC, Saar Werneck-de Castro JP (2012) Adipose-derived stem-cell treatment of skeletal muscle injury. J Bone Joint Surg Am 94: 609-17.

[122] Beier JP, Bitto FF, Lange C, Klumpp D, Arkudas A, Bleiziffer O, Boos AM, Horch RE, Kneser U (2011) Myogenic differentiation of mesenchymal stem cells co-cultured with primary myoblasts. Cell Biol Int 35: 397-406.

[123] Eom YW, Lee JE, Yang MS, Jang IK, Kim HE, Lee DH, Kim YJ, Park WJ, Kong JH, Shim KY, Lee JI, Kim HS (2011) Effective myotube formation in human adipose tissue-derived stem cells expressing dystrophin and myosin heavy chain by cellular fusion with mouse c2c12 myoblasts. Biochem Biophys Res Commun 408: 167-73.

[124] Choi YS, Vincent LG, Lee AR, Kretchmer KC, Chirasatitsin S, Dobke MK, Engler AJ (2012) The alignment and fusion assembly of adipose-derived stem cells on mechanically patterned matrices. Biomaterials 33: 6943-51.

[125] Holle AW, Engler AJ (2011) More than a feeling: discovering, understanding, and influencing mechanosensing pathways. Current Opinion in Biotechnology 22: 648-654.

[126] Meligy FY, Shigemura K, Behnsawy HM, Fujisawa M, Kawabata M, Shirakawa T (2012) The efficiency of in vitro isolation and myogenic differentiation of mscs derived from adipose connective tissue, bone marrow, and skeletal muscle tissue. In Vitro Cell Dev Biol Anim 48: 203-15.

[127] Tatsumi R, Hattori A, Ikeuchi Y, Anderson JE, Allen RE (2002) Release of hepatocyte growth factor from mechanically stretched skeletal muscle satellite cells and role of ph and nitric oxide. Molecular biology of the cell 13: 2909–2918.

[128] Peterson JM, Pizza FX (2009) Cytokines derived from cultured skeletal muscle cells after mechanical strain promote neutrophil chemotaxis in vitro. Journal of Applied Physiology 106: 130–137.

[129] Aguado BA, Mulyasasmita W, Su J, Lampe KJ, Heilshorn SC (2011) Improving viability of stem cells during syringe needle flow through the design of hydrogel cell carriers. Tissue Engineering Part A 18: 806–815.

[130] Boudoulas KD, Hatzopoulos AK (2009) Cardiac repair and regeneration: the rubik's cube of cell therapy for heart disease. Disease models & mechanisms 2: 344–358.

[131] Hagège AA, Carrion C, Menasché P, Vilquin JT, Duboc D, Marolleau JP, Desnos M, Bruneval P (2003) Viability and differentiation of autologous skeletal myoblast grafts in ischaemic cardiomyopathy. The Lancet 361: 491–492.

[132] Ott HC, Kroess R, Bonaros N, Marksteiner R, Margreiter E, Schachner T, Laufer G, Hering S (2005) Intramyocardial microdepot injection increases the efficacy of skeletal myoblast transplantation. European journal of cardiothoracic surgery 27: 1017–1021.

[133] Menasché P (2008) Skeletal myoblasts and cardiac repair. Journal of molecular and cellular cardiology 45: 545–553.

[134] McGinn AN, Nam HY, Ou M, Hu N, Straub CM, Yockman JW, Bull DA, Kim SW (2011) Bioreducible polymer-transfected skeletal myoblasts for vegf delivery to acutely ischemic myocardium. Biomaterials 32: 942–949.

[135] Borselli C, Cezar CA, Shvartsman D, Vandenburgh HH, Mooney DJ (2011) The role of multifunctional delivery scaffold in the ability of cultured myoblasts to promote muscle regeneration. Biomaterials 32: 8905-14.

[136] Borselli C, Storrie H, Benesch-Lee F, Shvartsman D, Cezar C, Lichtman JW, Vandenburgh HH, Mooney DJ (2010) Functional muscle regeneration with combined delivery of angiogenesis and myogenesis factors. Proc Natl Acad Sci U S A 107: 3287-92.

[137] Eschenhagen T, Zimmermann WH, Kléber AG (2006) Electrical coupling of cardiac myocyte cell sheets to the heart. Circulation research 98: 573–575.

[138] Johnson TD, DeQuach JA, Gaetani R, Ungerleider J, Elhag D, Nigam V, Behfar A, Christman KL (2014) Human versus porcine tissue sourcing for an injectable myocardial matrix hydrogel. Biomaterials Science .

[139] Singelyn JM, DeQuach JA, Seif-Naraghi SB, Littlefield RB, Schup-Magoffin PJ, Christman KL (2009) Naturally derived myocardial matrix as an injectable scaffold for cardiac tissue engineering. Biomaterials 30: 5409-5416.

[140] Seif-Naraghi SB, Salvatore MA, Schup-Magoffin PJ, Hu DP, Christman KL (2010) Design and characterization of an injectable pericardial matrix gel: A potentially autologous scaffold for cardiac tissue engineering. Tissue Engineering Part A 16: 2017-2027.

[141] Levenberg S, Rouwkema J, Macdonald M, Garfein ES, Kohane DS, Darland DC, Marini R, van Blitterswijk CA, Mulligan RC, D'Amore PA (2005) Engineering vascularized skeletal muscle tissue. Nature biotechnology 23: 879–884.

[142] Robin E, Guzy RD, Loor G, Iwase H, Waypa GB, Marks JD, Hoek TLV, Schumacker PT (2007) Oxidant stress during simulated ischemia primes cardiomyocytes for cell death during reperfusion. Journal of Biological Chemistry 282: 19133–19143.

[143] Clanton TL (2007) Hypoxia-induced reactive oxygen species formation in skeletal muscle. Journal of Applied Physiology 102: 2379–2388.

[144] Gute DC, Ishida T, Yarimizu K, Korthius RJ (1998) Inflammatory responses to ischemia, and reperfusion in skeletal muscle. Molecular and cellular biochemistry 179: 169–187.

[145] Correa RS, Samson WD, Quiroz MA (2003). Needle design for live microorganisms. US Patent 6,629,962.

[146] Ruan J, Song H, Li C, Bao C, Fu H, Wang K, Ni J, Cui D (2012) Dir-labeled embryonic stem cells for targeted imaging of in vivo gastric cancer cells. Theranostics 2: 618.

[147] Imanishi Y, Miyagawa S, Fukushima S, Ishimaru K, Sougawa N, Saito A, Sakai Y, Sawa Y (2013) Sustained-release delivery of prostacyclin analogue enhances bone marrow-cell recruitment and yields functional benefits for acute myocardial infarction in mice. PloS one 8: e69302.

[148] Celso CL, Fleming HE, Wu JW, Zhao CX, Miake-Lye S, Fujisaki J, Côté D, Rowe DW, Lin CP, Scadden DT (2009) Live-animal tracking of individual haematopoietic stem/progenitor cells in their niche. Nature 457: 92–96.

[149] Ohno Si, Takanashi M, Sudo K, Ueda S, Ishikawa A, Matsuyama N, Fujita K, Mizutani T, Ohgi T, Ochiya T (2013) Systemically injected exosomes targeted to egfr deliver antitumor microrna to breast cancer cells. Molecular Therapy 21: 185–191.

[150] Ye J, Ma C, Wang F, Hsueh EC, Toth K, Huang Y, Mo W, Liu S, Han B, Varvares MA (2013) Specific recruitment of ÎşÎť regulatory t cells in human breast cancer. Cancer research 73: 6137–6148.

[151] Somanchi SS, Somanchi A, Cooper LJ, Lee DA (2012) Engineering lymph node homing of ex vivo–expanded human natural killer cells via trogocytosis of the chemokine receptor ccr7. Blood 119: 5164–5172.

[152] Yoshikawa HY, Kawano T, Matsuda T, Kidoaki S, Tanaka M (2013) Morphology and adhesion strength of myoblast cells on photocurable gelatin under native and non-native micromechanical environments. The Journal of Physical Chemistry B 117: 4081–4088.

[153] Engler AJ, Griffin MA, Sen S, Bönnemann CG, Sweeney HL, Discher DE (2004) Myotubes differentiate optimally on substrates with tissue-like stiffness pathological implications for soft or stiff microenvironments. The Journal of cell biology 166: 877–887.

[154] Westerweel PE, Rookmaaker MB, van Zonneveld AJ, Bleys RL, Rabelink TJ, Verhaar MC (2005) A study of neovascularization in the rat ischemic hindlimb using araldite casting and spalteholtz tissue clearing. Cardiovascular Pathology 14: 294–297.

[155] Tsurumi Y, Takeshita S, Chen D, Kearney M, Rossow ST, Passeri J, Horowitz JR, Symes JF, Isner JM (1996) Direct intramuscular gene transfer of naked dna encoding vascular endothelial growth factor augments collateral development and tissue perfusion. Circulation 94: 3281–3290.